

# MODELING, ANALYSIS, AND NETWORK IDENTIFICATION OF CANCER SIGNAL TRANSDUCTION NETWORKS

A Dissertation

Presented to the Faculty of the Graduate School

of Cornell University

in Partial Fulfillment of the Requirements for the Degree of

Doctor of Philosophy

by

Katharine Rogers

December 2015

© 2015 Katharine Rogers  
ALL RIGHTS RESERVED

MODELING, ANALYSIS, AND NETWORK IDENTIFICATION OF CANCER  
SIGNAL TRANSDUCTION NETWORKS

Katharine Rogers, Ph.D.

Cornell University 2015

Cancer involves the dysregulation of multiple signaling pathways in which computational modeling can be applied to understand complex network responses. A computational modeling approach can be used to determine the development of drug resistance in cancers, predict combination therapies, and determine individualized treatment for cancer patients. To this end we have employed mechanistic modeling to a variety of cancer networks. In Chapter 1, we review current methods and progress toward using computational methods for cancer biology. Cancer is no longer considered one gene one disease and computational modeling is an important tool in understanding the development of many cancer types. In Chapter 2, we constructed a mechanistic model of the development of castration resistant prostate cancer (CRPC). Analysis of the model suggested that simultaneously targeting the PI3K and MAPK pathways in addition to anti-androgen therapies could be an effective treatment for CRPC. We experimentally tested this hypothesis in both androgen dependent prostate cancer (ADPC) LNCaP cell lines and LNCaP derived CRPC C4-2 cells using three inhibitors: the androgen receptor inhibitor MDV3100 (enzalutamide), the Raf kinase inhibitor sorafenib, and the PI3K inhibitor LY294002. Consistent with model predictions, cell viability decreased at 72 hrs in the dual and triple inhibition cases in both the LNCaP and C4-2 cell lines. In Chapter 3, we look at the importance of network identification in mechanistic modeling of cancer networks.

Cancer is a complex disease and complete biological knowledge of the system is often unknown. Using a small three node protein example we were able to obtain a correct model structure with no *a priori* knowledge of the system. We then applied this method to determine transcription factor network structures for six leukemia cell lines: K562, HL60, NB4, U937, HL60 R38+ and HL60 R38-. Starting with an initial best guess model structure we were able to determine additional network modifications for each cell line to improve model fit of experimental data. Potential future directions and closing remarks are offered in Chapter 4. Taken together, the results of these studies demonstrated that computational modeling can aid in identifying therapeutic targets and combination treatments for cancer. Also, the use of computational modeling can improve cancer network identification in the absence of complete biological knowledge.

## **BIOGRAPHICAL SKETCH**

Katharine Rogers graduated summa cum laude in 2010 from Rensselaer Polytechnic Institute with a Bachelors of Science in Chemical Engineering and Bachelors of Science in Mathematics. At Cornell University, she joined Dr. Jeffrey Varner's research group in the Department of Chemical and Biomolecular Engineering. As a Ph.D. candidate she received a National Science Foundation GK12 Fellowship. Her research focus involved modeling pathways involved in cancer progression of prostate cancer as well as determining unknown model structures in leukemia cell lines.

This work is dedicated to my friends, family, and Louie.

## **ACKNOWLEDGEMENTS**

Firstly, I would like to thank my mother for her unwavering love, support, and valuable advice over the years. Also, I want to thank my brothers, Harris and Ted, for all their support and help. I would also like to thank my late father and late grandparents for inspiring my interest in math and science.

Thanks to Dr. Jeffrey Varner for choosing me as a student, even with minimal prior coding experience. Jeff has been a great mentor, allowing me to explore both computational and experimental projects. I would also like to thank Dr. Matthew DeLisa for his guidance in the lab. Also, a big thanks to Dr. Brian Kirby for his class and his guidance. Thanks also to Dr. Paulette Clancy and Dr. Julie Nucci for their advising through the NSF GK12 program.

Thanks to all the Varner Group members. First, I would like to thank Joseph Wayman for being an excellent proofreader, soundboard, and friend. I would like to thank all of the undergrads and M.Eng students who helped conduct research related to my project: Caitlin Gee, Yalin Zhao, Mark Unter, Timothy Chu, Kyriakos Tsahalis, Spencer Davis, Rohit Yallamraju, and Gongcheng Lu. Thanks to the graduate students both old and new for their help: in particular, Holly Jensen for teaching me in the lab and Adithya Sagar and Anirikh Chakrabarti for their help with computational projects.

## TABLE OF CONTENTS

Biographical Sketch . . . . .	iii
Dedication . . . . .	iv
Acknowledgements . . . . .	v
Table of Contents . . . . .	vi
List of Tables . . . . .	viii
List of Figures . . . . .	ix
<b>1 Introduction</b>	<b>1</b>
1.1 Current approaches: Kinetic Models . . . . .	3
1.2 Current approaches: Logical Models . . . . .	7
1.3 Current Approach: Multiscale Models . . . . .	10
1.4 Using Signal Transduction Models to Identify Drug Therapies . . . . .	12
1.5 Conclusion . . . . .	14
<b>2 Modeling and Analysis of Hormone and Mitogenic Signal Integration in Prostate Cancer</b>	<b>15</b>
2.1 Introduction . . . . .	16
2.2 Results . . . . .	20
2.2.1 Estimating an ensemble of prostate signaling models. . . . .	20
2.2.2 Validation simulations revealed missing network structure. . . . .	23
2.2.3 Sensitivity analysis identified differentially important features of the prostate architecture. . . . .	28
2.2.4 Robustness analysis identified key regulators of prostate cancer. . . . .	32
2.2.5 Experimental results confirm the need for dual therapies in prostate cancer. . . . .	36
2.3 Discussion . . . . .	39
2.4 Materials and Methods . . . . .	45
2.4.1 Prostate model signaling architecture. . . . .	45
2.4.2 Formulation and solution of the model equations. . . . .	47
2.4.3 Sensitivity and robustness analysis. . . . .	49
2.4.4 Experimental Validation. . . . .	52
2.4.5 Cell culture and treatments . . . . .	52
2.4.6 Protein Extraction and Western Blot . . . . .	52
2.4.7 MTT Assay . . . . .	53
2.5 Acknowledgements . . . . .	54
<b>3 Model Identification of Leukemia Transcription Factor Networks</b>	<b>55</b>
3.1 Introduction . . . . .	55
3.2 Results . . . . .	58
3.2.1 Three Node Example Network . . . . .	58
3.2.2 Leukemia Transcription Factor Network . . . . .	62

3.3	Discussion . . . . .	76
3.4	Materials and Methods . . . . .	79
3.4.1	Formulation of Network Model Equations . . . . .	79
3.4.2	Estimation of top parameter sets using Particle Swarm Optimization (PSO) . . . . .	81
<b>4</b>	<b>Conclusion and Future Work</b>	<b>85</b>
4.0.1	Closing Remarks . . . . .	85
<b>A</b>	<b>Chapter 1 of appendix</b>	<b>90</b>
<b>B</b>	<b>Chapter 2 of appendix</b>	<b>103</b>
	<b>Bibliography</b>	<b>128</b>

## LIST OF TABLES

3.1	Initial myelomonocytic transcription factor network list with transcription factor, effect, target gene, and reference . . . . .	70
A.1	Objective function list along with species measured, stimulus, cell-type, steady state (SS) vs dynamic (D) and the corresponding literature reference. . . . .	94
A.2	Blind Prediction list along with species measured, stimulus, cell-type, steady state (SS) vs dynamic (D) and the corresponding literature reference. . . . .	96
B.1	Training objective function list with objective number, species measured, experiment and trials used in . . . . .	105
B.2	Prediction function list with prediction number, species measured, experiment and trials used in . . . . .	105
B.3	Experiment list with stimulus, species for training, and species for validation . . . . .	106
B.4	Training objective function list with objective number, species measured, stimulus, and time points. The same 39 objective functions were used for all cell lines with data from [122]. . . . .	107
B.5	Model Updates for K562 cell line with edge number, action, transcription factor, general effect, target gene, and new references .	111
B.6	Model Updates for NB4 cell line with edge number, action, transcription factor, general effect, target gene, and new references .	114
B.7	Model Updates for WT-HL60 cell line with edge number, action, transcription factor, general effect, target gene, and new references	117
B.8	Model Updates for HL60 R38+ cell line with edge number, action, transcription factor, general effect, target gene, and new references . . . . .	120
B.9	Model Updates for HL60 R38- cell line with edge number, action, transcription factor, general effect, target gene, and new references	123
B.10	Model Updates for U937 cell line with edge number, action, transcription factor, general effect, target gene, and new references .	126

## LIST OF FIGURES

1.1	Schematic of ODE analysis of the androgen receptor (AR) pathway. <b>A.</b> Simplified AR signal transduction network. <b>B.</b> The rate of change of network species $x$ , $dx/dt$ , is calculated from the stoichiometric matrix, $S$ , and the rate vector, $r$ . The stoichiometric matrix is formulated from the network shown in A. <b>C.</b> Continuos protein trajectory of PSA after addition of DHT. . . . .	5
1.2	Schematic of a logical model framework. <b>A.</b> Simple logical model example based on EGFR and HER2 signaling. <b>B.</b> Boolean network truth table of the network in A. A value of zero denotes no expression and one denotes high expression, with pERK expression as the output. <b>C., D.</b> Boolean and fuzzy logic states of pERK, respectively. In the boolean model pERK can either be 1 or 0, while fuzzy logic allows for members to be in multiple groups. . . . .	8
2.1	Schematic overview of the prostate signaling network. The model describes hormone and growth factor induced expression of several proteins, including PSA. In the absence of outside hormones/growth factors, overactive HER2 can stimulate the MAPK and AKT pathways. AR can be activated directly by the MAPK pathway. . . . .	22
2.2	Simulation results versus experimental results for training and validation data. Experiment numbers 1 through 43 were used for training, while experiments 44 through 72 were validation. Gray means the ensemble member qualitatively fit experimental data in both models. White means the the ensemble member only fit the data using the new model that included HER2 heterodimerization. Red means the ensemble member fit using only the old model. Black corresponds to an incorrect cellular response in both models. <b>A., C.</b> Training and validation results, respectively, for entire ensemble population using both the original model and an updated model including HER2 heterodimerization ( $N = 5000$ ). <b>B., D.</b> Simulation results for training and validation of a random set of 100 members using both models. . . .	24



- 2.6 Robustness analysis of a population of CR prostate models with Raf knock-out ( $N = 500$ ). A scaled log fold change of greater than zero implies that the concentration of the protein increased with the knock-out of Raf, while a log fold change of less than zero indicates that the concentration of protein decreased. A log of fold change equal to 0, shows no response due to Raf knock-out. Three distinct regions emerge in Raf knock-out case: (1) PSA increases, (2) cyclin D concentration increases, and (3) PSA and cyclin D concentration decrease. The grey ellipse is centered at the mean values with an x-radius and y-radius of one standard deviation of the scaled log fold change of PSA values and cyclin D values, respectively. The blue ellipse denotes two standard deviations from the mean and the orange denotes three standard deviations from the mean. Values denote percentage of total parameter sets that fall in each quadrant, while values in parenthesis denote the percentage that fall at least one standard deviation from the mean. . . . .

2.7 Robustness analysis of a population of CR prostate models with seven protein knock-out cases ( $N = 500$ ). A scaled log fold change of greater than zero implies that the concentration of the protein increased with the knock-out, while a scaled log fold change of less than zero indicates that the concentration of protein decreased. A scaled log fold change equal to 0, shows no response due to the knock-out. **A., B., C., D.** Log robustness of PSA, p70p, cyclin D, and AKTp versus protein knock-out. A CR LNCaP cell was assumed for all knock-out cases. The bottom and top of each box denotes 25th and 75th percentiles, while the red line indicates the median. The whiskers on the plot are plus and minus 1.5 the interquartile range (IQR) from the top and bottom values of the box, respectively. The grey dots denote outliers and the blue dots denote the mean. . . . .

2.8	Experimental results for multiple drug combinations on two prostate cancer cell lines, LNCaP and C4-2. <b>A.</b> Western blot analysis of AR, pS6, AKT, pAKT, ERK and cleaved PARP in LNCaP and C4-2 cell lines treated for 24 hrs with DMSO (control), sorafenib (5 $\mu$ M), LY294002 (40 $\mu$ M), and MDV3100 (10 $\mu$ M) alone or in combination (at least 3 repeats). <b>B.</b> Cells (LNCaP and C4-2) were treated for 24, 48 and 72 hrs with sorafenib (5 $\mu$ M), LY294002 (40 $\mu$ M), and MDV3100 (10 $\mu$ M) and cell viability was measured using MTT Assay. Values were normalized to DMSO (control). <b>C.</b> Cell viability results for LNCaP and C4-2 cells at varying concentration of sorafenib, LY294002, and MDV3100 after 24 hrs of treatment. Values were normalized to DMSO (control). Error bars represent standard error (at least 3 repeats with triplicates performed in each experiment). . . . .	38
3.1	Model for three node protein network. Arrows denote activation and lines denote inhibition. The model includes three proteins ( $P_1$ , $P_2$ , and $P_3$ ), the corresponding mRNA ( $mRNA_1$ , $mRNA_2$ , and $mRNA_3$ ), RNA polymerase (RNAP), ribosomes (RIBO), and Inducer. <b>A.</b> The true model for the three node protein network. <b>B.</b> The best fit model after parameter estimation using data from only one experiment. <b>C.</b> The best fit model after parameter estimation using data from experiments 1, 2 and 3. Red lines denote interactions not in original model and blue lines denote interactions that are opposite of the original model. <b>D.</b> Gene transcription activation and repression in the model (figure modified from [7]). . . . .	60
3.2	Experiment 1 results for the top 20 models with respective best parameter sets determined from particle swarm optimization. In experiment 1, inducer was added at Time = 100. <b>A, B, C.</b> Plots of mRNA concentration profiles for species 1, 2, and 3 after inducer added at Time = 100. <b>D.</b> Plot of protein concentration profile for species 1 which was used for validation. <b>E, F.</b> Plots of protein concentration profiles for species 2 and 3. Red dots denote synthetic experimental data used for fitting. Red lines represent the true model with optimized parameters, blue denotes the best fitting model (3.1B), and the grey lines represent remaining top 18 models. . . . .	63

3.3	Structures of top 20 three protein node models. Models are arranged from lowest error (best fit) to highest error, with the true model at number 12. Red denotes interactions not in original model, blue denotes interactions that are opposite of the original model, and dotted lines denote interactions in true model that are missing in structure. Numbers (i.e. 3147) denote the specific model number out of the total 19683 structures. . . . .	64
3.4	Experiment 2 results for the top 20 models with respective best parameter sets determined from particle swarm optimization. In experiment 2, inducer and an inhibitor for $P_2$ were added at Time = 100. <b>A, B.</b> Plots of mRNA concentration profiles for species 1 and 2 after inducer and inhibitor added at Time = 100. <b>C.</b> Plot of mRNA concentration profile for species 3 which was used for validation. <b>D, E, F.</b> Plots of protein concentration profiles for species 1, 2, and 3. Red dots denote synthetic experimental data used for fitting. Red lines represent the true model with new optimized parameters, blue denotes the best fitting model after experiment 1 (3.1B), green denotes the new best fitting model, orange denotes the third best fit model, and the grey lines represent remaining top 18 models. . . . .	65
3.5	Initial myelomonocytic transcription factor network structure from literature sources. Figure shows interactions between protein nodes with arrows indicating transcriptional activation and lines indicating transcriptional repression. Phenotypic markers are shown on the right side, with black indicating activation and red repression. RXR (shown in the figure) was assumed to exist in an active form to dimerize with RAR $\alpha$ , VDR, and PPAR $\gamma$ and was excluded in this network identification problem. . . . .	67
3.6	Selected training results for the HL60 R38- cell line. <b>A., B., C.</b> Simulation and experimental results of change in VDR concentration due to RA, D3, and RA/D3 stimulus, respectively. Green denotes experimental data, pink denotes simulation data from the initial network, and blue denotes simulation data from the best network. The top parameter set is used, and error bars denote standard experimental error. . . . .	72
3.7	Selected training results for the HL60 cell line. <b>A., B., C.</b> Simulation and experimental results of change in cells expressing CD38 due to RA, D3, and RA/D3 stimulus, respectively. Green denotes experimental data, pink denotes simulation data from the initial network, and blue denotes simulation data from the best network. The top parameter set is used, and error bars denote standard experimental error. . . . .	73

3.8	Selected training results for the NB4 cell line. <b>A., B., C.</b> Simulation and experimental results of change in CD11b concentration due to RA, D3, and RA/D3 stimulus, respectively. Green denotes experimental data, pink denotes simulation data from the initial network, and blue denotes simulation data from the best network. The top parameter set is used, and error bars denote standard experimental error. . . . .	74
3.9	Selected training results for the K562 cell line. <b>A., B., C.</b> Simulation and experimental results of change in PU.1 concentration due to RA, D3, and RA/D3 stimulus, respectively. Green denotes experimental data, pink denotes simulation data from the initial network, and blue denotes simulation data from the best network. The top parameter set is used, and error bars denote standard experimental error. . . . .	75
A.1	Coefficient of variation (CV) of model parameters estimated using POETs. The solid line denotes the mean CV calculated over the entire ensemble ( $N = 5000$ ). The points denote the mean CV of the 500 ensemble members used for sensitivity and robustness calculations. Over the ensemble, the coefficient of variation (CV) of the kinetic parameters spanned 0.59 - 5.8, with 33% of the parameters having a CV of less than one. . . . .	98
A.2	Blind model predictions for the ensemble with the original and updated model (EGFR and HER2 heterodimer). <b>A, B.</b> Time course data for HER2 phosphorylation due to a stimulus of 1.6 nM EGF (LNCaP C-33, P7) for the old and new model, respectively. Dark grey shows only parameters improved by the updated model ( $N=2870$ ) while light grey show all parameter sets ( $N=5000$ ). <b>C, D.</b> Shc phosphorylation levels at 16 hrs in the presence and absence of 1.6 nM EGF (LNCaP C-33, P29) for the old and new model, respectively. Light grey denotes experimental data, mid grey denotes simulation results for all parameters ( $N=5000$ ), and black denotes only parameters improved by the updated model ( $N=3142$ ). Error bars denote plus and minus one standard deviation above the mean. . . . .	99

A.3	Sensitivity analysis of a population of prostate models (N = 500). Species with a low sensitivity are considered robust, while species with a high sensitivity ranking are considered fragile. <b>A</b> . Sensitivity ranking of network species in CR cells in the absence and presence of DHT. <b>B</b> . Sensitivity ranking of network species in CR cells in the presence of enzalutamide in the presence and absence of a DHT stimulus. <b>C., D.</b> Sensitivity ranking of network species in CR cells in the presence and absence of sorafenib and lapatinib, respectively, with a DHT stimulus. Error bars denote standard error with N = 500. . . . .	100
A.4	Robustness analysis of protein markers. Expression level of key proteins was altered by a factor of 2, 0.1, or 0 (knock-in, knock-down, or knock-out) and robustness coefficients were calculated for five key protein markers. Simulations shown were from CR cells, with indicated perturbation. Mean of 500 ensemble members is shown. . . . .	101
A.5	Dual knock-out of AR and PI3K leads to decreased expression of activated p70. A., B, C. Robustness coefficient of activated p70 (S6) in the PI3K knock-out, AR knock-out, and dual knock-out cases, respectively. The control was the basil CR LNCaP wild type case. Error bars denote plus and minus one standard error above the mean with N = 500. Experimental data is from Carver, <i>et al.</i> [34]. . . . .	102
B.1	Synthetic data running experiment 1 for true model of three node protein network. In experiment 1, inducer was added at Time = 100. <b>A, B, C.</b> Plots of mRNA concentration profiles for species 1, 2, and 3 after inducer added at Time = 100. <b>D, E, F.</b> Plots of protein concentration profiles for species 1, 2, and 3. Red dots denote data used for fitting (0, 24, 48, and 72 AU after stimulus). . . . .	104
B.2	Selected training results for the U937 cell line. <b>A., B., C.</b> Simulation and experimental results of change in AhR concentration due to RA, D3, and RA/D3 stimulus, respectively. Green denotes experimental data, pink denotes simulation data from the initial network, and blue denotes simulation data from the best network. The top parameter set is used, and error bars denote standard experimental error. . . . .	109

B.3 Selected training results for the HL60 R38+ cell line. <b>A.</b> , <b>B.</b> , <b>C</b> . Simulation and experimental results of change in C/EBP $\alpha$ concentration due to RA, D3, and RA/D3 stimulus, respectivelyl. Green denotes experimental data, pink denotes simulation data from the initial network, and blue denotes simulation data from the best network. The top parameter set is used, and error bars denote standard experimental error. . . . .	110
---	-----

## CHAPTER 1

### INTRODUCTION

Cancer<sup>1</sup>, once considered a monolithic disease, is a vast repertoire of diseases divided into carcinomas (epithelial-originating cancers), sarcomas (connective tissue cancers), leukemias (blood cancers), lymphomas, myelomas, and mixed types like teratocarcinoma. All these diseases exhibit the “Hallmarks of Cancer” as described by Hanahan and Weinburg in 2000 [95]. These characteristics are (1) sustained proliferative signaling, (2) insensitivity to or evasion of growth-suppressive signals, (3) resistance to or evasion of apoptosis, (4) limitless renewal potential, (5) promotion of angiogenesis and (6) tissue invasion and metastasis. In a more recent review, to this list Hanahan and Weinburg added (7) altered metabolic signaling, and (8) resistance to immune destruction and resulting inflammation [96]. These proposed hallmarks have in fact been criticized: it was pointed out that 5 of the original 6 (excluding ability to metastasize) are in fact characteristics of benign tumors as well [144]. Nonetheless, a general consensus exists that cancers do exhibit the above listed attributes, which can parsimoniously be described as notably harmful uncontrolled cell proliferation. Cancer can unfortunately arise in essentially any tissue type, resulting in “hundreds of different cancers” [246].

Cancer treatments have progressed over the years from surgery and chemotherapy to targeted therapies. Currently, there are a multitude of small molecule inhibitors on the market, including tyrosine kinase inhibitors, growth factor receptor inhibitors, mTOR inhibitors, and angiogenesis inhibitors. In addition, cancer vaccines are another up-and-coming therapy; Sipuleucel-T

---

<sup>1</sup>Adapted with permission from: Rogers K, Jensen H, Varner J. Physical and Logical Models of Signal Transduction Processes in Cancer, (in prep).

(Provenge) is an approved autologous vaccine for castration resistant prostate cancer [250]. However, targeted therapies are proving less promising than previously anticipated. Of all anticancer agents tested in the preclinical setting, only 5% are successfully licensed after making it to Phase III clinical testing [115]. This low success rate is mainly due to poor candidate selection in the preclinical arena, which arises from shortcomings on how cancer therapies are pursued. Individual cell lines do not represent whole cancers; mouse xenografts do not reflect the human case; treatments are tested as monotherapeutics rather than combination therapies. Bevacizumab (Avastin) was a previously approved angiogenesis inhibitor for breast cancer treatment, until the FDA revoked approval in 2011 (despite slowing metastatic growth, it did not help patients live longer or improve prognosis, and had some harmful side effects) [192]. Emergent resistance is also a major obstacle in cancer therapy, and can arise in response to chemotherapeutic agents, kinase inhibitors, hormonal agents and immunomodulatory treatments. In some cases chemotherapeutic combinations have been successful at overcoming resistance developed in response to single agents; but often cancerous cells exhibit cross-resistance to alternative compounds, or are *de novo* resistant to treatment [82]. Resistance, especially in relation to kinase inhibitors, is often associated with an acquired mutation(s) in the intended target; examples include the emergence of a mutation in Bcl-Abl in chronic myelogenous leukemia (CML) cells treated with imatinib, mutation in PML-RAR in acute promyelocytic leukemia (APL) cells treated with retinoic acid, and an EGFR mutation in gefitinib-treated non-small cell lung cancer. These mutations are likely not produced by the treatment *per se* but exist in subpopulations that are then positively selected [82]. However, such acquired mutations are not the whole story of resistance. Genetic alterations can

arise in signaling factors upstream or downstream of the target. Enhanced ERK activation results from MEK1 mutation or a mutant NRas that acts through c-Raf; both of these mechanisms render B-Raf inhibition ineffectual [82]. Bypass mechanisms result when a downstream effector of the target is activated via an alternative pathway, or when feedback inhibition is inadvertently relieved [82]. Beyond this, sometimes no resulting mutations can be identified. Even pathway-independent resistance is possible, such as altered tumor angiogenesis in response to both EGFR inhibitors and therapeutic anti-EGFR antibody [82]. Resistance is, overall, poorly understood at present.

It is evident that cancers are diseases epitomized by dysregulation of entire networks. Although all cancers have a genetic basis, with genome alterations either inherited or induced from external factors (viruses, carcinogens, radiation), holistic understanding at the genetic, intracellular, tissue and extracellular (tumor environment) and physiological level is still necessary to develop successful future therapeutics for such a complex disease. It is also necessary to cease considering cancers as one gene one disease and begin exploring combination treatments [203]. A computational modeling approach can be used to determine the development of drug resistance in cancers, predict combination therapies, and determine individualized treatment for cancer patients. Below we address some of the current methods and progress toward using computational methods for cancer biology.

## 1.1 Current approaches: Kinetic Models

Cancer involves the dysregulation of multiple signaling pathways in which computational modeling can be applied to understand complex network re-

sponses. One of the most common modeling approaches for signal transduction networks is through a set of coupled ordinary differential equations (ODEs), using mass action kinetics [5]. The equations used are derived from established chemical and physical theory [5]. ODE kinetic models often require extensive prior knowledge of network structure, rate constants and initial conditions [135]. Even with this, the ability of ODE models to capture dynamics makes it a particularly useful tool in studying cell signaling. A small example ODE model is shown in Figure 1.1. In the early 1990s, Lauffenburger and coworkers developed early biophysical and kinetic models of epidermal growth factor receptor (EGFR) signaling in fibroblastic cells and interleukin 2 receptor signaling in T-cells [229, 76]. Both models provided key insights into critical network parameters involved in cell proliferation. A more potent ligand for EGFR was later developed using these models [197]. Additional ODE models were developed focusing on downstream signaling due to the presence of growth factors and its effect on cell fate decisions [134, 214].

Almost two decades later, multiple cancer signal transduction systems have been studied using an ODE framework. DNA damage response was studied with a p53/MdM2 network model [45]. The model contained negative and positive feedback loops, that subsequently led to oscillations in p53 protein levels. Apoptosis through caspase regulatory networks has been explored using experimental training data from HeLa cells [198, 3, 4]. Analysis of the mammalian NF- $\kappa$ B system by Hoffman and coworkers, predicted bimodal signal characteristics of the I $\kappa$ B-NF- $\kappa$ B signaling module [110]. Other important cancer signaling systems that have been explored include RTK and MAPK (mitogen-activated protein kinase) cascades [20, 214, 23, 41], JAK-STAT signaling [232, 254], and Wnt signaling [249, 248, 136].

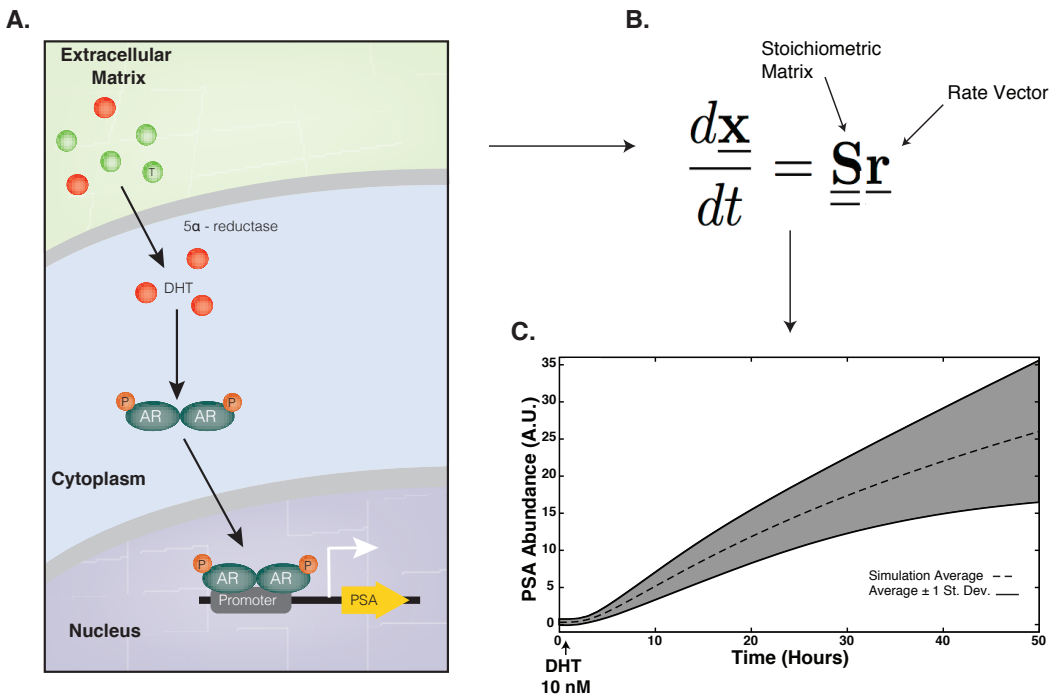


Figure 1.1: Schematic of ODE analysis of the androgen receptor (AR) pathway. **A.** Simplified AR signal transduction network. **B.** The rate of change of network species  $x$ ,  $dx/dt$ , is calculated from the stoichiometric matrix,  $S$ , and the rate vector,  $r$ . The stoichiometric matrix is formulated from the network shown in A. **C.** Continuous protein trajectory of PSA after addition of DHT.

As cancer often involves dysregulation of multiple signaling pathways as well as crosstalk and feedback between pathways, larger systems need to be developed to provide a more accurate portrayal of cancer networks. For example, a model by Kim *et al.* discovered a positive feedback loop between the Wnt and ERK pathways [136]. A model by Borisov *et al.* predicted increased mitogenic signaling due to crosstalk between insulin and EGF signaling networks [23]. This model predicted and experiments confirmed that inhibition of PIP3 positive feedback abolished the increased mitogenic signaling due to insulin. Tasseff *et al.* developed a model to reveal new targets for androgen

independent prostate cancer [241]. Initially, treatments for prostate cancer target the androgen receptor signaling pathway, but often the cancer progresses into an androgen independent phenotype. The model includes androgen receptor signaling as well as crosstalk between the androgen receptor and the MAPK pathway, itself a predicted mechanism for the development of androgen independent prostate cancer [72]. As more complete knowledge of interactions between signaling pathways is elucidated, computational models will become even more important in aiding in the understanding of these complex networks.

Often, the option of adding all known biology to computational models of cancer signal transduction networks is not possible. Model size is often limited due to the difficulty in solving for unknown model parameters. Gadkar *et al.* showed that it was often impossible to identify all the parameters in signal transduction methods even with near perfect knowledge of the system and high frequency sampling [80]. A report by Apgar *et al.* examined the importance of experimental design in generating better training and validation data sets for model identification [10]. Alternatively, it was suggested by Bailey, more than a decade ago, that qualitative and quantitative knowledge of complex biological systems could be achieved in the absence of complete structural and parameter knowledge [13]. Later, Sethna and coworkers showed that the sensitivity of model behavior and predictive ability was dependent on only a few parameter combinations, a characteristic common to multiparameter signaling models referred to as “sloppiness” [55]. Thus, even with limited parameter information reasonable model predictions could be possible. Taking advantage of this sloppy model hypothesis, we have developed techniques for parameter identification using ensembles of deterministic models. A multi-objective optimization approach, Pareto optimal ensemble techniques (POETs), explores

parameter space while accounting for uncertainty and conflicts in experimental training data [227]. We have proposed that the sloppiness of biological models may be a source of cell-to-cell [148] or even patient-to-patient heterogeneity [164]. Recently, cell-to-cell heterogeneity has been explored through Bayesian techniques of parameter estimation [101, 127]. This cell-to-cell heterogeneity is applicable to cancer in that often resistance can occur due to a small subpopulation of drug-resistant cells [47]. By studying how individual cells will react to external stimuli we can understand how drug resistance occurs and determine additional therapeutic targets.

## 1.2 Current approaches: Logical Models

Due to the size constraint in kinetic models, other computational methods have been utilized for modeling cancer networks. One such method is known as logic based modeling. Logic based models are graphical representations of signaling networks in which the nodes of the graph represent proteins and the edges represent interactions [174]. The components are connected with logical gates, where each gate relates inputs to outputs. A subset of these, known as Boolean logic models, divide network components into one of two activation states (on and off). These models are simpler than mechanistic models, but one limitation is relating nonbinary data to two distinct activation states (on and off) [135]. Multiple approaches have been added to logic based models to allow for the modeling of intermediate states of activity. For example, in multistate discrete models additional levels between 0 and 1 are specified [174]. Additionally, fuzzy logic has been utilized to allow for component values to range continuously from 0 to 1 [174]. Figure 1.2 shows a schematic logical model framework

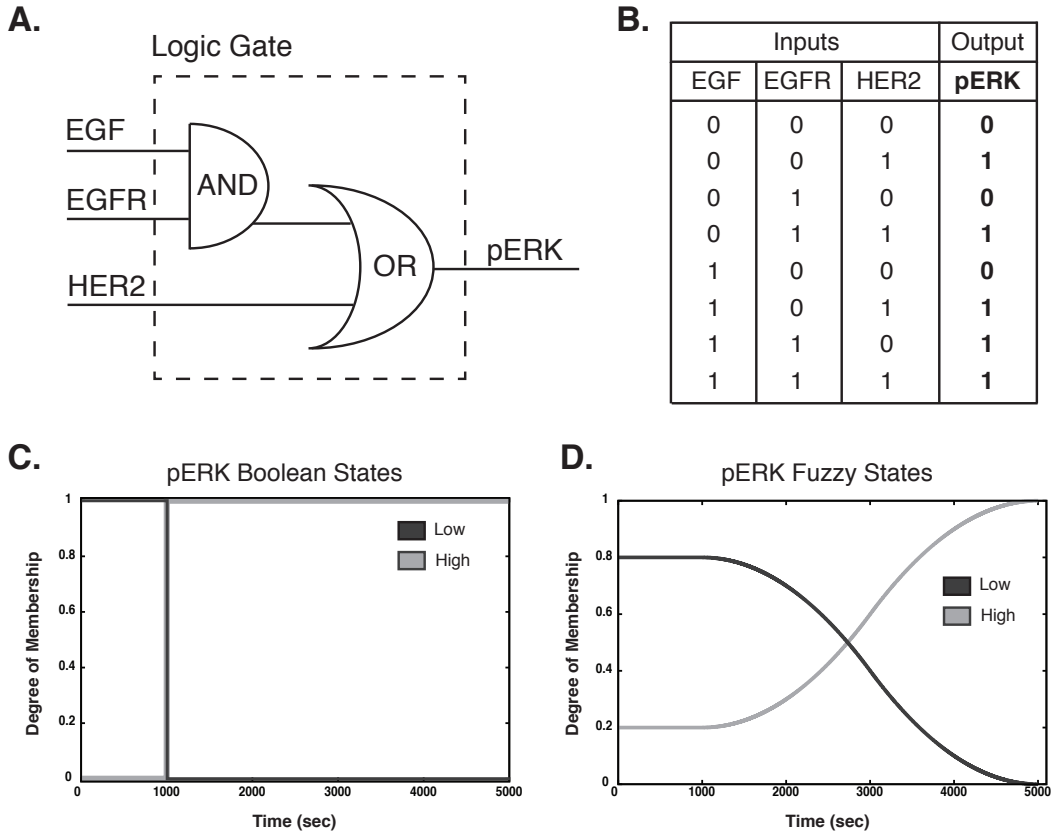


Figure 1.2: Schematic of a logical model framework. **A.** Simple logical model example based on EGFR and HER2 signaling. **B.** Boolean network truth table of the network in A. A value of zero denotes no expression and one denotes high expression, with pERK expression as the output. **C., D.** Boolean and fuzzy logic states of pERK, respectively. In the boolean model pERK can either be 1 or 0, while fuzzy logic allows for members to be in multiple groups.

and the difference in outputs from using boolean states vs fuzzy states.

Logic based models are important to cancer research, because they are typically simpler to solve than mechanistic models and less *a priori* knowledge is required. In the earliest known logical based biological model, Kauffman used discrete logic to model gene regulation [131]. In 2000, Huang and Ingber were

one of the first to develop a logic-based model of a cell-signaling network. The model explored different fates (proliferation, differentiation, apoptosis) of individual cells due to external stimuli and specific molecular cues [112]. Due to the large scale of cancer networks, many logical models of biological networks have been developed. A Boolean model, containing 94 nodes and 123 interactions, of T cell receptor signaling predicted unexpected signaling events that were experimentally validated [207]. Using a Boolean logic model of EGFR signaling, qualitative model predictions were compared to high-throughput data from human hepatocytes and liver cancer cells (HepG2) [210]. The use of logical models may also be able to give some insight into medical applications. Boolean models portraying the early response of liver cells to cytokines and small molecule inhibitors were developed by training against primary human hepatocytes and four liver cancer cell lines [205, 206]. These Boolean models, in combination with high-throughput data, predicted distinct models for each cell type with models clustering into normal and diseased sets. Heiser and coworkers utilized a Pathway Logic model to determine EGFR-MAPK signaling in 30 breast cancer lines [106]. The model identified Pak1 as a key node in regulating the MAPK cascade when over-expressed. Through experimental validation they determined that Pak1 over-expressing luminal breast cancer cell lines have increased sensitivity to MEK inhibition. Zhang *et al.* developed a Boolean model of T cell large granular lymphocyte (T-LGL) leukemia to understand signaling components leading to survival of cytotoxic T lymphocytes [276]. The model predicted that apoptosis in T-LGL leukemia could be induced by inhibiting PDGF signaling and that Sphingosine kinase 1 and NF- $\kappa$ B were both essential for survival of cytotoxic T lymphocytes. Using fuzzy logic can be an improvement of boolean models by allowing for intermediate states of activity, instead

of assuming genes as on or off. Aldridge *et al.* modeled cell signaling of TNF, EGF, and insulin receptors in human colon carcinoma cells using fuzzy logic [6]. The model predicted a pro-survival relationship between MK2 and ERK pathways. Logical models can be extremely useful in cases where mechanistic knowledge of the system is incomplete.

### 1.3 Current Approach: Multiscale Models

Cancer is a multiscale disease. As mentioned previously, holistic understanding at the genetic, intracellular, tissue, extracellular (tumor environment), and physiological level is required in order to develop successful future therapeutics. The next step from *in silico* intracellular signaling network models is multiscale models that dynamically recapitulate tumor cell migration (metastasis), angiogenesis, and other microenvironment effects like cell-cell interactions and/or nutrient delivery. Multiscale mathematical angiogenesis models (reviewed in [196]) were developed as early as the 1970s. Now, there is a vast array of literature for modeling multiscale systems using different methods. Multiscale models [59] are generally either continuous (employing partial differential equations), discrete (employing stochastic methods), or hybrid models. Continuum models [233, 170] are advantageous for describing an entire range of spatial and temporal properties, but often result in a population-averaged view of the modeled tumor. Discrete methods [36, 102] are better suited for revealing the emergent properties of individual cell decisions, but these methods tend to be less scalable [35]. The most prevalent hybrid method is agent based modeling (ABM) in which discrete autonomous “agents” (which exist in different states) act within a spatially and temporally continuous environment. A set of rules determines

how the continuous environment influences the agents, and/or vice versa.

Multiscale ABM models [132] can follow a top-down or bottom-up approach and may (bottom-up) or may not (top-down) be coupled to intracellular signaling dynamics. Top-down approaches employ coarse-grained empirical rules to describe global system characteristics, and are easy to implement with software packages like NetLogo [223] or CompuCell [9]. Meanwhile bottom-up approaches are becoming more popular for modeling biological complexity, using signaling networks to guide the action of agents [35]. Avascular cancer growth was modeled by Ferreira *et al.* using nutrient reaction-diffusion, cell proliferation and death, and cell motility; the model qualitatively captured commonly observed morphologies for primary tumors [73]. In 2005, Jiang *et al.* described another model for avascular multicellular tumors, which employed a Boolean network at the subcellular level, a lattice Monte Carlo model for proliferation and adhesion at the cellular level, and reaction-diffusion dynamics for extracellular chemicals concentrations [123]. CancerSim is an agent based simulation developed by Abbott *et al.* that recapitulates the “Hallmarks of Cancer” put forth by Hanahan and Weinberg [1]. Implemented in CancerSim are cells that can develop very crude and simplified “mutations” (characteristics), such as “evade apoptosis” or “ignore growth inhibition”. The simulation typically results in a heterogeneous cell population and predicts that when mutation rates are low, certain pathways will dominate [1]. In 2009, Wang *et al.* expanded upon their earlier work to develop a 3D model of non-small-cell lung cancer that also incorporated previously omitted TGF $\beta$ , and showed that targeted monotherapy could be ineffective [259]. Perfahl *et al.* reported a bottom-up 3D lattice-based model of vascular tumor growth that incorporated subcellular signaling mechanisms and stochastic elements like endothelial tip cell emergence [189].

Overall, the use of multiscale modeling may be a promising approach for target discovery due to the additional considerations of metastasis, angiogenesis, and cell-cell interactions.

## 1.4 Using Signal Transduction Models to Identify Drug Therapies

The use of computational models of cancer networks to discover new drug targets, particularly in resistant cancers, and to allow for personalized treatment are relatively new ideas. Often, primary targets for cancer types are known, but crosstalk and feedback of other signaling pathways can lead to resistance even in the presence of inhibitors [133]. In particular, one receptor system which has been extensively modeled is that of the epidermal growth factor receptor (EGFR), reviewed in [265]. EGFR is a receptor that is overexpressed in many human tumors including breast, lung, head and neck, colorectal, and more [209]. Other ErbB family members have also been studied [270]. Some progress has recently been made in using computational models to discover novel targets in cancers where ErbB signaling is important. For example, Schoeberl *et al.* developed MM-121, a human monoclonal antibody against ErbB3, after revealing through sensitivity analysis that ErbB3 was a key node in their computational model of the ErbB signaling network [215]. Currently, many ErbB receptor inhibitors are used as treatments in several cancers, although resistance is an issue [116]. Models have been developed to find new targets in resistant cancers, including cancers resistant to trastuzumab [70, 208]. Faratian *et al.* developed a kinetic model which included AKT/MAPK crosstalk, PTEN, HER2/HER3 dimer-

ization and inhibition, and receptor tyrosine kinase (RTK) inhibitor binding [70]. The model hypothesized that PTEN expression levels predict cell sensitivity to RTK inhibitors and was experimentally confirmed using primary breast cancer samples. Sahin *et al.* developed a Boolean logic model to find novel targets for trastuzumab resistant breast cancer [208]. The model, which combined ErbB signaling with G1/S transition of the cell cycle, identified c-MYC as a potential new target.

Computational models can also be utilized to determine combination treatments for cancer and possibly even preferred treatment regimens. Recently, Kirouac *et al.* developed a multiscale systems model of HER2 positive breast cancer to predict combination therapies [137]. Signal transduction events were modeled using a quantitative logic framework, while tumor growth kinetics and feedback regulation were modeled using an ODE framework. Model predictions in combination with experiments in mice, showed dual inhibition of HER3 and HER2 as a treatment for HER2 positive breast cancer. Additionally, a signal transduction model of EGFR in colon cancer cells predicted dual inhibition of MEK and EGFR as a treatment [138]. Decreased tumor growth due to this dual inhibition was experimentally confirmed in a xenograft tumor model of KRAS-mutant colon cancer. A mass action kinetic model of insulin-like growth factor (IGF-1) signaling in breast cancer cells predicted optimal drug combinations [117]. Computational modeling may also be useful in determining drug regimens. A recent study by Lee *et al.* predicted that pretreatment with an EGFR inhibitor sensitizes a subset of triple-negative breast cancer cells to DNA-damaging chemotherapy [145]. Taken together computational models of cancer networks can be used to discover new drug targets, particularly in resistant cancers, allow for personalized treatment, and to determine combination treat-

ments and drug regimens.

## 1.5 Conclusion

In this chapter we outlined the current status of modeling techniques in cancer networks. The choice of method depends on the system, data available, and goal of the analysis. ODE kinetic models allow for the most detailed mechanistic system analysis, but require extensive prior knowledge of network structure. In cases where complete network structure is unknown this may not be the best option. Logic based models are typically simpler than ODE models and require less *a priori* knowledge. These models can be useful in cases where mechanistic knowledge of the system is incomplete. In addition to logic and kinetic based models, multiscale models are necessary to recapitulate the multiple length and time scales involved in cancer initiation, invasion and metastasis. Multiscale models can be either continuous (partial differential equations), discrete (stochastic) or hybrid models. The use of multiscale modeling may be a promising approach for target discovery due to the additional considerations of metastasis, angiogenesis, and cell-cell interactions. Studies have shown that computational models of cancer networks can be used to discover new drug targets, particularly in resistant cancers, allow for personalized treatment, and to determine combination treatments and drug regimens. Taken together, we expect computational modeling of cancer networks to become increasingly important in discovering advanced treatment options for patients.

## CHAPTER 2

### MODELING AND ANALYSIS OF HORMONE AND MITOGENIC SIGNAL INTEGRATION IN PROSTATE CANCER

Prostate<sup>1</sup> cancer is the most common cancer in men and the second leading cause of cancer related death in the United States. Androgens, such as testosterone, are required for androgen dependent prostate cancer (ADPC) growth. Androgen ablation in combination with radiation or chemotherapy remains the primary non-surgical treatment for ADPC. However, androgen ablation typically fails to permanently arrest cancer progression, often resulting in castration resistant prostate cancer (CRPC). CRPC is closely related to metastasis and decreased survival. In this study, we developed and analyzed a population of mathematical models describing growth factor and hormone signal integration in androgen dependent, intermediate and resistant prostate cancer cells. The model describes the integration of two simultaneous extracellular signaling inputs, androgen and mitogenic growth factors. Model parameters were identified from 43 studies in androgen dependent and castration resistant LNCaP cell lines. The model was validated by comparing simulations with an additional 29 data sets from LNCaP cell lines that were not used during training. Additionally, data from four drug trials was also used to evaluate the models performance. Sensitivity and robustness analysis, conducted over the population of prostate signaling models, suggested that simultaneously targeting the PI3K and MAPK pathways in addition to anti-androgen therapies could be an effective treatment for CRPC. We tested this hypothesis in both ADPC LNCaP cell lines and LNCaP derived CRPC C4-2 cells using three inhibitors: the androgen

---

<sup>1</sup>Adapted with permission from: Rogers K, Wayman J, Tasseff R, Gee C, DeLisa M, Varner J. Modeling and Analysis of Hormone and Mitogenic Signal Integration in Prostate Cancer, (in prep).

receptor inhibitor MDV3100 (enzalutamide), the Raf kinase inhibitor sorafenib, and the PI3K inhibitor LY294002. Consistent with model predictions, cell viability decreased at 72 hrs in the dual and triple inhibition cases in both the LNCaP and C4-2 cell lines.

## 2.1 Introduction

Prostate cancer (PCa) is the most commonly diagnosed cancer and the second leading cause of cancer-related death in men in the United States [221]. Initially, PCa cells depend upon the activation of cytosolic androgen receptors (AR) by androgen hormones, such as testosterone, for survival and growth. Androgen ablation in combination with radiation or chemotherapy remains the primary non-surgical treatment for androgen dependent prostate cancer (ADPC) [113]. However, androgen ablation typically fails to permanently arrest cancer progression as malfunctioning cells eventually lose androgen sensitivity and proliferate without hormone. The loss of androgen sensitivity results in castration resistant prostate cancer (CRPC), a phenotype closely linked with metastasis and greatly reduced survival [99]. Currently, there are six approved treatments that demonstrate a survival advantage in patients with metastatic CRPC, each of these target diverse aspects of the disease [211]. The taxane family members docetaxel and cabazitaxel interact with microtubule stability [240, 57], while abiraterone [211] or enzalutamide [213] interfere with androgen signaling by blocking androgen formation or nuclear translocation, respectively. Other approved treatments are non-specific to PCa. For example, general treatments such as sipuleucel-T, a first generation cancer vaccine [128], and radium-223, an alpha emitter which targets bone metastasis [186], are both approved to treat CRPC.

Unfortunately, regardless of the therapeutic approach, the survival advantage of these treatments is typically only a few months. Thus, understanding the molecular basis of the loss of androgen sensitivity in CRPC could be an important step for the development of the next generation of therapies with a prolonged survival advantage.

Androgen-induced proliferation and survival depends upon many coordinated signal transduction and gene expression events. Androgen Receptor (AR) is part of the nuclear hormone receptor superfamily, which includes other important cancer targets such as progesterone receptor (PR) and estrogen receptor (ER) in breast cancer [11]. Nuclear hormone receptors act as ligand dependent transcription factors interacting with specific DNA sequences of target genes as either monomers, heterodimers, or homodimers; AR, PR, and ER act as homodimers. In the case of AR these specific DNA sequences are known as androgen response elements (ARE) [167]. In the absence of androgen, AR is predominately found in the cytoplasm bound to heat shock proteins (HSP) [195]. Androgen, either testosterone or testosterone metabolites such as  $5\alpha$ -dihydrotestosterone (DHT), enter prostate cells and interact with the cytosolic androgen receptor (AR). The interaction of DHT with AR promotes the dissociation of AR from chaperones such as HSP [194] and its subsequent dimerization, phosphorylation and translocation to the nucleus (reviewed by Brinkmann *et al.* [24]). Activated nuclear AR drives a gene expression program broadly referred to as androgen action, that promotes both proliferation and survival. In addition to many genes including itself, activated nuclear AR promotes the expression and secretion of prostate specific antigen (PSA), arguably the best known PCa biomarker [72]. PSA is commonly used as a prostate cancer indicator, although its prognostic ability is controversial [12, 109, 175]. In CRPC, AR sig-

nals in the absence of androgens. Androgen dependent (AD) prostate cells can become castration resistant (CR) through several possible mechanisms, including constitutively amplified AR expression and altered AR sensitivity to testosterone or other non-androgenic molecules [72]. In this study, we focused on the aberrant activation of AR by kinase signaling cascades, sometimes called the outlaw pathway. Outlaw pathway activation is driven by over-activated receptor tyrosine kinases (RTKs), a common pathology in many cancer types including PCa [224, 49]. RTKs stimulate downstream kinases, including the AKT and mitogen-activated protein kinase (MAPK) pathways, which promote AR phosphorylation and dimerization in the absence of an androgen signal [49, 271]. Interestingly, among the few genes activated AR represses is cellular prostatic acid phosphatase (cPAcP), itself a key regulatory of RTK activation [253]. Thus, in CRPC the androgen program is initiated without the corresponding extracellular hormone cue, potentially from crosstalk between growth factor and hormone receptor pathways.

In this study, we developed a mathematical model of growth factor and hormone signal integration in androgen dependent, intermediate and resistant prostate cancer cells. We used this model to better understand which components and processes were differentially important in AD versus CR cells. The new model architecture was a significant advance over our previous prostate signaling model [241]. We added the regulated expression of ten additional proteins, including the cell cycle restriction point proteins cyclin D (and the differentially spliced variants cyclin D1a and cyclin D1b), cyclin E, cyclin-dependent kinase inhibitor 1A (p21Cip1), and cyclin-dependent kinase inhibitor 1B (p27Kip1). Also, we included the Rb/E2F pathway, expanded our description of the activation of the mammalian target of rapamycin (mTOR)

protein and its role in translation initiation, and included the regulation of AR action by cyclin D1a and E2F. However, this upgraded architecture, while increasing the biological scope of the model, also expanded the challenge of estimating the unknown model parameters. To estimate these parameters, we used multiobjective optimization in combination with dynamic and steady-state data sets generated in AD, intermediate and CR LNCaP cell lines. We identified a population of approximately  $N = 5000$  models (from well over a million candidate models) which described both AD and CR data sets using a single model structure. Furthermore, we tested the model using an additional 29 LNCaP data sets not used for model training, along with data from four clinical studies. We analyzed the model population using sensitivity and robustness analysis to uncover differentially important mechanisms in AD versus CR cell lines. In the presence of androgen, the sensitivity profile was similar between AD and CR cells. Components of the MAPK and PI3K pathways were sensitive, irrespective of the level of androgen dependence. Thus, the MAPK and PI3K pathways represented globally important targets. However, in the absence of androgen, there were 108 statistically significant shifts in species sensitivity between AD and CR cells. In CR cells, HER2 activation of the MAPK and PI3K pathways was significantly more important, as was AR activation through the MAPK pathway. On the other hand, components of the translation and transcription infrastructure were differentially more important in AD cells in the absence of androgen. Taken together, our analysis suggested that independently targeting the PI3K or MAPK pathways in combination with anti-androgen therapies could perhaps be an effective treatment strategy for CRPC. We tested this hypothesis in both ADPC LNCaP cell lines and LNCaP derived CRPC C4-2 cells using three inhibitors: the androgen receptor inhibitor MDV3100 (enzalutamide), the Raf

kinase inhibitor sorafenib, and the PI3K inhibitor LY294002. Consistent with model predictions, cell viability decreased at 72 hrs in the dual and triple inhibition cases for both LNCaP and C4-2 cell lines.

## 2.2 Results

### 2.2.1 Estimating an ensemble of prostate signaling models.

We modeled the integration of growth factor, cell cycle and hormone signaling pathways in AD and CR LNCaP cells (Fig. 2.1). The signaling architecture was curated from over 80 primary literature sources in combination with biological databases. The model equations were formulated as a system of ordinary differential equations (ODEs), where biochemical reaction rates were modeled using mass action kinetics. ODEs and mass action kinetics are common modeling tools [260], however, ODEs have the disadvantage of requiring estimates for unknown model parameters. Many techniques have been developed to estimate ODE model parameters, often from noisy and sparse experimental data [173]. Typically these identification problems are underdetermined, hence no unique parameter values can be estimated [255]. Thus, instead of estimating a single yet highly uncertain parameter set, we estimated an ensemble of possible parameter sets using the Pareto Optimal Ensemble Techniques (POETs) algorithm [227]. POETs uses a combination of simulated annealing and local optimization techniques coupled with Pareto optimality-based ranking to simultaneously optimize multiple objective functions. Starting from an initial best fit set, we estimated the unknown model parameters using 43 *in vitro* data sets

taken from six AD, intermediate and CR LNCaP cell lines (Table A.1). Each of the training data sets was a separate objective in the multiobjective optimization calculation. The training data were steady-state or dynamic immunoblots from which we extracted relative species abundance using their optical density profiles. POETs sampled generated over a million possible parameter sets, from which we selected  $N = 5000$  sets for further analysis. The coefficient of variation (CV) of the population of model parameters spanned 0.59 - 5.8, with 33% of the parameters having a CV of less than one (Fig. A.1). As a control, we also performed simulations for  $R = 100$  random parameter sets to compare against the parameters estimated by POETs.

The population of signaling models recapitulated training data in both AD and CR cell lines with only two experimentally mandated parameter changes (Fig. 2.2 and Fig. 2.3). Data from the LNCaP clones C-33 (dependent), C-51 (intermediate), and C-81 (resistant) [154, 118, 111] along with the CR LNCaP cell lines LNCaP-Rf [178], LNCaP-AI [40] and LNAI [88] were used for model identification. To simulate the effective difference between LNCaP cell lines, the parameter controlling the maximum rate of PAcP gene expression was scaled by 0.1 and 0.5, respectively, for the C-81 and C-51 cell-lines compared to C-33. This modification was based upon steady-state PAcP data from the three LNCaP clones [147]. Similarly, the expression of p16INK4 was adjusted in accordance with the study of Lu *et al.* [163]. These two parameters were the only adjustable parameter differences between AD and CR cells. To simulate an increased mTOR activation in the presence of a DHT stimulus, we added a first order activation term for mTOR activation with a DHT stimulus. Androgens have been shown to increase expression of proteins involved in cellular metabolism, which may lead to an increase in mTOR activation [268]. The model fit 36 of the

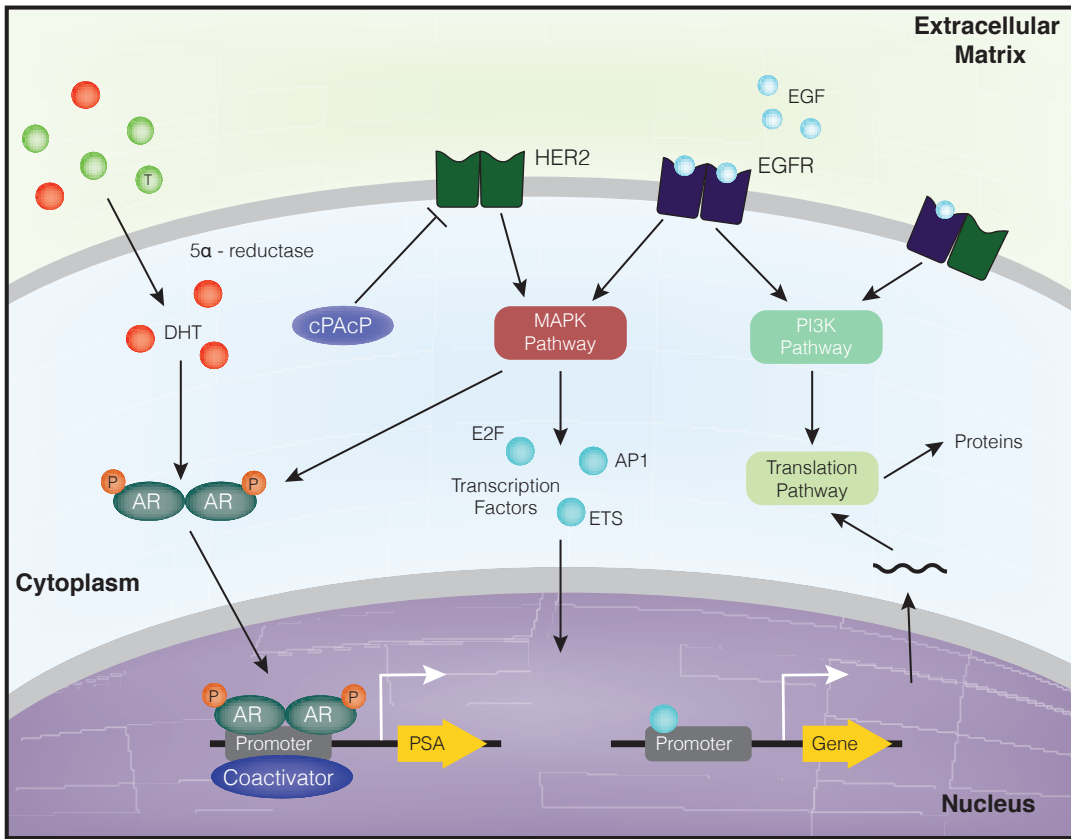


Figure 2.1: Schematic overview of the prostate signaling network. The model describes hormone and growth factor induced expression of several proteins, including PSA. In the absence of outside hormones/growth factors, overactive HER2 can stimulate the MAPK and AKT pathways. AR can be activated directly by the MAPK pathway.

43 training objectives (Fig. 2.2A). Conversely, only 10 of the 43 training objectives were captured with the random parameter control (Fig. 2.2B). The model captured the crosstalk between RTK activation and androgen action (Fig. 2.3). The model described DHT-induced PSA expression in both C-33 (Fig. 2.3A) and C-81 (Fig. 2.3B) cells. Interestingly, simulations with the HER2 inhibitor AG879 also recapitulated decreased PSA expression in C-81 cells in the absence of androgen stimulation (Fig. 2.3C). AR action decreased the PAcP mRNA message,

presumably leading to increased HER2 activity (Fig. 2.3D). The model also recapitulated the integration of androgen action with AR expression, G1/S cell cycle protein expression and AKT phosphorylation. For example, the model captured AR-induced AR expression following a DHT stimulus (Fig. 2.3H). Conversely, the transcription factor E2F inhibits AR transcription in LNCaP cells (Fig. 2.3I). Other cell cycle proteins were also integrated with androgen action. For example, the cyclin D1 abundance increased in CR compared to AD cells in the absence of androgen (Fig. 2.3E), while DHT induced p21Cip1 expression in C-33 cells (Fig. 2.3F). The level of phosphorylated AKT also increased in higher passage number cells (Fig. 2.3G). Taken together, the estimated model population recapitulated signaling events in both AD and CR LNCaP cell lines, above a random control, for a wide range of data at both the protein and transcript level.

### 2.2.2 Validation simulations revealed missing network structure.

The model was validated against 29 *in vitro* and four *in vivo* clinical studies (Table A.2). For 15 of the 29 cases, greater than 40% of the ensemble was qualitatively consistent with the experimental data (Fig. 2.2C). However, for the random parameter control, only 7 of the 29 cases were satisfied (Fig. 2.2D). We correctly predicted positive feedback between HER2 auto-activation and androgen action (Fig. 2.4A and Fig. 2.4B). We also captured the dose-dependence of AR abundance on DHT (Fig. 2.4C). In addition to the cell line studies, we simulated the outcome of enzalutamide, lapatinib, and sorafenib clinical trials in

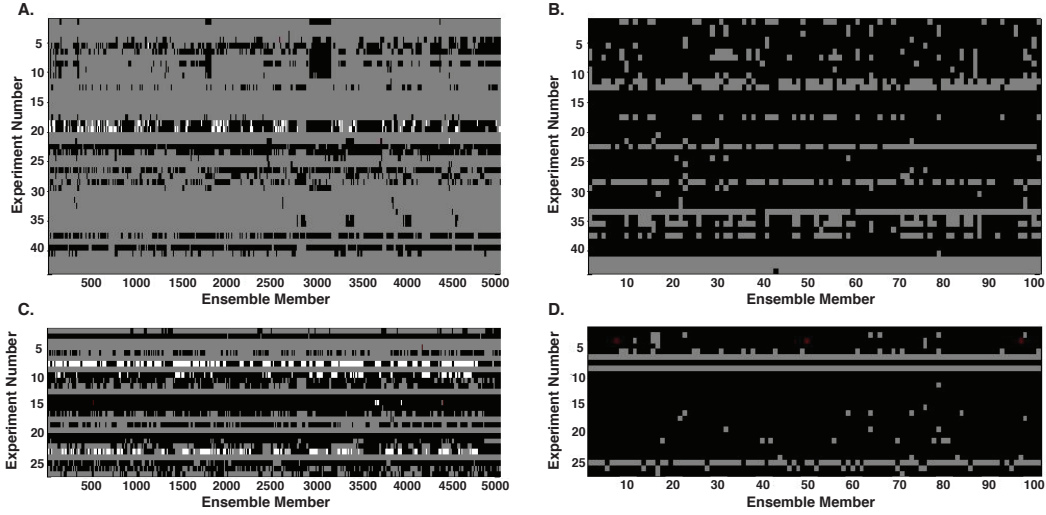


**Figure 2.2:** Simulation results versus experimental results for training and validation data. Experiment numbers 1 through 43 were used for training, while experiments 44 through 72 were validation. Gray means the ensemble member qualitatively fit experimental data in both models. White means the ensemble member only fit the data using the new model that included HER2 heterodimerization. Red means the ensemble member fit using only the old model. Black corresponds to an incorrect cellular response in both models. **A., C.** Training and validation results, respectively, for entire ensemble population using both the original model and an updated model including HER2 heterodimerization ( $N = 5000$ ). **B., D.** Simulation results for training and validation of a random set of 100 members using both models.

AD and CRPC patients. The trial end points were the reduction in PSA expression relative to an untreated baseline. Enzalutamide acts on AR by inhibiting its nuclear translocation, DNA binding, and coactivator recruitment [213]. In the enzalutamide trial, 54% of the patients that received the drug showed a PSA decline of  $\geq 50\%$  while 25% showed a decline  $\geq 90\%$ . We simulated enzalutamide exposure by reducing the rate constants governing activated AR binding to nuclear importer, cyclin E, and CDK6 to 1% of their initial values. Consistent with the trial, 62% of ensemble members showed a  $\geq 50\%$  decline

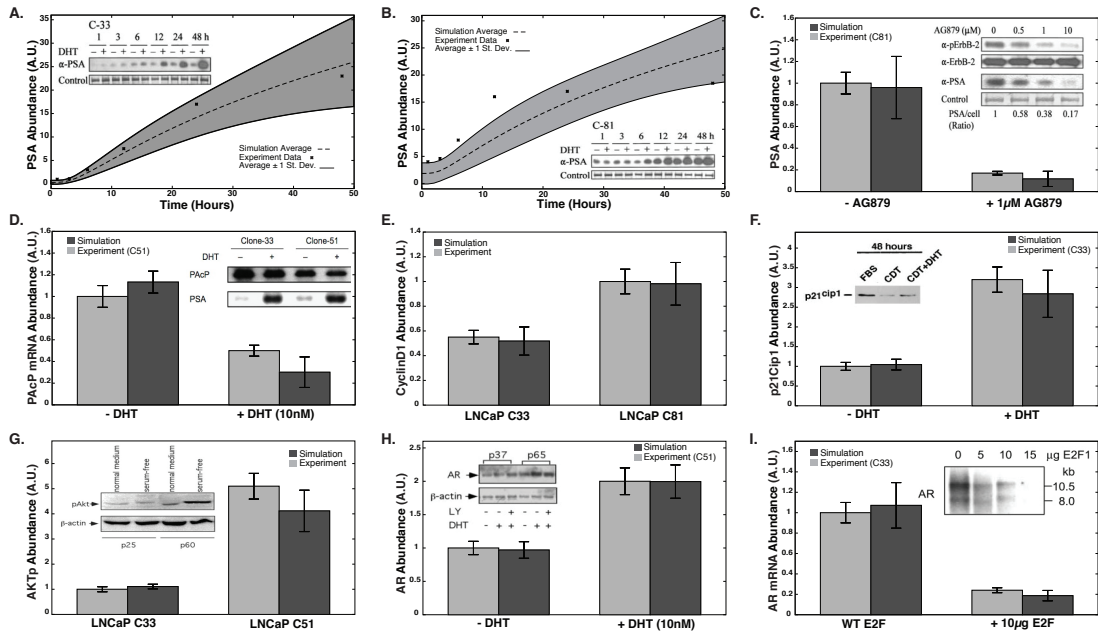


**Figure 2.3:** Ensemble performance against selected training objectives ( $N = 5000$ ). **A, B.** Time course data for PSA concentration due to a stimulus of 10 nM DHT in LNCaP C-33 cells and LNCaP C-81 cells, respectively (O2, O3). **C.** PSA levels in the presence and absence of a HER2 inhibitor (LNCaP C-81 cells, O7). **D.** PAcP mRNA levels at 72 hours in the presence and absence of DHT (LNCaP C-51 cells, O14). **E.** Steady-state cyclin D levels in LNCaP C-33 vs. C-81 (O17). **F.** p21Cip1 levels at 48 hrs in the presence and absence of DHT (LNCaP C-33, O25). **G.** Steady-state AKT phosphorylation levels in LNCaP C-33 vs. C-51 (O30). **H.** AR expression levels at 24 hours in the presence and absence of DHT (LNCaP C-51, O31). **I.** AR mRNA levels in the presence and absence of E2F over expression (LNCaP C-33, O34). Error bars denote plus and minus one standard deviation above the mean.

in PSA abundance, while 14% showed a  $\geq$  90% decline (Fig. 2.4G). The second trial we simulated involved exposure of CRPC patients to sorafenib. Sorafenib is a kinase inhibitor with activity against Raf, vascular endothelial growth factor receptor (VEGFR), platelet-derived growth factor receptor (PDGFR), c-kit and c-Ret [52]. We considered only the effects of sorafenib on the protein kinase Raf, as VEGFR, PDGFR, c-kit and c-Ret were not included in the model. None of the 22 patients in the sorafenib study showed a PSA decline of  $> 50\%$ . However, our simulations showed that approximately 55% of the ensemble members had a PSA decline of  $\geq 50\%$ . The last drug we considered was lapatinib, an inhibitor of epidermal growth factor receptor (EGFR) and HER2 tyrosine kinase activity [157]. Two lapatinib drug trials were considered: one in which patients had CRPC and one in which patients had biochemically relapsed ADPC [263, 157]. In the CRPC lapatinib drug trial, two of the 21 enrolled patients had a PSA response  $\geq 47\%$  [263]. For the CRPC case, our model showed 26.5% of ensemble members with a PSA response  $\geq 47\%$ . Of the 35 patients enrolled in the ADPC lapatinib study, no PSA decreases was observed [157]. In this case, our model showed 9.2% of ensemble members with a PSA response  $\geq 50\%$ . Although no response to lapatinib was seen in ADPC clinical trials, *in vitro* AD LNCaP experiments showed decreased PSA expression in response to lapatinib, most notably with the addition of DHT [161].

Validation and training failures suggested the original signaling architecture was missing critical components. Several of the failed training and validation simulations involved the response of the network to epidermal growth factor (EGF) stimulation. For example, Chen *et al.* showed that HER2 phosphorylation increased within five minutes following EGF stimulation of LNCaP-AI cells [40]. We predicted no connection between HER2 phosphorylation and

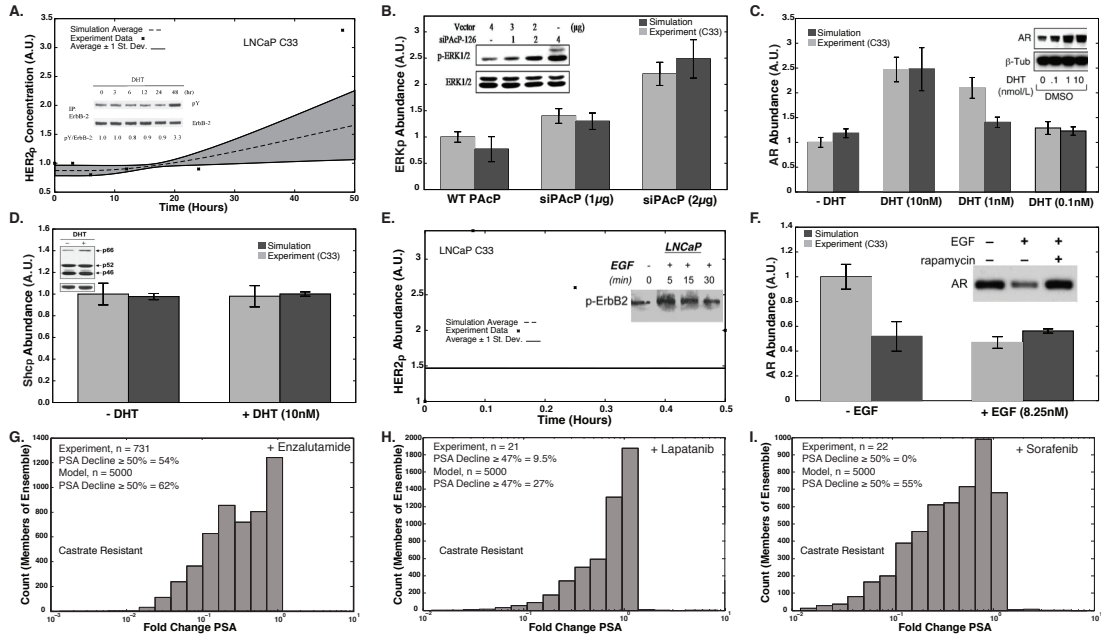


**Figure 2.4:** Blind model predictions for the ensemble ( $N = 5000$ ). The model ensembles predictive ability was assessed by comparing simulation versus experimental data not used for training. **A.** Time course data for HER2 phosphorylation due to a stimulus of 10 nM DHT (LNCaP C-33, P1). **B.** ERK phosphorylation levels in the presence and absence of a PAcP inhibitor (LNCaP C-33 cells, P3). **C.** AR expression levels at 24 hrs in varying levels of DHT (LNCaP C-33, P17). **D.** Shc phosphorylation levels at 24 hrs in the presence and absence of DHT (LNCaP C-33, P22). **E.** Time course data for HER2 phosphorylation due to a stimulus of 1.6 nM EGF (LNCaP C-33, P7). **F.** AR expression levels in varying levels of EGF (LNCaP C-33, P14). **G, H, I.** Fold change in PSA concentration due to drug stimulus: enzalutamide, lapatinib, and sorafenib. Error bars denote plus and minus one standard deviation above the mean.

EGF stimulation on this short timescale (Fig. 2.4E). Interestingly, we initially neglected the heterodimerization of HER2 with other ErbB family members in order to simplify the model. However, Chen *et al.* suggested that HER2-EGFR heterodimerization could be an important factor in EGF-driven activation of HER2 [40]. We tested this hypothesis by developing a new model that included HER2 and EGFR heterodimerization. We set the rate constants governing the assembly of HER2/EGFR heterodimers equal to EGFR homodimer assembly; all other parameters were unchanged. This was a reasonable first approximation, as the affinity of HER2/EGFR heterodimerization and EGFR homodimerization is thought to be similar [107]. With the inclusion of HER2-EGFR heterodimerization, we qualitatively fit the EGF-induced HER2 activation case and improved our training for experiments that involved an EGF stimulus, e.g., cyclin D mRNA and protein abundance following an EGF stimulus in C-33 cells (Fig. 2.2A and C, white pixels and Fig. A.2).

### **2.2.3 Sensitivity analysis identified differentially important features of the prostate architecture.**

We used sensitivity analysis to identify important signaling components in AD versus CR cells (Fig. 2.5). We calculated first order steady-state sensitivity coefficients under different stimuli for 500 parameter sets selected from the ensemble. Signaling components were rank-ordered based upon analysis of their sensitivity coefficient values. In the presence of DHT, the sensitivity profile was similar for AD versus CR cells, with only a few differences (Fig. 2.5B). The top 2% of sensitive species, regardless of androgen dependence, involved components

from the MAPK and PI3K pathways. In particular, activated Ras, Raf, phosphorylated MEK, as well as PIP3 localized AKT, phosphorylated AKT, and PI3K were sensitive in both AD and CR cells. Species involving PAcP and p16INK4 were more sensitive in AD cells, which was expected since the expression of these two proteins were the only parameters changed between AD and CR cells. Other species such as E2F, cyclin E, and DHT-activated AR were also more sensitive in AD cells. On the other hand, HER2-Grb2-Gab activation of PI3K and AKT inhibition of Raf were more sensitive in CR cells.

The importance of signaling components varied with androgen dependence in the absence of DHT (Fig. 2.5A). There were 609 statistically significant shifts in species sensitivity (318 more and 291 less sensitive) between CR and AD cells in a non-androgen environment. However, only 108 of these shifts were greater than one standard deviation above the mean. In CR cells, HER2 activation of ERK and PI3K was more sensitive, as was AR activation through the MAPK pathway. This was expected, as outlaw pathway activity was elevated in castration resistant cells. Species in the MAPK pathway were in general more sensitive in CR cells (128 out of 140 significant), with all forms of sPAcP more robust in CR cells. On the other hand, infrastructure pathways encoding transcription and translation were more sensitive in AD cells. PSA and cyclin D1b (mRNA and mRNA complexes) were the only species involved in translation that were more robust in AD cells (14 out of 116). The transcription factor, E2F was more fragile in AD cells, while the transcription factors ETS and AP1 were more robust. ETS and AP1 are activated by phosphorylated ERK, and ETS is also activated by active PKC [266, 156]. E2F is deactivated through binding to Rb, which is deactivated by cyclin D1 and CDK phosphorylation [142]. The model also included AP1 suppression of AR transcriptional activity (more sensitive in CR)

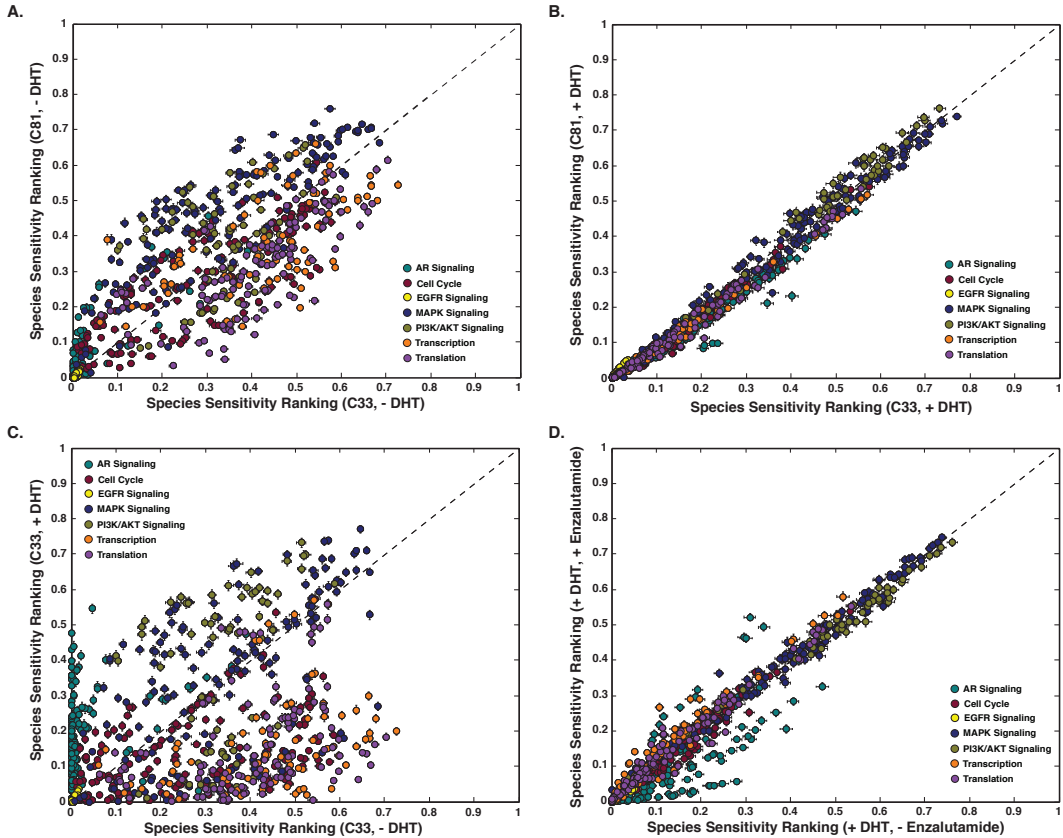


Figure 2.5: Sensitivity analysis of a population of prostate models ( $N = 500$ ). Species with a low sensitivity are considered robust, while species with a high sensitivity ranking are considered fragile. **A, B.** Sensitivity ranking of network species in AD versus CR cells in the absence (presence) of DHT. **C.** Sensitivity ranking of network species in AD cells in the absence and presence of DHT. **D.** Sensitivity ranking of network species in CR cells in the presence and absence of enzalutamide with a DHT stimulus. Error bars denote standard error with  $N = 500$ .

[212], as well as inhibition of transcription of the AR gene by E2F (more sensitive in AD) [56]. Species in the PI3K pathway that were more fragile in AD cells included Rheb and TOR complexes. Interestingly, these species were included as the last step in the PI3K pathway prior to translation, with the phosphorylation of 4E-BP1 by TOR being considered the beginning of translation in this model. This again indicates that in the absence of DHT general translation is more fragile in AD cells.

There was a large shift in sensitive species between an androgen and a non-androgen environment in both AD and CR cell lines (Fig. 2.5C and Fig. A.3). Of the 664 statistically significant shifts in AD cells, 288 were more sensitive between androgen versus non-androgen environments. However, only 119 shifts were larger than one standard deviation above the mean. Unsurprisingly, AR activation through DHT binding, with and without coactivators, in a DHT environment was more sensitive, as was AR inhibition of PAcP transcription (repressed by AR in the model). Species further upstream, such as HER2 activation of the MAPK and PI3K/AKT pathways, were also more sensitive in a DHT environment. Cell cycle species that were more fragile in the presence of DHT, included complexes involving p21Cip1 and CDC25A. In a non-androgen environment, basal transcription (68 out of 72) and translation (114 out of 120) were more fragile. Other fragile species in the absence of DHT included Rb, E2F, Sam68, cyclin D1a complexes, phosphatases in the MAPK pathway, Rheb complexes, and TOR complexes.

We also considered the sensitivity of CR cells following the application of the AR inhibitor enzalutamide in the presence of DHT (Fig. 2.5D). Species which were more sensitive in an androgen environment with enzalutamide included

cytosolic AR, cPAcP, and p21Cip1. As we would expect, AR species found in the nucleus and/or bound to coactivators, were more robust in the presence of enzalutamide. The top two percent of sensitive species with and without enzalutamide were conserved. In a CR cell, enzalutamide had no effect on the sensitivity of PI3K/AKT species as well as many MAPK species (ERK, Raf, and MEK). Next, we looked at the effect of enzalutamide on a CR cell in both a non-androgen and DHT environment (Fig. A.3). More sensitive species in a non-androgen environment included dimerized HER2, ERK, and PAcP. Species which were more robust in the non-androgen environment included, AR activated by DHT, AKT, p70, and AR bound to HSP. The results of our sensitivity analysis indicated that instead of inhibiting solely the AR pathway (enzalutamide), a combination therapy targeting the PI3K or MAPK pathways in addition to AR may be more effective.

#### **2.2.4 Robustness analysis identified key regulators of prostate cancer.**

Robustness analysis was conducted for 80 proteins to quantify the effects of amplifying or knocking down key model components in both AD and CR cells using  $N = 500$  models. Gene expression parameters were altered by a factor 10, 0.5, and 0 for knock-in, knock-down, or knock-out perturbations, respectively. We calculated the effect of these perturbations on the expression of different protein markers, such as PSA, AR, and cyclin D. A knock-out of Raf, MEK or ERK showed an overall increase in cyclin D levels in CR cells (Fig. A.4). This was unexpected and we saw a similar increase in cyclin D due to the knock-in of

Raf, MEK or ERK. We found that individual models showed different response to a Raf knock-out, in both cyclin D and PSA abundance. We saw three distinct regions: (1) increased PSA expression, (2) increased cyclin D expression, and (3) decrease in both PSA and cyclin D expression. Of the 500 models, 126 models had increased PSA expression, and 62 models had increased cyclin D expression due to the knock-out of Raf (Fig. 2.6). We explored the flux vectors of the outlying parameter sets to understand the mechanistic effect of Raf knock-out on PSA and cyclin D. Outlying parameter sets in region 1 displayed high activation of PI3K through HER2 signaling as well as high association of AP1 with AR. AP1 is known to bind and suppress AR transcriptional activity in LNCaP cells [212]. Knocking out Raf lowered AP1 levels and, therefore, freed AR for increased transcription of PSA. Models in region 2 also had high activation of PI3K through HER2, as well as higher association of E2F with Rb and cyclin D1a with AR. Cyclin D levels in region 2 increased due to an increase in E2F levels caused by the Raf knock-out. Models in region 3 had high association of mTOR. Interestingly, the drug sorafenib, a multi-kinase inhibitor that has activity against Raf, showed no measurable PSA decline in prostate cancer patients in clinical trials [52]. The robustness analysis showed that network perturbation can result in unexpected responses due to heterogeneity in signal transduction and gene expression processes.

We also used robustness analysis to observe the effect of knocking out combinations of key species found in our sensitivity analysis. We calculated the effect of perturbation in CR cells on different protein markers for seven cases: (1) Raf knock-out, (2) PI3K knock-out, (3) AR knock-out, (4) Raf and PI3K knock-outs, (5) Raf and AR knock-outs, (6) PI3K and AR knock-outs, and (7) Raf, PI3K and AR knock-outs. Over the 500 ensemble member set, the overall decrease in

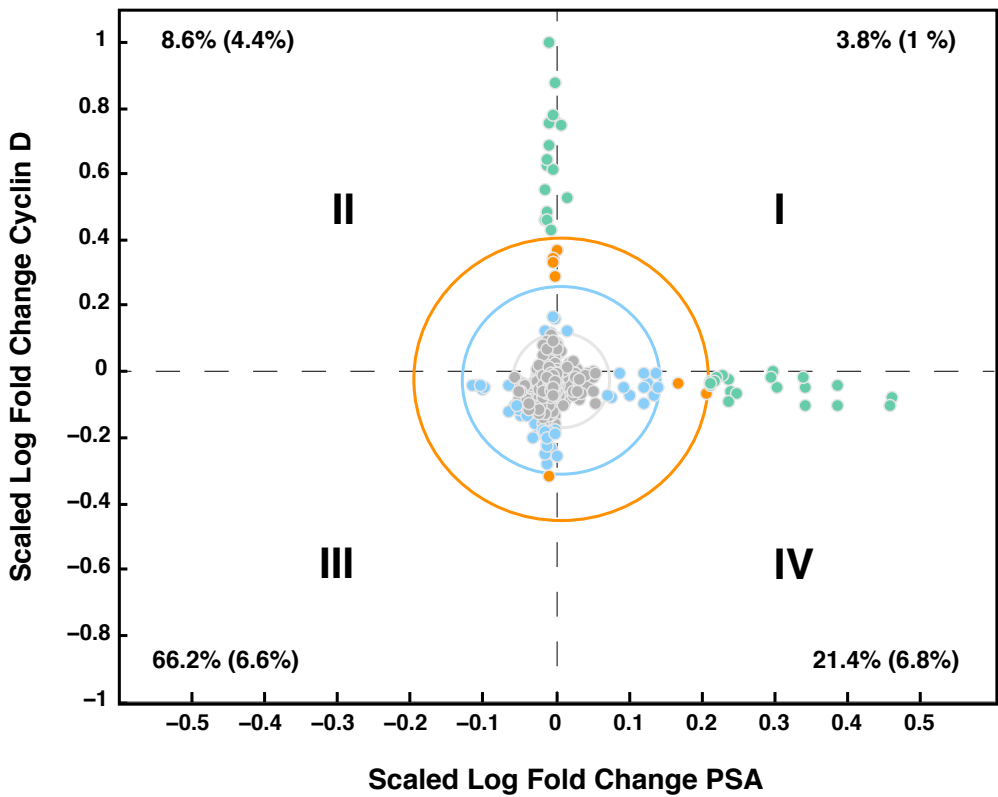


Figure 2.6: Robustness analysis of a population of CR prostate models with Raf knock-out ( $N = 500$ ). A scaled log fold change of greater than zero implies that the concentration of the protein increased with the knock-out of Raf, while a log fold change of less than zero indicates that the concentration of protein decreased. A log of fold change equal to 0, shows no response due to Raf knock-out. Three distinct regions emerge in Raf knock-out case: (1) PSA increases, (2) cyclin D concentration increases, and (3) PSA and cyclin D concentration decrease. The grey ellipse is centered at the mean values with an x-radius and y-radius of one standard deviation of the scaled log fold change of PSA values and cyclin D values, respectively. The blue ellipse denotes two standard deviations from the mean and the orange denotes three standard deviations from the mean. Values denote percentage of total parameter sets that fall in each quadrant, while values in parenthesis denote the percentage that fall at least one standard deviation from the mean.

PSA expression levels was greatest in all cases which included the knock-out of AR (Fig. 2.7A). The decreased expression of activated p70 was most prominent in the double PI3K/AR knock-out case and the triple Raf/PI3K/AR knock-out case (Fig. 2.7B). Although the change in expression level of cyclin D varied for individual ensemble members (increased and decreased), the median and mean behavior for all knock-out cases is approximately zero suggesting no change due to perturbation (Fig. 2.7C). Individual ensemble members do show a decline in cyclin D expression in cases involving PI3K in double and triple knock-outs and in these cases we also see fewer ensemble members that have an increased expression of cyclin D. Fig. 2.7D shows that in the PI3K knock-out case we see a complete inhibition of AKTp expression (a value of -1 is essentially zero expression due to knock-out). This is a trivial result in the model because AKTp only occurs through PIP3 recruitment to the membrane, and PIP3 is only activated by PI3K in the model. All other knock-out cases show a median response of no fold change in AKTp expression, but we do see a group of ensemble members that have an increased expression of AKTp in the RAF knock-out and RAF/AR knock-out cases. Overall, these results are consistent with our hypothesis that a combination therapy will be more effective.

## **2.2.5 Experimental results confirm the need for dual therapies in prostate cancer.**

Sensitivity and robustness analysis, conducted over a subpopulation of prostate signaling models, suggested that simultaneously targeting the PI3K and MAPK pathways in addition to anti-androgen therapies could be an effective treatment for CRPC. To test this hypothesis we used the well characterized ADPC cell line LNCaP as well a LNCaP derived CRPC cell line C4-2 [244]. Three inhibitors were used: the AR inhibitor MDV3100 (enzalutamide), the Raf kinase inhibitor sorafenib, and the PI3K inhibitor LY294002. In both cell lines, inhibition of either the AR or MAPK pathways promoted activation of the PI3K pathway, as seen by the increase in phosphorylated AKT (S473) (Fig. 2.8A). The addition of the PI3K inhibitor, LY294002, alone or in combination diminished PI3K activity (phosphorylated AKT (S473) in Fig. 2.8A). Interestingly, the inhibition of PI3K alone, increased AR expression in both LNCaP and C4-2 cell lines (Fig. 2.8A). Since, AR transcriptionally upregulates its own expression [86, 153], this may indicate increased AR activity. The ribosomal protein pS6 was completely inhibited only in the presence of the PI3K inhibitor LY294002. Expression of cleaved PARP (c-PARP), an indicator for apoptosis, was highest in the triple inhibition case for both LNCaP and C4-2 cell lines. We also saw an increase in c-PARP in the dual inhibition of RAF and PI3K in both cell lines and in the dual inhibition of PI3K and AR in C4-2 cells. Cell viability results show a large decrease in cell viability at 72 hrs in the dual inhibition cases as well as the triple inhibition case for both LNCaP and C4-2 cell lines (Fig. 2.8B). In both cell lines, MDV3100 ( $10 \mu\text{M}$ ), has only a modest effect on cell viability versus control (DMSO). Figure 2.8C shows cell viability of both cell lines in varying concentrations of inhibitors at 24

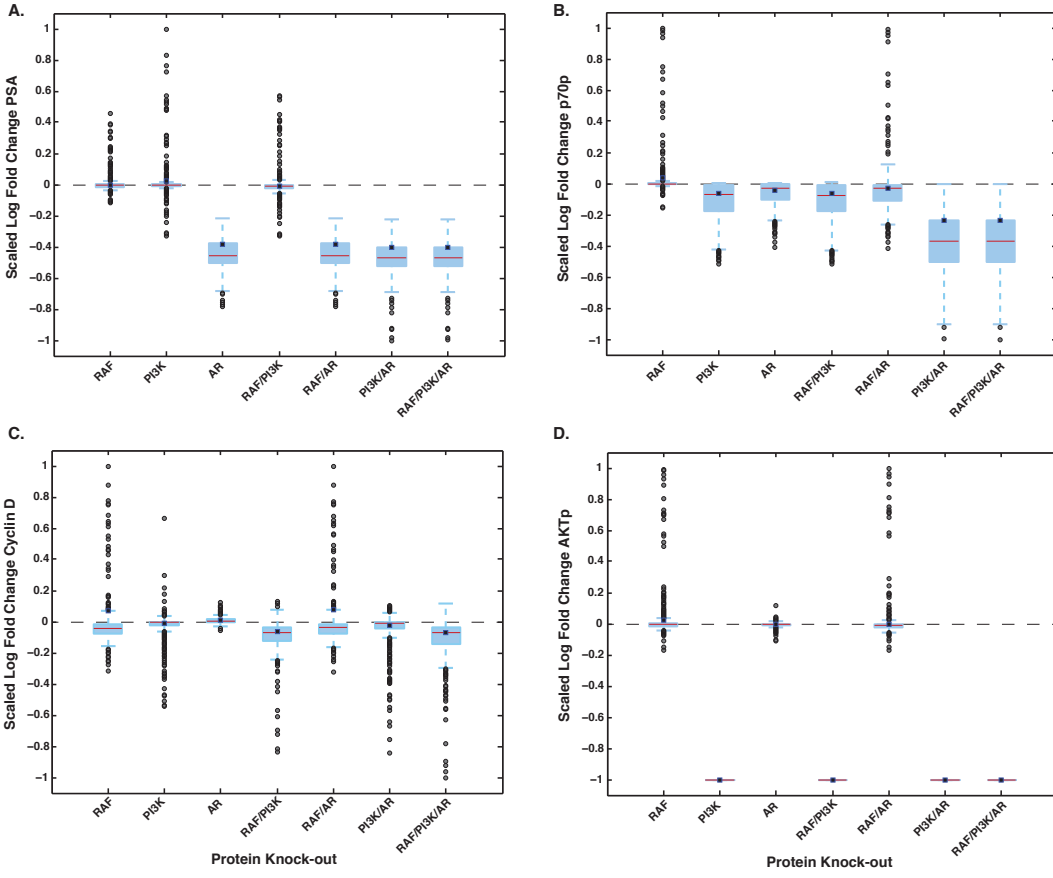


Figure 2.7: Robustness analysis of a population of CR prostate models with seven protein knock-out cases ( $N = 500$ ). A scaled log fold change of greater than zero implies that the concentration of the protein increased with the knock-out, while a scaled log fold change of less than zero indicates that the concentration of protein decreased. A scaled log fold change equal to 0, shows no response due to the knock-out. A., B., C., D. Log robustness of PSA, p70p, cyclin D, and AKTp versus protein knock-out. A CR LNCaP cell was assumed for all knock-out cases. The bottom and top of each box denotes 25th and 75th percentiles, while the red line indicates the median. The whiskers on the plot are plus and minus 1.5 the interquartile range (IQR) from the top and bottom values of the box, respectively. The grey dots denote outliers and the blue dots denote the mean.

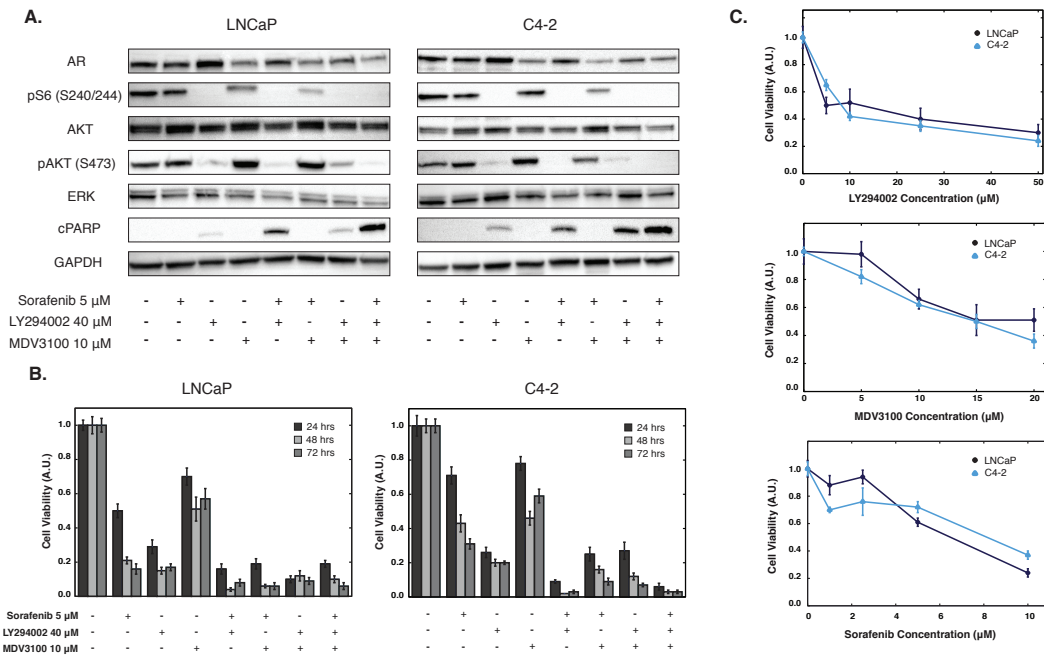


Figure 2.8: Experimental results for multiple drug combinations on two prostate cancer cell lines, LNCaP and C4-2. **A.** Western blot analysis of AR, pS6, AKT, pAKT, ERK and cleaved PARP in LNCaP and C4-2 cell lines treated for 24 hrs with DMSO (control), sorafenib (5  $\mu$ M), LY294002 (40  $\mu$ M), and MDV3100 (10  $\mu$ M) alone or in combination (at least 3 repeats). **B.** Cells (LNCaP and C4-2) were treated for 24, 48 and 72 hrs with sorafenib (5  $\mu$ M), LY294002 (40  $\mu$ M), and MDV3100 (10  $\mu$ M) and cell viability was measured using MTT Assay. Values were normalized to DMSO (control). **C.** Cell viability results for LNCaP and C4-2 cells at varying concentration of sorafenib, LY294002, and MDV3100 after 24 hrs of treatment. Values were normalized to DMSO (control). Error bars represent standard error (at least 3 repeats with triplicates performed in each experiment).

hrs. Taken together the experimental results suggest combination treatments are necessary in prostate cancer due to interactions between signaling pathways.

## 2.3 Discussion

In this study, we developed a population of mathematical models describing growth factor and hormone signal integration in androgen dependent, intermediate and resistant prostate cancer cells. These models described the regulation of androgen receptor expression and activation through androgen binding as well as a ligand-independent, MAPK-driven mechanism referred to as the outlaw pathway. An ensemble of model parameters was estimated using 43 steady-state and dynamic data sets taken from androgen dependent, intermediate and independent LNCaP cell lines using multiobjective optimization. Further, we tested the predictive power of the model by comparing model predictions against 33 novel data sets (including four *in vivo* drug studies) not used during model training. The model ensemble captured 84% of the training data and 52% of the validation data relative to 23% and 24% for a random control population. Interestingly, during the initial round of parameter estimation, we identified several potentially missing structural components not present in the original connectivity. One such component, EGF-induced HER2/EGFR heterodimerization, was added to the current generation model. Inclusion of this structural component significantly improved both training and validation performance using the same rate constants as the EGFR-homodimer case (no additional parameter fitting). We then analyzed the population of signaling models, using both sensitivity and robustness analysis, to identify the critical components controlling network performance in a variety of conditions.

In addition, three of the validation cases involved the effect of EGF on AR and AR-activated genes, i.e., PSA. Cai *et al.* showed decreased expression of endogenous AR as well as androgen-regulated PSA in AD LNCaP cells due to

an EGF stimulus [32]. Cinar *et al.* also showed decreased AR protein expression due to EGF, an effect reversed by the mTOR inhibitor, Rapamycin [46]. Model simulations show either the opposite trend or no effect due to EGF stimulus (Fig. 2.4F) [46]. These results suggest missing network structure. From additional literature searches, the inhibition of AR activation through EGF is still an open question, with many groups debating the biology involved, predominately in the PI3K/AKT pathway. Lin *et al.* found that in low passage number LNCaP cells (C-33), AKT negatively regulates AR by destabilizing it and marking it for ubiquitylation. In high passage number LNCaP (C-81), AKT levels are high which contribute to AR stability and less degradation [153]. Wen *et al.* showed that HER2 could induce AKT activation and LNCaP cell growth in the presence and absence of androgen [262]. Another study shows AKT phosphorylation of AR at S213 and S790 suppresses AR transactivation and AR-mediated apoptosis of LNCaP [152]. The study from Cai *et al.* showed the reduction in AR was not due to degradation or PI3K/AKT signaling, but instead was due to decreased AR mRNA levels [32]. They found that AR protein levels in CR cells were not affected by EGF. Others though have found that PSA expression, even in C-81 cells, is decreased by EGF [93]. In other prostate cell lines, EGF has been shown to increase AR transactivation [90, 193]. The MAPK pathway, which is downstream of EGFR, may also enhance AR responses to low levels of androgen [91, 261]. Due to the discrepancies in the literature, experiments should be performed before adding additional network connectivity to the model.

The population of PCa models was analyzed using sensitivity analysis to identify key signaling components and processes in both AD and CR cells. There was very little difference between sensitive and robust components in AD versus CR cells in the presence of androgen. MAPK and PI3K pathway

components were consistently ranked in the top 2% of sensitive species in the presence of androgen for both AD and CR cells. On the other hand, cell cycle species, such as cyclin D-CDK4/6 complexes bound to cell cycle inhibitors (p27Kip1, p21Cip1, p16INK4), were consistently robust. However, this profile changed considerably in the absence of androgen. The activation of PI3K and ERK by HER2 dimerization and autophosphorylation was significantly more important in CR versus AD cells. Interestingly, AR activation by ERK was also more sensitive in CR versus AD cells in the absence of androgen. Lastly, although AR-regulated transcriptional processes were equally sensitive between the cell types, general translational and transcriptional components were more robust in CR versus AD cells. This evidence supports the current theory that CR cells will still respond to androgen and, thus, AR is still an active target in therapeutics against CRPC [129]. Supporting the argument that AR can be activated in the absence of androgens by MAPK activation [72]. Advanced prostate cancers often have higher levels of E2F and other transcription factors [56]. Interestingly, E2F was more sensitive in AD cells, while other transcription factors (ETS and AP1) were more robust. The drug enzalutamide had no effect on the top 2% of sensitive species. Species in the PI3K/AKT and MAPK pathways in the presence of enzalutamide were still highly sensitive. The application of enzalutamide, increased sensitivity of AR species found outside of the nucleus as well as PAcP species. Robustness analysis indicated diverse effects of Raf knock-out on PSA and cyclin D concentrations. Clinical studies of sorafenib, a multi-kinase inhibitor that has activity against Raf, showed increase PSA levels in patients [52]. Our results indicate that cell-to cell heterogeneity in gene expression can play a significant role in determining cell response. Thus, combination therapies need to be considered even in the case of a Raf knock-out.

The results of the model suggest that an inhibition of either the PI3K pathway or the MAPK pathway in combination with an AR inhibitor as a possible therapy for CRPC. Sensitivity analysis revealed no change in the top sensitive species in the presence or absence of the AR inhibitor, enzalutamide. PI3K/AKT and MAPK species continued to fall in the top two percent of sensitive species. A study by Carver *et al.* looked at dual inhibition of AR and PI3K signaling in LNCaP cells and in a Pten-deficient murine prostate cancer model [186]. Using both the PI3K inhibitor, BEZ235, and the AR inhibitor, MDV3100 (enzalutamide), the group saw a drastic decrease in the total number of cells. Each inhibitor on its own had a much smaller effect on total cell number. They saw an increase in the cell death marker, c-PARP, in the dual inhibition case. The group hypothesized that AKT inhibition leads to increased AR signaling activity through increased protein concentrations of HER3. On the other hand AR inhibition leads to increased AKT activity due to the down regulation of PHLPP, a protein phosphatase that regulates AKT. For the simplicity of this model, the HER3 pathway and also cell death were not included in the model. Dual knock-out studies of PI3K and AR in our model show only a slight additive effect on cell cycle protein cyclin D through the dual knock-out compared to solely inhibiting PI3K (Fig. 2.7). The triple case, with PI3K, AR, and RAF knock-outs, also only showed a slight additive effect (Fig. 2.7). This could indicate that the combined decrease in cell population due to the dual inhibition of PI3K and AR is entirely due to cell death. The Carver *et al.* study did not consider cell cycle proteins or cell growth. Our model does show a decrease in cell cycle proteins in the PI3K knock-out as well as in the PI3K and AR dual knock-out case in some ensemble members (Fig. 2.7). This result seems to be consistent with the decreased cell count in the PI3K knock-out case which is not dependent on

cell death, as c-PARP levels are low. The decrease in cell cycle proteins in the model is due to a decrease in general translation, including free eIF4E levels and activated 40S ribosome subunit. The decrease in p70 (S6) activation due to inhibition of PI3K is shown in both the model and in the Carver *et al.* study , indicating this result is due to the PI3K pathway (Fig. A.5). Our experimental results confirm the Carver *et al.* study in that a dual inhibition of AR and PI3K signaling led to a more prominent decrease in cell viability then each of the inhibitors alone in LNCaP cells. We extended the study to look at the addition of a third inhibitor, sorafenib, that inhibits Raf kinase in the MAPK pathway and an additional cell line, C4-2, which was CR. In both cell lines, there was not a significant decrease in cell viability between the three dual inhibitor cases and the triple inhibition case at 74 hours, indicating that a dual inhibition (PI3K/AR, AR/MAPK, or PI3K/MAPK) may be a sufficient treatment.

The PCa signaling architecture was assembled after extensive literature review and hand curation of the biochemical interactions. However, there are a number of areas where model connectivity could be refined, e.g., the regulation of AR phosphorylation. We assumed a single canonical activating AR phosphorylation site (S515), with ERK being the major kinase and PP2A or PP1 being the major phosphatases responsible for regulating this site. MAPK activation following EGF treatment increases AR transcription and cell growth, partially through AR phosphorylation on MAPK consensus site S515 [193]. However, there are at least 13 phosphorylation sites identified on AR, with phosphorylation at six of these being androgen induced [83]. Moreover, other kinases such as AKT, protein kinase C (PKC) family members, as well as Src-family kinases can all phosphorylate AR in prostate cells [91, 193]. For example, AKT activation leads to AR phosphorylation at both S213 and S791 (however, the role of

these sites remains unclear) [262, 152, 238, 153]. AKT effects on AR may also be passage number dependent, with AKT repressing AR transcription in low passage number cells and enhancing transcription in higher passage numbers [153]. Androgen independent phosphorylation of AR by Src family kinases (not currently in model) at Y534 [91] or by protein kinase C (PKC) family members at the consensus site S578 could also be important for understanding the regulation of AR activity. A second area we will revisit is the gene expression program associated with androgen action, and particularly the role of AR coregulators. Currently, we included only two AR coactivators, cyclin E and CDK6 [269, 151] and three corepressors AP1, Cdc25A, and cyclin D1a in the model [212, 43, 191]. However, there are at least 169 proteins classified as potential AR coregulators [104, 103] with many of these being differentially expressed in malignant cells. For example, the expression of steroid receptor coactivator-1 (Src-1) and transcriptional intermediary factor 2 (Tif-2), both members of the steroid receptor coactivator family, are elevated in prostate cancer [89, 90]. Src-1 is phosphorylated by MAPK and interacts directly with AR to enhance AR-mediated transcription [103]. Another class of potentially important AR coregulators are the cell cycle proteins Cdc25 and Rb. Unlike Cdc25A, Cdc25B (not in the model) can act as an AR coactivator leading to enhanced AR transcription activity [181]. The Rb protein, in addition to being a key cell cycle regulator, has been shown to be an AR coactivator in an androgen-independent manner in DU145 cells [272]. However, there is some uncertainty about the role of Rb as Sharma *et al.* showed that Rb decreased AR activation in multiple prostate cancer cell lines and xenografts [217]. Forkhead proteins have also been shown to activate as well as repress AR function. In prostate cancer, AKT suppresses AFX/Forkhead proteins, which diminishes expression of AFX target genes, such as p27Kip1

[87, 27, 171, 236]. Lastly, undoubtedly there are several other signaling axes important in PCa, such as cytokine or insulin- and insulin-like growth factor signaling [33, 105, 237, 216]. Understanding the pathways associated with these signals and how they relate to the current model, may give us a more complete picture of CR prostate cancer.

## 2.4 Materials and Methods

### 2.4.1 Prostate model signaling architecture.

We modeled the expression, translation and post-translational modifications of key components of the signaling architecture. The model, which consisted of 780 protein, lipid or mRNA species interconnected by 1674 interactions, was a significant extension to our previous model [241] in several important areas. First, we included well-mixed nuclear, cytosolic, membrane and extracellular compartments (including transfer terms between compartments). Next, we expanded the description of growth factor receptor signaling, considering both homo- and heterodimer formation between ErbB family members and the role of cellular and secreted prostatic acid phosphatase (cPAcP and sPAcP, respectively). Both forms of PAcP were included because cPAcP downregulates HER2 activity, while sPAcP promotes modest HER2 activation [253]. Third, we expanded the description of the G1/S transition of the cell cycle (restriction point). The previous model used the abundance of cyclin D as a proliferation marker, but did not include other proteins or interactions potentially important to the restriction point. Toward this shortcoming, we included cyclin E expres-

sion (and its role as a coregulator of androgen receptor expression), enhanced the description of cyclin D expression and the alternative splicing of cyclin D mRNA (including the role of the splice variants in androgen action), included the Rb/E2F pathway as well as E2F inhibition of androgen receptor expression [56], and the cyclin-dependent kinases cyclin-dependent kinase 4 (CDK4) and cyclin-dependent kinase 6 (CDK6). We also included key inhibitors of the restriction point including cyclin-dependent kinase inhibitor 1 (p21Cip1), cyclin-dependent kinase inhibitor 1B (p27Kip1), and cyclin-dependent kinase inhibitor 2A (p16INK4) [220]. Fourth, we enhanced the description of growth factor induced translation initiation. One of the key findings of the previous model was that growth factor induced translation initiation was globally sensitive (important in both androgen dependent and independent conditions). However, the description of this important subsystem was simplified in the previous model. Here, we expanded this subsystem, using connectivity similar to previous study of Lequieu *et al.* [148], and re-examined the importance of key components of this axis, such as mammalian target of rapamycin (mTOR), phosphatidylinositol 3-kinase (PI3K) and AKT. Lastly, we significantly expanded the description of the role of androgen receptor. The previous model assumed constant AR expression, consistent with studies in androgen dependent and independent LNCaP sublines [147]. However, other prostate cancer cell lines vary in their AR expression [225]. Thus, to capture androgen signaling in a variety of prostate cancer cells, we included the transcriptional regulation governing androgen receptor expression, updated our description of the regulation of androgen receptor activity and androgen action (gene expression program driven by activated androgen receptor). At the expression level, we included AR auto-regulation in combination with the co-activators cyclin E and CDK6 [269, 151].

We also assumed androgen receptor could be activated through androgen binding or a ligand-independent, MAPK-driven mechanism referred to as the outlaw pathway [72, 271]. We assumed a single canonical activating AR phosphorylation site (S515), with phosphorylated extracellular-signal-regulated kinase 1/2 (ppERK1/2) being the major kinase and protein phosphatase 2 (PP2A) or phosphoprotein phosphatase 1 (PP1) being the major phosphatases responsible for regulating this site. Finally, we modeled androgen receptor induced gene expression, including prostate specific antigen (PSA), cPAcP and p21Cip1.

#### 2.4.2 Formulation and solution of the model equations.

The prostate model was formulated as a coupled set of non-linear ordinary differential equations (ODEs):

$$\frac{d\mathbf{x}}{dt} = \mathbf{S} \cdot \mathbf{r}(\mathbf{x}, \mathbf{k}) \quad \mathbf{x}(t_o) = \mathbf{x}_o \quad (2.1)$$

The quantity  $\mathbf{x}$  denotes the vector describing the abundance of protein, mRNA, and other species in the model ( $780 \times 1$ ). The stoichiometric matrix  $\mathbf{S}$  encodes the signaling architecture considered in the model ( $780 \times 1674$ ). Each row of  $\mathbf{S}$  describes a signaling component while each column describes a particular interaction. The  $(i, j)$  element of  $\mathbf{S}$ , denoted by  $\sigma_{ij}$ , describes how species  $i$  is involved with interaction  $j$ . If  $\sigma_{ij} > 0$ , species  $i$  is produced by interaction  $j$ . Conversely, If  $\sigma_{ij} < 0$ , then species  $i$  is consumed in interaction  $j$ . Lastly, if  $\sigma_{ij} = 0$ , then species  $i$  is not involved in interaction  $j$ . The term  $\mathbf{r}(\mathbf{x}, \mathbf{k})$  denotes the vector of interactions rates ( $1674 \times 1$ ). Gene expression and translation processes as well as all biochemical transformations were decomposed into simple elementary steps, where all reversible interactions were split into two irreversible steps

(supplemental materials). We modeled each network interaction using elementary rate laws where all reversible interactions were split into two irreversible steps. Thus, the rate expression for interaction  $q$  was given by:

$$r_q(\mathbf{x}, k_q) = k_q \prod_{j \in \{\mathbf{R}_q\}} x_j^{-\sigma_{jq}} \quad (2.2)$$

The set  $\{\mathbf{R}_q\}$  denotes reactants for reaction  $q$ , while  $\sigma_{jq}$  denotes the stoichiometric coefficient (element of the matrix  $\mathbf{S}$ ) governing species  $j$  in reaction  $q$ . The quantity  $k_q$  denotes the rate constant (unknown) governing reaction  $q$ . Model equations were generated in the C-programming language using the UNIVERSAL code generator, starting from an text-based input file (available in supplemental materials). UNIVERSAL, an open source Objective-C/Java code generator, is freely available as a Google Code project (<http://code.google.com/p/universal-code-generator/>). Model equations were solved using the CVODE solver in the SUNDIALS library [108] on an Apple workstation (Apple, Cupertino, CA; OS X v10.6.8).

We ran the model to steady-state before calculating the response to DHT or growth factor inputs. The steady-state was estimated numerically by repeatedly solving the model equations and estimating the difference between subsequent time points:

$$\|\mathbf{x}(t + \Delta t) - \mathbf{x}(t)\|_2 \leq \gamma \quad (2.3)$$

The quantities  $\mathbf{x}(t)$  and  $\mathbf{x}(t + \Delta t)$  denote the simulated abundance vector at time  $t$  and  $t + \Delta t$ , respectively. The  $L_2$  vector-norm was used as the distance metric, where  $\Delta t = 100$  hr of simulated time and  $\gamma = 0.001$  for all simulations.

We estimated an ensemble of model parameter sets using the Pareto Optimal Ensemble Techniques (POETs) multiobjective optimization routine [228,

227, 148]. POETs minimized the residual between model simulations and 43 separate training objectives taken from protein and mRNA signaling data generated in androgen dependent, intermediate and independent LNCaP cell lines (Table A.1). From these training objectives, POETs generated  $> 10^6$  candidate parameter vectors from which we selected  $N = 5000$  Pareto rank-zero vectors for further analysis. The set-to-set correlation between selected sets was approximately 0.60, suggesting only modest similarity between ensemble members. Approximately 33%, or 560 of the 1674 parameters had a coefficient of variation (CV) of less than 1.0, where the CV ranged from 0.59 to 5.8 over the ensemble. Details of the parameter estimation problem and POETs are given in the supplemental materials.

### 2.4.3 Sensitivity and robustness analysis.

Steady-state sensitivity coefficients were calculated for  $N = 500$  parameter sets selected from the ensemble by solving the augmented kinetic-sensitivity equations [61]:

$$\begin{bmatrix} \mathbf{S} \cdot \mathbf{r}(\mathbf{x}, \mathbf{k}) \\ \mathbf{A}(t_s)\mathbf{s}_j + \mathbf{b}_j(t_s) \end{bmatrix} = \begin{pmatrix} \mathbf{0} \\ \mathbf{0} \end{pmatrix} \quad j = 1, 2, \dots, \mathcal{P} \quad (2.4)$$

where

$$s_{ij}(t_s) = \left. \frac{\partial x_i}{\partial k_j} \right|_{t_s} \quad (2.5)$$

for each parameter set. Steady-state was calculated as described previously. The quantity  $j$  denotes the parameter index,  $\mathbf{A}$  denotes the Jacobian matrix, and  $\mathcal{P}$  denotes the number of parameters in the model. The vector  $\mathbf{b}_j$  denotes the  $j$ th column of the matrix of first-derivatives of the mass balances with respect to the parameters. Steady-state sensitivity coefficients were used because of the

computational burden associated with sampling several hundred parameters sets for each of the 1674 parameters. The steady-state sensitivity coefficients  $\mathcal{N}_{ij} \equiv s_{ij}$  were organized into an array for each parameter set in the ensemble:

$$\mathcal{N}^{(\epsilon)} = \begin{pmatrix} \mathcal{N}_{11}^{(\epsilon)} & \mathcal{N}_{12}^{(\epsilon)} & \dots & \mathcal{N}_{1j}^{(\epsilon)} & \dots & \mathcal{N}_{1P}^{(\epsilon)} \\ \mathcal{N}_{21}^{(\epsilon)} & \mathcal{N}_{22}^{(\epsilon)} & \dots & \mathcal{N}_{2j}^{(\epsilon)} & \dots & \mathcal{N}_{2P}^{(\epsilon)} \\ \vdots & \vdots & & \vdots & & \vdots \\ \mathcal{N}_{M1}^{(\epsilon)} & \mathcal{N}_{M2}^{(\epsilon)} & \dots & \mathcal{N}_{Mj}^{(\epsilon)} & \dots & \mathcal{N}_{MP}^{(\epsilon)} \end{pmatrix} \quad \epsilon = 1, 2, \dots, N_\epsilon \quad (2.6)$$

where  $\epsilon$  denotes the index of the ensemble member,  $P$  denotes the number of parameters,  $N_\epsilon$  denotes the number of parameter sets sampled ( $N = 500$ ) and  $M$  denotes the number of model species. To estimate the relative fragility or robustness of species and reactions in the network, we decomposed  $\mathcal{N}^{(\epsilon)}$  using Singular Value Decomposition (SVD):

$$\mathcal{N}^{(\epsilon)} = \mathbf{U}^{(\epsilon)} \Sigma^{(\epsilon)} \mathbf{V}^{T,(\epsilon)} \quad (2.7)$$

Coefficients of the left singular vectors corresponding to largest  $\theta \leq 15$  singular values of  $\mathcal{N}^{(\epsilon)}$  were rank-ordered to estimate important species combinations, while coefficients of the right singular vectors were used to rank important reaction combinations. Only coefficients with magnitude greater than a threshold ( $\delta = 0.001$ ) were considered. The fraction of the  $\theta$  vectors in which a reaction or species index occurred was used to quantify its importance (sensitivity ranking). We compared the sensitivity ranking between different conditions to understand how control in the network shifted in different cellular environments.

Robustness coefficients were calculated as shown previously [242]. Robustness coefficients denoted by  $\alpha(i, j, t_o, t_f)$  are defined as:

$$\alpha(i, j, t_o, t_f) = \left( \int_{t_o}^{t_f} x_i(t) dt \right)^{-1} \left( \int_{t_o}^{t_f} x_i^{(j)}(t) dt \right) \quad (2.8)$$

Robustness coefficients quantify the response of a marker to a structural or operational perturbation to the network architecture. Here  $t_o$  and  $t_f$  denote the initial and final simulation time respectively, while  $i$  and  $j$  denote the indices for the marker and the perturbation respectively. A value of  $\alpha(i, j, t_o, t_f) > 1$ , indicates increased marker abundance, while  $\alpha(i, j, t_o, t_f) < 1$  indicates decreased marker abundance following perturbation  $j$ . If  $\alpha(i, j, t_o, t_f) \sim 1$  the  $j$ th perturbation does not influence the abundance of marker  $i$ . Robustness coefficients were calculated (starting from steady-state) from  $t_o = 0$  hr to  $t_f = 72$  hr following the addition of 10nM DHT at  $t_o$ . For scaled log fold change we used the following equation:

$$\alpha_{scaled}(i, j) = \begin{cases} \frac{\log_{10}(\alpha(i, j))}{\max \log_{10}(\alpha(i))}, & \text{if } \log_{10}(\alpha(i, j)) \geq 0 \\ -\frac{\log_{10}(\alpha(i, j))}{\min \log_{10}(\alpha(i))}, & \text{if } \log_{10}(\alpha(i, j)) < 0 \end{cases} \quad (2.9)$$

A value of  $\alpha_{scaled}(i, j) > 0$ , indicates increased marker abundance, while  $\alpha_{scaled}(i, j) < 0$  indicates decreased marker abundance following perturbation  $j$ . If  $\alpha_{scaled}(i, j) \sim 0$  the  $j$ th perturbation does not influence the abundance of marker  $i$ . A value of  $\alpha_{scaled}(i, j) = 1$ , indicates max increase of marker abundance, while  $\alpha_{scaled}(i, j) = -1$  indicates the max decrease of marker abundance. Robustness coefficients were calculated for the same  $N = 500$  models selected for sensitivity analysis.

#### **2.4.4 Experimental Validation.**

#### **2.4.5 Cell culture and treatments**

Androgen dependent LNCaP prostate cancer cells were a gift from Dr. Brian Kirby (Cornell University), and the castration resistant C4-2 prostate cancer cell line was purchased from MD Anderson Cancer Center, University of Texas. Cell lines were maintained in RPMI 1640 media (Life Technologies, Inc., Grand Island, NY) with 10% fetal calf serum (FBS; Hyclone) and 1x antibiotic/antimycotic (Sigma, St. Louis, MO) in a 5% CO<sub>2</sub> humidified atmosphere at 37°C. The AR inhibitor MDV3100 (enzalutamide) and the Raf inhibitor sorafenib were purchased from SantaCruz Biotechnology (Santa Cruz, CA). The PI3K inhibitor LY294002 was purchased from Cell Signaling Technologies (Danvers, MA, USA). All stock solutions were diluted in DMSO and stored at -20°C (Sigma, St. Louis, MO). Stock solution concentrations for western blotting experiments were 10 mM Sorafenib, 50 mM LY294002, and 10 mM MDV3100. For the cell viability assays, stock solution concentrations were 0.5 mM Sorafenib, 4 mM LY294002, and 1 mM MDV3100.

#### **2.4.6 Protein Extraction and Western Blot**

LNCaP and C4-2 cells were seeded in 60 mm dishes at a density of 4 × 10<sup>5</sup>. After 96 and 72 hrs, for LNCaP and C4-2 cells respectively, the media was replaced with fresh media and drug treatments were added. After 24 hours, cells were washed twice in PBS buffer, scraped in 250 µL ice-cold lysis buffer (Pierce, Rockford, IL) supplemented with protease and phosphatase inhibitors (Sigma,

St. Louis, MO), and lysed for 30 min on ice. Lysates were centrifuged at 13,000 rpm for 30 min at 4°C. After quantification of total protein by BCA assay, equal amounts of total protein lysates (25 µg) were resolved by SDS-PAGE and transferred onto PVDF membranes. Membranes were blocked in 5% fat free milk and then probed with antibodies. The primary antibodies used for western blot analysis were pAKT Ser473, AKT, pS6 Ser240/244 , pERK Thr202/Tyr204, ERK, AR, cleaved PARP, and GAPDH were from Cell Signaling Technologies (Danvers, MA, USA). For detection, enhanced chemiluminescence ECL reagent (GE Healthcare, Pittsburgh, PA) was used and signals were visualized using the ChemiDoc XRS system (Bio-Rad).

#### **2.4.7 MTT Assay**

LNCaP and C4-2 cells were seeded at a density of 1x10<sup>4</sup> cells per well in 96 well plates. After 48 hrs the media was refreshed and drug treatments added. Cell growth at 24, 48, and 72 hrs was determined using a 3-(4,5-dimethyl thiazol-2-yl)-2,5-diphenyl tetrazolium bromide (MTT) assay. At the specified time point 10 µL MTT reagent (stock of 5 mg/mL in PBS) was added to each well and the cells were further incubated for 4 hrs. At 4 hrs, the media was removed and 50 µL of dissolving reagent DMSO was added to each well. After an additional 10 min incubation, the absorbance was measured at 540 nm on a microplate reader. Each reading was adjusted by subtracting the absorbance value for the blank (media only) and the results were then scaled to the DMSO-treated (control) case.

## **2.5 Acknowledgements**

This study was supported by award number U54CA143876 from the National Cancer Institute. The content is solely the responsibility of the authors and does not necessarily represent the official views of the National Cancer Institute or the National Institutes of Health. The authors acknowledge the financial support of the National Science Foundation, award no. DGE-1045513, for a GK12 training grant entitled “Grass Roots: Advancing Education in Renewable Energy and Cleaner Fuels through collaborative graduate fellow/teacher/grade-school student interactions”. We would also like to thank Timothy Chu, Kyriakos Tsahalis, Spencer Davis, Rohit Yallamraju, Gongcheng Lu, and Yalin Zhao for their support on the project.

# CHAPTER 3

## MODEL IDENTIFICATION OF LEUKEMIA TRANSCRIPTION FACTOR NETWORKS

### 3.1 Introduction

It<sup>1</sup> was suggested by Bailey, more than a decade ago, that qualitative and quantitative knowledge of complex biological systems could be achieved in the absence of complete structural and parameter knowledge [13]. Although this is true, the incomplete knowledge of biological phenomenon often limits the impact of computational models. As we saw in Chapter 2.2.2, unknown or even disputed network structures can lead to incomplete fitting of computation models, requiring additional experiments and updating of the model. Since ODE kinetic models typically require extensive prior knowledge of network structure, rate constants and initial conditions [135], often a single “correct” network structure is assumed. Villaverde *et al.* discussed three main strategies in the reverse engineering of dynamic models: (1) full network inference, (2) network selections, and (3) kinetic parameter estimations [255]. Strategy 1, where the kinetic model structure and kinetic parameters are unknown, is typically solved by identifying the model interaction network without dynamics and then identifying the kinetic parameters. Strategy 3 was used in chapter 2, where we assumed a network structure and estimated the unknown parameters. In this chapter we will consider strategy 2; we have an initial model network structure that will be perturbed to find modifications to fit the experimental data for six different leukemia cell lines.

---

<sup>1</sup>Adapted with permission from: Rogers K, Sagar A, Jensen H, Varner J. Model Identification of Leukemia Transcription Factor Networks, (in prep).

Leukemia is the 6th leading cause of cancer death in both males and females in the United States [222]. Approximately 72% of cancer related leukemia deaths were caused by four main types of leukemia; acute lymphocytic leukemia (ALL), chronic lymphocytic leukemia (CLL), acute myeloid leukemia (AML), and chronic myeloid leukemia (CML). ALL and CLL are characterized by accumulation of lymphocytes in the bone marrow, with ALL progressing at a faster rate (i.e. acute vs. chronic). ALL occurs in both children and adults and has a 90% five year survival rate in children [114], while CLL is rare in children and has a 66% five year survival rate (2001-2009) [179]. The 10 year survival rate for CML has improved to 80-90% due to the use of targeted treatments for BCR-ABL and adenosine triphosphate (ATP) [119]. AML is characterized by the accumulation of abnormally differentiated cells of the hematopoietic system in the bone marrow and blood, with a survival rate of 35 to 40% in adults under the age of 60 (5 to 15% in patients older than 60) [64]. AML is a group of extremely heterogeneous diseases, with over 200 known chromosome translocations and mutations in patient leukemic cells [85]. The use of differentiation induction therapy agents like all-*trans* retinoic acid (RA) and 1,25-dihydroxyvitamin D3 (D3) have been explored in many cancer cell types, including myeloid leukemias, and lung, liver, prostate, and breast cancer (RA treatment) [31, 239] and in prostate, breast, colorectal, leukemia, and brain (D3 treatment) [42]. Acute promyelocytic leukemia (APL), a subtype of AML, was once one of the most fatal forms of acute leukemia until the introduction of RA increased remission rates of patients to between 80 and 90 % [48]. Failure of RA treatment can occur initially in patients with RA resistant variants (PLZF-RARA-positive APL), and relapse occurs in 5-20% of cases due to the emergence of RA resistance. To understand the response of multiple leukemia cell lines to RA and D3 treatments, we developed

a network structure of well known transcription factors governing myelomonocytic lineage selection (granulocytic or monocytic).

In this study we considered data from RA, D3, and RA plus D3 treatments on six human myeloid leukemia cell lines; (1) K562 (FAB M1), (2) HL60 (FAB M2), (3) NB4 (FAB M3), (4) U937 (FAB 5), (5) HL60 R38+ and (6) HL60 R38- (5 and 6 are described previously [121]). K562, a CML cell line with a Bcr-Abl fusion protein [162], was used as a control because the cells are not responsive to both RA [200] and D3 treatment [177]. HL60 cells, an AML cell line, are lineage-bipotent myelobasts [75, 54] that can differentiate to either granulocytic lineage (using RA) or monocytic lineage (using D3). The two RA-resistant HL60 cell lines, R38+ and R38-, were described previously [121, 120]. NB4, an APL cell line, are highly RA-responsive, but require combination treatments for monocytic differentiation (i.e. low response to D3) [21, 243]. U937, histiocytic lymphoma cell line, are highly responsive to D3 induced monocytic differentiation, but have ambiguous differentiation effects due to RA (either monocytic or granulocytic) [182, 180, 58]. The model network contained two inputs (RA and D3) and 18 main species. We included two receptors, reinoic acid receptor alpha (RAR $\alpha$ ) and vitamin D receptor (VDR), but excluded their heterodimer receptor pair, retinoid receptor (RXR), for simplicity (assumption RXR is readily available). Also, included in the model were transcription factors important in myelomonocytic lineage selection (listed in Table 3.1). Finally upstream markers for differentiation were included, including CD38, CD11b, CD14, G1/G0 cell cycle arrest and inducible oxidative metabolism. CD38 and CD11b are myelomonocytic markers and CD14 is a monocytic specific marker.

In this study we first determined that a network structure of a small three

node protein model could be identified with sufficient experimental data. A model structure search in combination with particle swarm optimization to determine parameter values narrowed down total possible model structures from 19683 to twenty. After additional experimental data was implemented, we were able to find the synthetic model structure with no *a priori* knowledge. Next we investigated possible network structures for transcription factor and upstream markers in six leukemia cell lines treated with RA and D3 (data from [122]). The upstream markers CD38 and CD11b (myelomonocytic markers) and CD14 (monocytic specific marker) were included in the model. Also, included in the model were transcription factors important in myelomonocytic lineage selection. Starting from an initial best model structure curated from literature sources, we were able to improve the model fits for six leukemia cell lines versus experimental data.

## 3.2 Results

### 3.2.1 Three Node Example Network

To determine if we could distinguish between possible model structures, we began by first modeling a simple three protein node network. The model we designated as the true model is shown in Figure 3.1A and the results for the synthetic data generated are given in Figure B.1. All proteins in the model could act as either transcription factors or transcription repressors. The two examples of transcriptional regulation, activation and repression, are given in Figure 3.1D. Assuming no prior knowledge, other than number of nodes and inducer loca-

tion, we were able to narrow down possible network structures with just one experiment and ultimately determine the true network structure with a small set of additional experiments (Table B.3). For an  $n$  node protein network with three possible interactions between nodes (activation, inhibition, or no interaction) and allowing for self regulation (i.e.  $P_1$  can be a transcription factor for itself), we had a total of  $3^{n^2}$  possible structures, where  $n$  is the number of protein nodes. The simple  $n = 3$  case had a total of 19683 possible model structures, which we exhaustively searched and determined a best fit parameter set for each model using particle swarm optimization. For particle swarm optimization we designated a ten particle system and 30 operations, for 300 total iterations. The initial ten particles were each a set of parameters containing 35 randomized parameters (20 control parameters and 15 kinetic parameters). Using the data from five species (one saved for validation) in experiment 1 (Table B.3), we narrowed our results to the 20 best model structures (top 0.1%). For these 20 best models, we ran a second particle swarm optimization with 300 total iterations to determine if a better solution could be found. In this case we started with ten particles randomized from the best parameter set from each model obtained from the first trial. As shown in Figure 3.2, the true model was not selected as the best fit and we did not find the “true” parameter set. The top model was similar to the true model with two additional interactions and two opposite sign interactions (i.e. activation instead of inhibition) (Fig. 3.1B). Therefore, by using data from just one experiment we were able to obtain a subset of 20 possible model structures.

From the possible 20 model structures we wanted to determine if we could narrow down the possibilities to one structure with the use of additional experimental data. All top 20 models show qualitatively the correct response (Fig. 3.2) and therefore, the simulation error could be caused either by a model structure

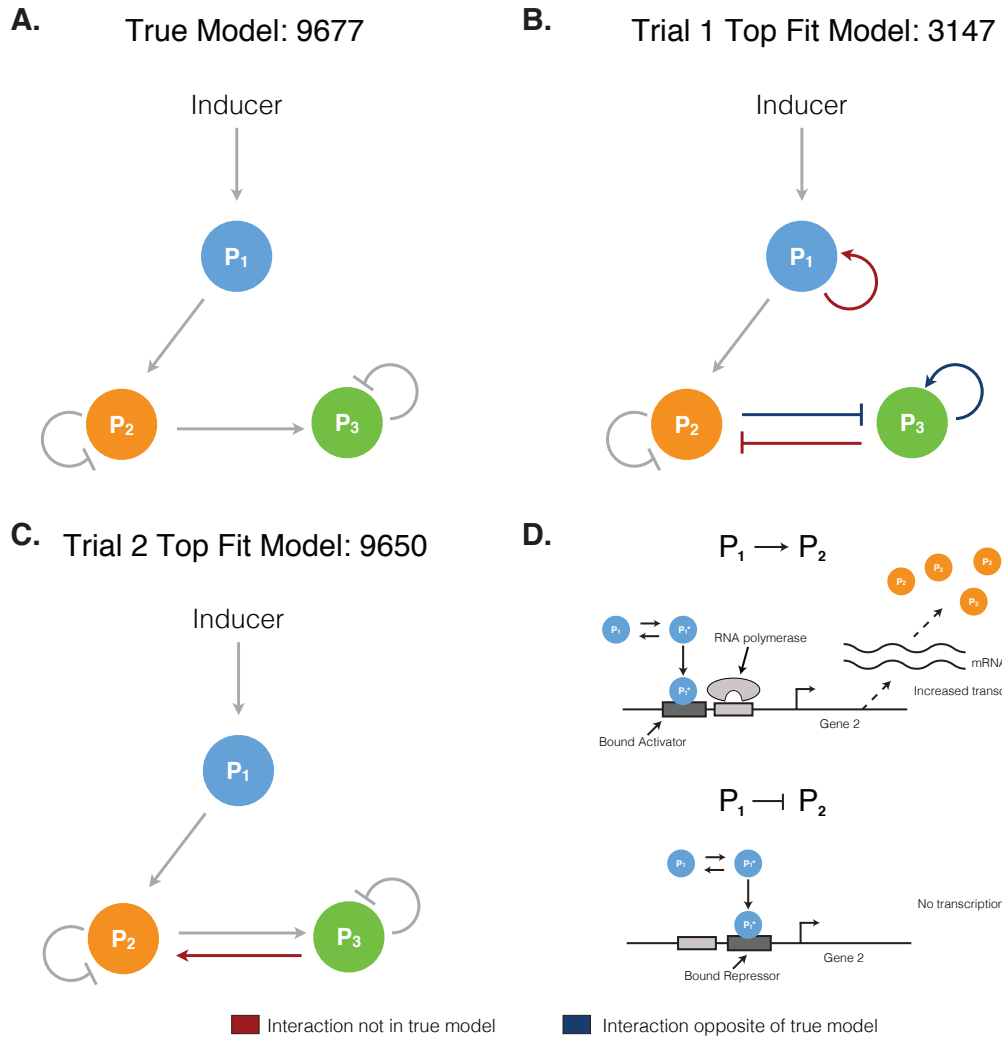


Figure 3.1: Model for three node protein network. Arrows denote activation and lines denote inhibition. The model includes three proteins ( $P_1$ ,  $P_2$ , and  $P_3$ ), the corresponding mRNA ( $mRNA_1$ ,  $mRNA_2$ , and  $mRNA_3$ ), RNA polymerase (RNAP), ribosomes (RIBO), and Inducer. **A.** The true model for the three node protein network. **B.** The best fit model after parameter estimation using data from only one experiment. **C.** The best fit model after parameter estimation using data from experiments 1, 2 and 3. Red lines denote interactions not in original model and blue lines denote interactions that are opposite of the original model. **D.** Gene transcription activation and repression in the model (figure modified from [7]).

issue or a parameter set estimation issue (did we find the correct parameters?). The top 20 models have many features in common (Fig. 3.3): (1) All 20 models designated  $P_1$  as a transcription factor activator for species two, (2) 19 models showed  $P_2$  inhibits itself, (3) 20 models showed  $P_2$  as a transcriptional regulator (activator or repressor) for species three, with four having the opposite interaction (i.e. repression instead of activation), and (4) 18 models showed  $P_3$  regulated itself, but 12 of these cases are opposite (activation instead of repression). Many of the structures also had added interactions: (1) ten models added regulation from  $P_3$  to species two, (2) eight models added self-regulation of  $P_1$  (all activation), and (3) eight models added regulation of species three by  $P_1$ . After studying the possible structures we performed two additional experiments to obtain synthetic data (Table B.3). In experiment two an inducer was added at  $t=100$  A.U. and the binding domain of  $P_2$  was inhibited (i.e.  $P_2$  could not act as a transcription factor). Finally, in experiment three an inducer was added every 24 A.U. starting at  $t = 100$  A.U., to represent step inputs on the system. Again we ran a particle swarm optimization method to find a new best fit parameter set for the top 20 models, this time using a total of three experiments and five species per experiment to calculate experimental error (Table B.1). With the additional two experiments we were able to exclude the previous top model (Fig. 3.1B). In figure 3.4C and 3.4F, we see that the previous top model (in blue) does not qualitatively fit mRNA or protein data for species three. The true model (red) is the second best fitting model after optimization with three experiments, while the new top fitting model is in green. In experiment two,  $mRNA_3$  decreased due to the inhibition of  $P_2$  activity ( $P_2$  is a transcription factor activator for  $mRNA_3$  in the true model). The previous top model (3147) was not able to obtain this result due to the incorrect interaction between  $P_2$  and species three

(inhibition instead of activation). The new top model (Fig. 3.1C) had one additional interaction that occurred between  $P_3$  and species two. After finding that the control parameter value,  $\kappa_{3,2}$ , was 9.9e-7 (essentially zero), for this interaction we were able to ignore the additional interaction (in equation 3.14, if  $\kappa_{3,2} = 0$  then  $f_{3,2} = 0$ ). Therefore, with using only three experiments and 15 objective functions we were able to obtain the correct model structure after exhaustively searching all 19683 possible structures. From the small three node network we determined that the correct model structure could be identified with sufficient experimental data after an exhaustive network search.

### 3.2.2 Leukemia Transcription Factor Network

Next we investigated possible network structures for transcription factor and upstream markers in six leukemia cell lines treated with RA and D3 (data from [122]). The six cell lines, K562, HL60, NB4, U937, HL60 R38+ and HL60 R38-, had diverse reactions to the stimuli and thus, we assumed that network structures could differ between cell lines. The leukemia transcription factor network with two inducers (RA and D3), contained 42 differential equations (RXR was included but set to zero in this case), 652 control parameters, and 90 kinetic parameters. In this case, with  $n = 18$  protein nodes, if no prior knowledge was assumed, other than number of nodes and inducer location, we would have a total of  $3^{18^2}$  possible model structures. To narrow down our search space we first assumed proteins which do not act as transcription factors always have no interaction from the protein to another species: CD38, CD11b, CD14 and p47. Also, we designated the protein Gfi-1 as always acting as a repressor if the interaction existed. Next we created an initial guess transcription factor network

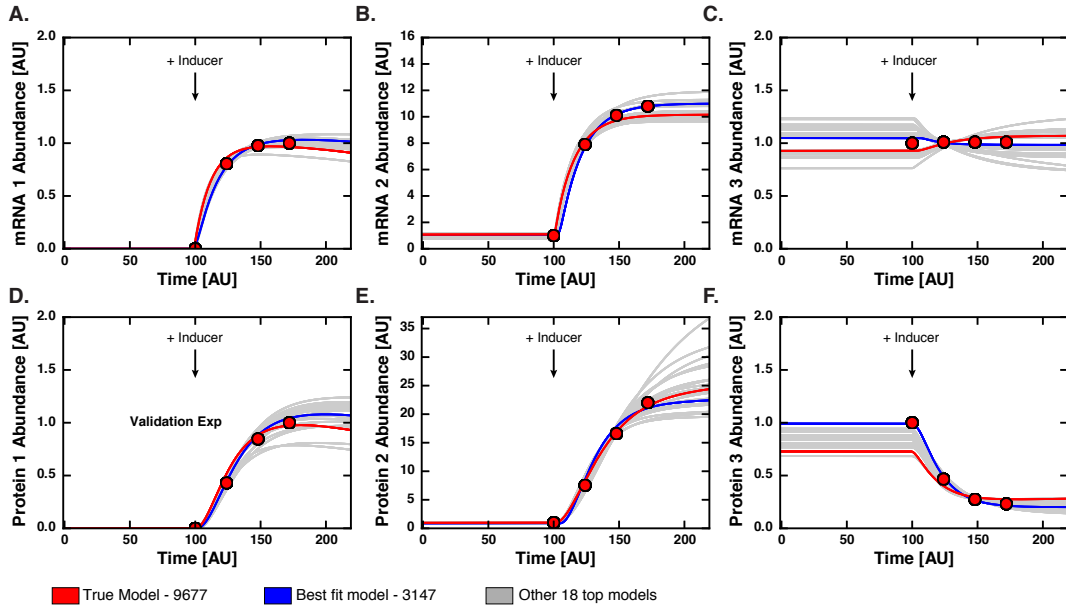


Figure 3.2: Experiment 1 results for the top 20 models with respective best parameter sets determined from particle swarm optimization. In experiment 1, inducer was added at Time = 100. **A, B, C.** Plots of mRNA concentration profiles for species 1, 2, and 3 after inducer added at Time = 100. **D.** Plot of protein concentration profile for species 1 which was used for validation. **E, F.** Plots of protein concentration profiles for species 2 and 3. Red dots denote synthetic experimental data used for fitting. Red lines represent the true model with optimized parameters, blue denotes the best fitting model (3.1B), and the grey lines represent remaining top 18 models.

by searching the literature, which is shown in Figure 3.5 (interactions and references shown in Table 3.1). We began by calculating a top parameter set for each cell line using this initial network structure. A top parameter set was calculated using particle swarm optimization with 35 particles and 90 iterations per particle, for a total of 3150 iterations. Simulation data for each cell line was compared to 39 objective functions found in Table B.4. After finding the parameter set with the lowest error for each model based on this initial structure, we then perturbed the model by randomly changing one to three edges in the model

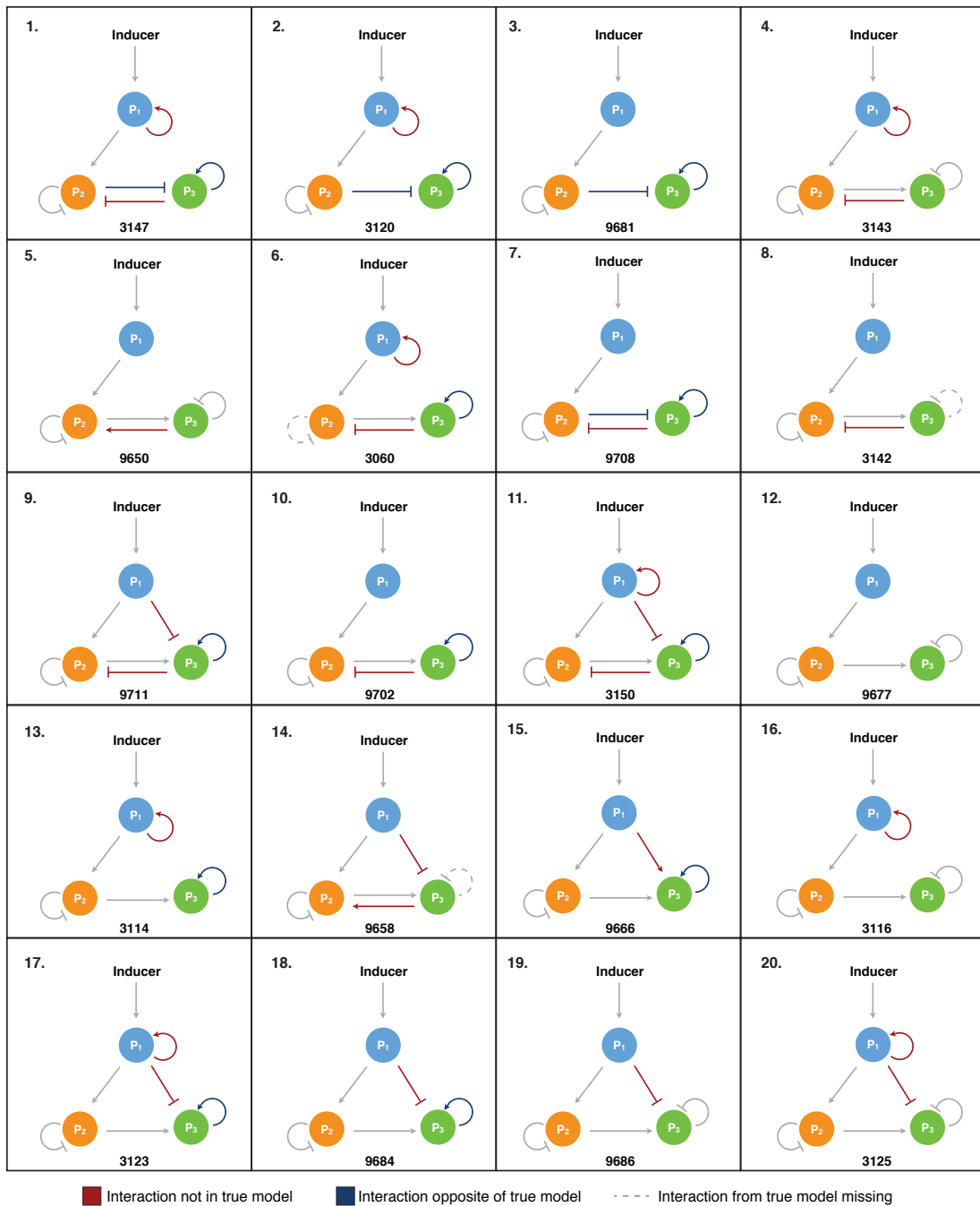


Figure 3.3: Structures of top 20 three protein node models. Models are arranged from lowest error (best fit) to highest error, with the true model at number 12. Red denotes interactions not in original model, blue denotes interactions that are opposite of the original model, and dotted lines denote interactions in true model that are missing in structure. Numbers (i.e. 3147) denote the specific model number out of the total 19683 structures.

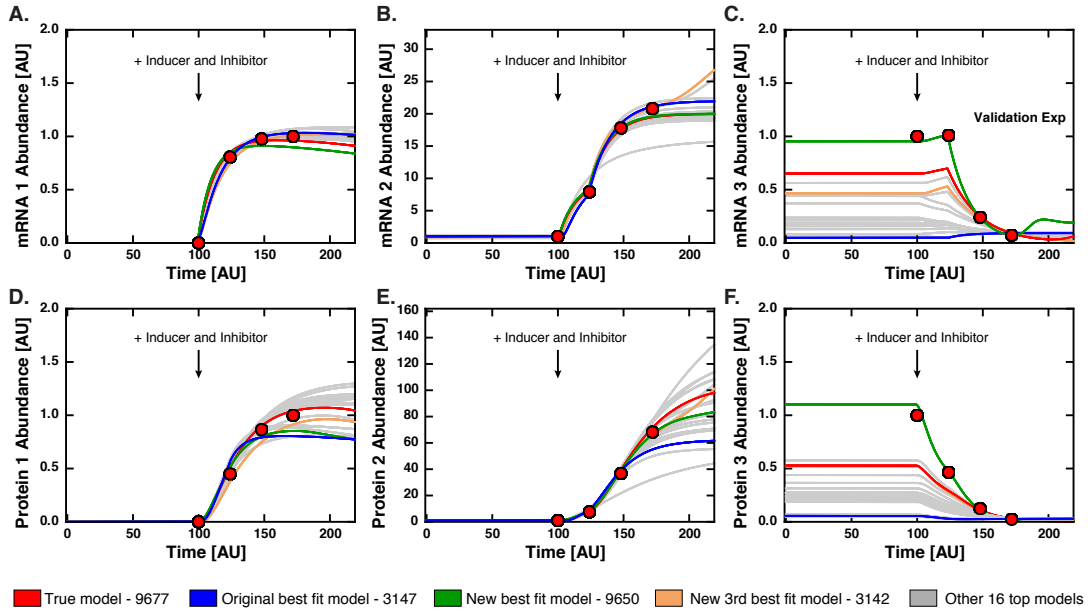


Figure 3.4: Experiment 2 results for the top 20 models with respective best parameter sets determined from particle swarm optimization. In experiment 2, inducer and an inhibitor for  $P_2$  were added at Time = 100. **A, B.** Plots of mRNA concentration profiles for species 1 and 2 after inducer and inhibitor added at Time = 100. **C.** Plot of mRNA concentration profile for species 3 which was used for validation. **D, E, F.** Plots of protein concentration profiles for species 1, 2, and 3. Red dots denote synthetic experimental data used for fitting. Red lines represent the true model with new optimized parameters, blue denotes the best fitting model after experiment 1 (3.1B), green denotes the new best fitting model, orange denotes the third best fit model, and the grey lines represent remaining top 18 models.

from our initial best guess to either no interaction (0), negative interaction (-1), or positive interaction (1). Again we used particle swarm optimization to find a new best parameter set for the updated model. If the error was less than the previous model we accepted the new model, and in the next iteration we would perturb this new model structure. Through this method, we looked at approximately 300 model structures for each cell line and were able to improve model

Transcription Factor Network

Phenotypic Markers

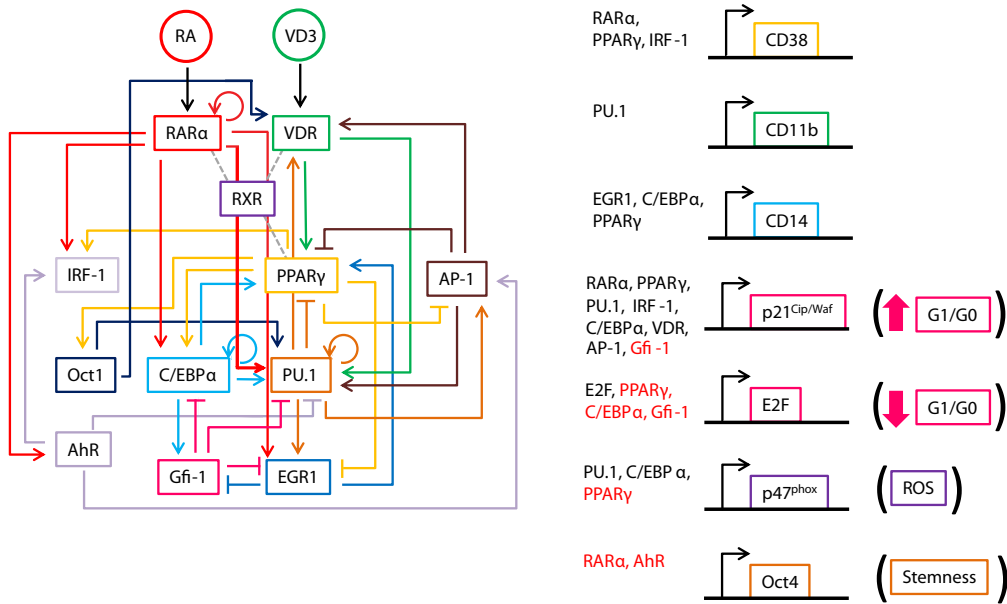


Figure 3.5: Initial myelomonocytic transcription factor network structure from literature sources. Figure shows interactions between protein nodes with arrows indicating transcriptional activation and lines indicating transcriptional repression. Phenotypic markers are shown on the right side, with black indicating activation and red indicating repression. RXR (shown in the figure) was assumed to exist in an active form to dimerize with RAR $\alpha$ , VDR, and PPAR $\gamma$  and was excluded in this network identification problem.

fits compared to the initial model structure.

Through model and parameter optimization we discovered improved network structures for the six cell lines: K562, HL60, NB4, U937, HL60 R38+ and HL60 R38-. The new network structures showed improved fits against a subset of the experimental data. For example the new model structure of the HL60 R38-cell line was able to accurately predict the increase in VDR concentration due to a D3 stimulus and RA+D3 stimulus which was missed in the original structure (Figure 3.6). The new model structure for the HL60 cell line was able to predict the CD38 expression shift due to RA and RA + D3 stimulus, but still missed the D3 stimulus experiment (Figure 3.7). In the NB4 case of CD11b concentration we again missed the D3 stimulus experiment, but were able to improve the results of the RA and RA + D3 stimulus experiments (Figure 3.8). Change in PU.1 concentration due to RA, D3, and RA + D3 treatments was accurately modeled with the new K562 model structure (Figure 3.9). Training experiments involving AhR in U937 cells and C/EBP $\alpha$  in HL60 R38+ cells are also shown (Figure B.2 and B.3). To improve the model fits many perturbations (adding, deleting, or switching edges) were made to the initial network structure for each cell line. For the K562 cell line, unresponsive to RA and D3, 100 changes were made to our initial best network structure (Table B.5). The model structure for the NB4 cell line, which is highly responsive to RA, contained 90 changes (Table B.6). For HL60 cells, 91 edges were changed in the model structure (Table B.7). The two RA resistant HL60, R38- and R38+, models had 76 and 74 changes, respectively (Table B.9 and Table B.8). Finally, the U937 model had 41 network changes in the best model solution (Table B.10). Taken together, through a combination of network perturbations we were able to better predict a subset of experiments in six leukemia cell lines: K562, HL60, NB4, U937, HL60 R38+ and HL60 R38-. We also developed new model structures specific to each cell line from our initial

shared model structure guess.

Table 3.1: Initial myelomonocytic transcription factor network list with transcription factor, effect, target gene, and reference

Transcription Factor	General Effect	Target Gene	Reference(s)
RAR $\alpha$	upregulates	RAR $\alpha$	[199]
RAR $\alpha$	upregulates	PU.1	[176]
RAR $\alpha$	upregulates	C/EBP $\alpha$	[77]
RAR $\alpha$	upregulates	IRF-1	[165]
RAR $\alpha$	represses	Oct4	[234]
RAR $\alpha$	upregulates	CD38	[65]
RAR $\alpha$	upregulates	p21	[159]
RAR $\alpha$	upregulates	AhR	[29]
RAR $\alpha$	upregulates	EGR1	[14]
VDR	upregulates	PPAR $\gamma$	[67]
VDR	upregulates	PU.1	
VDR	upregulates	p21	[160]
PPAR $\gamma$	upregulates	C/EBP $\alpha$	[202]
PPAR $\gamma$	upregulates	IRF-1	[251]
PPAR $\gamma$	upregulates	Oct1	[26]
PPAR $\gamma$	represses	AP-1	[60]
PPAR $\gamma$	represses	E2F	[8]
PPAR $\gamma$	represses	EGR1	[71]
PPAR $\gamma$	upregulates	CD38	[226]
PPAR $\gamma$	upregulates	CD14	[235]
PPAR $\gamma$	upregulates	p21	[94]
PPAR $\gamma$	represses	p47phox	[256]
PU.1	represses	PPAR $\gamma$	[62]
PU.1	upregulates	PU.1	[38]
PU.1	upregulates	AP-1	[230]
PU.1	upregulates	EGR1	[143]
PU.1	upregulates	CD11b	[183]
PU.1	upregulates	p21	[274]
PU.1	upregulates	p47phox	[149]
PU.1	upregulates	VDR	[84]
C/EBP $\alpha$	upregulates	PPAR $\gamma$	[202]
C/EBP $\alpha$	upregulates	PU.1	[51]
C/EBP $\alpha$	upregulates	C/EBP $\alpha$	[245]
C/EBP $\alpha$	upregulates	Gfi-1	[150]

C/EBP $\alpha$	represses	E2F	[53]
C/EBP $\alpha$	upregulates	CD14	[184]
C/EBP $\alpha$	upregulates	p21	[98]
IRF-1	upregulates	CD38	[15]
IRF-1	upregulates	p21	[188]
Gfi-1	represses	PU.1	[50]
Gfi-1	represses	C/EBP $\alpha$	[66]
Gfi-1	represses	E2F	[66]
Gfi-1	represses	EGR1	[143]
Gfi-1	represses	p21	[66]
Oct1	upregulates	VDR	[158]
Oct1	upregulates	PU.1	[39]
AP-1	upregulates	VDR	[158]
AP-1	represses	PPAR $\gamma$	[60]
AP-1	upregulates	PU.1	[16]
AP-1	upregulates	p21	[130]
E2F	upregulates	E2F	[124]
EGR1	upregulates	PPAR $\gamma$	[79]
EGR1	represses	Gfi-1	[166]
EGR1	upregulates	CD14	[37]
AhR	upregulates	AP-1	[231]
AhR	upregulates	IRF-1	[218]
AhR	represses	Oct4	[28]
AhR	represses	PU.1	

## HL60 R38-

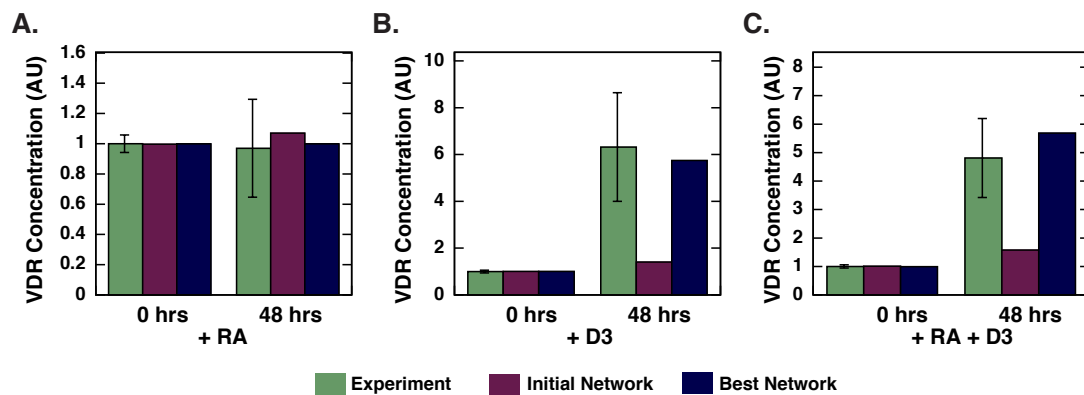


Figure 3.6: Selected training results for the HL60 R38- cell line. **A., B., C.** Simulation and experimental results of change in VDR concentration due to RA, D3, and RA/D3 stimulus, respectively. Green denotes experimental data, pink denotes simulation data from the initial network, and blue denotes simulation data from the best network. The top parameter set is used, and error bars denote standard experimental error.

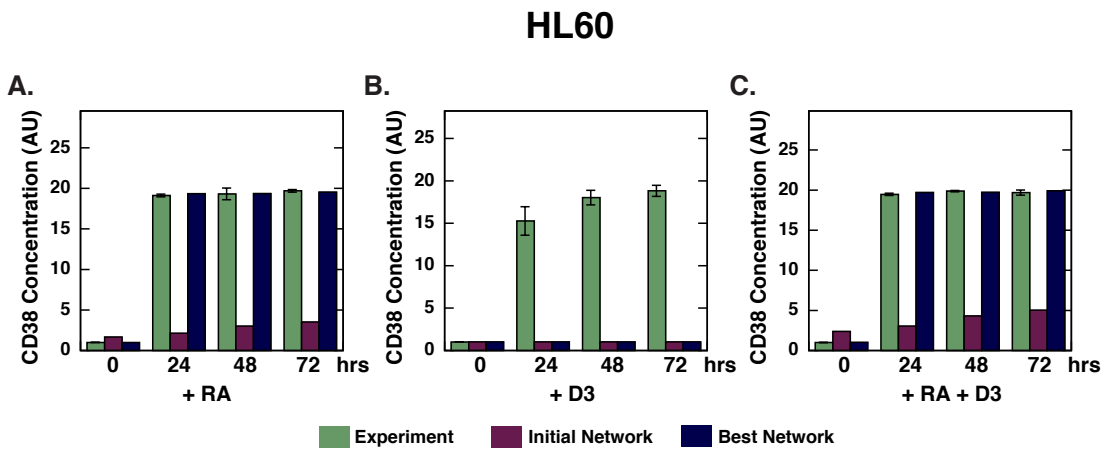


Figure 3.7: Selected training results for the HL60 cell line. A., B., C. Simulation and experimental results of change in cells expressing CD38 due to RA, D3, and RA/D3 stimulus, respectively. Green denotes experimental data, pink denotes simulation data from the initial network, and blue denotes simulation data from the best network. The top parameter set is used, and error bars denote standard experimental error.

## NB4

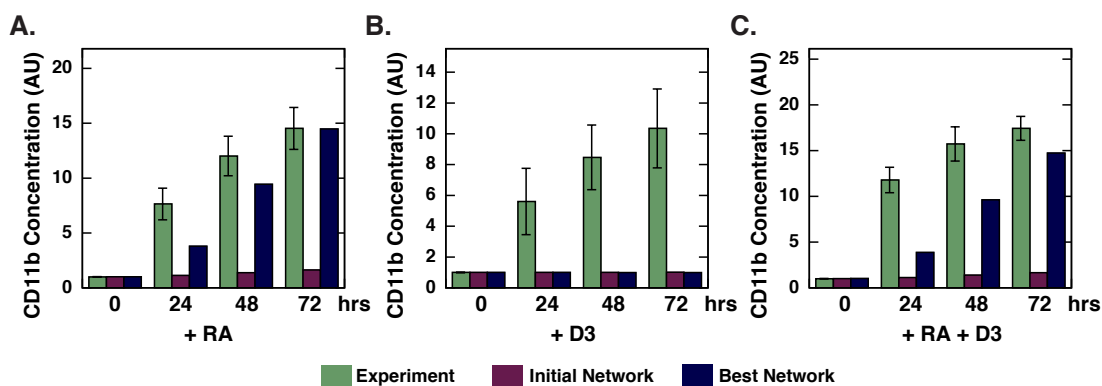


Figure 3.8: Selected training results for the NB4 cell line. **A., B., C.** Simulation and experimental results of change in CD11b concentration due to RA, D3, and RA/D3 stimulus, respectively. Green denotes experimental data, pink denotes simulation data from the initial network, and blue denotes simulation data from the best network. The top parameter set is used, and error bars denote standard experimental error.

## K562

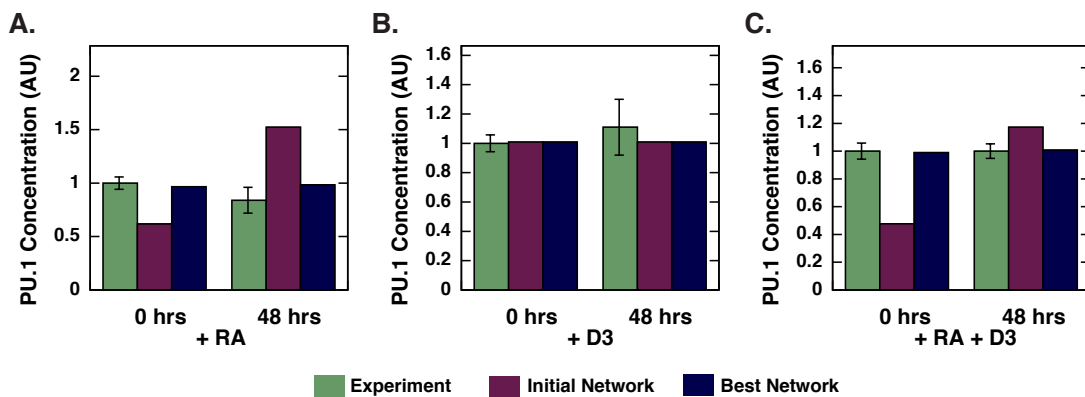


Figure 3.9: Selected training results for the K562 cell line. A., B., C. Simulation and experimental results of change in PU.1 concentration due to RA, D3, and RA/D3 stimulus, respectively. Green denotes experimental data, pink denotes simulation data from the initial network, and blue denotes simulation data from the best network. The top parameter set is used, and error bars denote standard experimental error.

### 3.3 Discussion

In this study, we developed a method for determining protein node network structures from experimental data with incomplete biological knowledge. The models described transcriptional regulation due to the input of inducers. First we were able to determine a toy three node protein network structure by searching through all possible structures and using particle swarm optimization to optimize parameters. The network structure was narrowed down to a subset of 20 models using data from one experiment and eventually found using two additional experiments. In total, 15 objective experiments were used for training and three experiments were saved for prediction. Of the top 20 network structures found many of the edges were conserved including: (1) All 20 models designated  $P_1$  as a transcription factor activator for species two, (2) 19 models showed  $P_2$  inhibits itself, (3) 20 models showed  $P_2$  as a transcriptional regulator (activator or repressor) for species three, with four having the opposite interaction (i.e. repression instead of activation), and (4) 18 models showed  $P_3$  regulated itself, but 12 of these cases are opposite (activation instead of repression). In many cases additional interactions were added. By adding data from two additional experiments to the training, we were able to narrow down the results further with the true model as the second best result. After determining the two models differed in only one additional interaction, which was essentially zero due to the kinetic parameter, we were able to exclude this interaction and therefore found the true model. One note, we were not able to find the true parameter set that was used to obtain the synthetic data with the number of iterations performed. Additional parameter estimation and the use of an ensemble of parameter sets may be necessary to find a more optimal parameter solution.

From this we determined that the correct network structure of a small transcriptional regulation network could be found with enough experimental data and model iterations.

Next we applied this method to determine transcription factor network structures for six leukemia cell lines: K562, HL60, NB4, U937, HL60 R38+ and HL60 R38-. All six cell lines have different reactions to RA, D3, and RA + D3 stimuli. RA, a current treatment for APL, is limited by RA resistance, variable efficacy in different cell types, and lack of understanding of the mechanism of action. Jensen *et al.*, studied transcriptional regulation in six leukemia cell lines to determine the changes in critical transcription factors in myelomonocytic differentiation between cell lines [122]. By using the experimental data from this study we wanted to find new network structures in each cell line and therefore, better understand the critical changes in the development of new cancer subtypes. The initial network structure curated from literature contained transcription factors as well as upstream markers for myelomonocytic lineage selection. Network perturbations included the addition and deletion of interactions as well as switching an interaction (i.e. upregulates to represses). We found new top network structures for all six cell lines and network perturbations can be found in Tables B.5 - B.10. Interestingly, there was no edge change that was consistent between all cell lines. Three network changes were made to five of six cell lines: switched or deleted AhR upregulates PU.1 (edge 100), added C/EBP $\alpha$  upregulates VDR (edge 110), and switched or deleted C/EBP $\alpha$  upregulates PU.1 (edge 118). Looking through the network perturbations we were able to find some literature evidence for a few interactions. For example upregulation of AP-1 by Oct1 was added to the network structure of four cell lines (K562, NB4, and WTHL60) and has been studied in [247]. This interaction was also added to

the HL60 R38- model, except in this case AP-1 was repressed by Oct1. By continuing to look through the data we can determine more biologically relevant interactions found in the new models. The new leukemia cell line specific transcription factor models were able to improve the fit of experimental data from a subset of experiments. Some issues that need to be resolved include the fitting of many D3 only experiments.

The initial leukemia transcription factor network was assembled after extensive literature review and hand curation of the biochemical interactions. One note was that interactions came from additional cell lines, including breast and prostate cancer, and therefore these interaction may or may not exist in leukemia cell lines. In this chapter we tried to determine new network structures by perturbing a best guess initial model network from literature. Data was limited to thirteen different proteins, out of 18 included in the model. Additional experiments with mRNA data would be useful in determining final model structures as we modeled mRNA. A population study should be performed on the flow cytometry data to see if population dynamics can be fit, not just single cell response. To improve the model network search a machine learning method could be used in which after each model perturbation error is calculated and based on this error a probability is given to the edges perturbed. For example, if we perturb edge ten and error triples, we can give the probability of making this step in the future very low. Also, it would be interesting to look at edges that have very little effect on model error. Another element that should be added to the model is the determination of granulocytic or monocytic differentiation in the cell lines in response to RA and D3 treatments. The ratio of PU.1 to C/EBPA $\alpha$  determines granulocytic vs. monocytic lineage selection [51]. CD38 and CD11b are myelomonocytic markers and CD14 is a monocytic specific marker. Overall

the goal was to determine network structures to explain varying responses to RA and D3 treatment in six leukemia cell lines. The network structures found can be studied further to determine important functional changes between cell lines.

## 3.4 Materials and Methods

### 3.4.1 Formulation of Network Model Equations

For each motif of N protein nodes, a mRNA and protein balance for each node is written as:

$$\frac{dm_j}{dt} = r_{X,j}v_{X,j} - k_{d,j}m_j - \mu m_j + \lambda \quad (3.1)$$

$$\frac{dp_j}{dt} = r_{T,j}v_{T,j} - k'_{d,j}p_j - \mu p_j \quad (3.2)$$

where  $j = 1, 2, 3 \dots N$ . Degradation rates are given as  $k_{d,j}$  and  $k'_{d,j}$ , and  $\lambda$  denotes a basal mRNA production rate.

The balances governing cellular infrastructure such as RNA polymerase (RNAP) and ribosomes (RIBO) are given by:

$$\frac{dRNAP}{dt} = (\alpha - RNAP)\mu \quad (3.3)$$

$$\frac{dRIBO}{dt} = (\beta - RIBO)\mu \quad (3.4)$$

where  $\alpha$  and  $\beta$  are constants. Balances governing a given inducer  $I_\pi$  and cellular growth rate  $\mu$ :

$$\frac{dI_z}{dt} = \delta \quad (3.5)$$

$$\frac{d\mu}{dt} = 0 \quad (3.6)$$

There are a total of  $2N + \Pi + 3$  differential equations for each motif, where  $\Pi$  is the number of inducers in the network.

The terms  $r_{X,j}$  and  $r_{T,j}$  denote the rate of transcription and translation respectively and are given by:

$$r_{X,j} = k_{X,j}(RNAP)\mu_j \quad (3.7)$$

$$r_{T,j} = k_{T,j}(RIBO)m_j\omega_j \quad (3.8)$$

where  $\mu_j$  and  $\omega_j$  describe the allocation of RNAP and RIBO resources to the expression and translation of node j:

$$\mu_j = k_{X,j}(RNAP) \left[ \sum_i k_{X,i}(RNAP) \right]^{-1} \quad (3.9)$$

$$\omega_j = k_{T,j}(RIBO)m_j \left[ \sum_i k_{T,i}(RIBO)m_i \right]^{-1} \quad (3.10)$$

The rate of expression and translation for node j is modified by control variables which describe the regulatory inputs controlling the node. One assumption is that translation is not actively regulated, thus  $v_{T,j} = 1$ . Transcription may be regulated by other proteins in the motif. If the expression of species j had m activating factors and n repressive factors, the control term was modeled as a mean:

$$v_j = \frac{\left( \sum_{i \in j^+} u_{i,j} + \sum_{i \in j^-} d_{i,j} \right)}{(m + n)} \quad (3.11)$$

where:

$$u_{ij} = f_{ij} \quad (3.12)$$

$$d_{ij} = 1 - f_{ij} \quad (3.13)$$

The quantities  $j^+$  and  $j^-$  denote the sets of activating and repressive factors for gene j. There are many possible functional forms for  $0 \leq f_{ij}(\mathcal{Z}) \leq 1$ . Each

individual transfer function took the form:

$$f_i(x) = \frac{\kappa_{ij}^\eta Z_j^\eta}{1 + \kappa_{ij}^\eta Z_j^\eta} \quad (3.14)$$

where  $Z_j$  denotes the abundance of the  $j$  factor (e.g. protein abundance), and  $\kappa_{ij}$  and  $\eta$  are control parameters. The  $\kappa_{ij}$  parameter was a gain parameter and  $\eta$  was a cooperativity parameter (similar to a Hill coefficient).

The small three protein network with one inducer contained 10 differential equations, 20 control parameters, and 15 kinetic parameters. For the small three protein network the model equations were encoded using the Python programming language and solved using the ODEINT routine of the SciPy module [125]. The leukemia transcription factor network with two inducers (RA and D3), contained 42 differential equations (RXR was included but set to zero in this case), 652 control parameters, and 90 kinetic parameters. Due to the increased size of the network, the model equations in this case were encoded using the Julia programming language [19] and solved using the CVODE solver in the SUNDIALS library [108].

### 3.4.2 Estimation of top parameter sets using Particle Swarm Optimization (PSO)

We used particle swarm optimization to estimate top parameter sets for each model. Particle swarm optimization employs a population of particles with their own coordinates, velocity and best fit error to find a global best fit error [68].

The mean squared error,  $\eta$ , of parameter set  $\mathbf{k}$  for training objective  $j$  was

defined as:

$$\eta_j(\mathbf{p}_k) = \frac{1}{N} \sum_i^N \frac{(\hat{x}_{i,j} - \beta_j x(\mathbf{p}_k)_{i,j})^2}{\hat{\sigma}_{i,j}^2} \quad (3.15)$$

The symbol  $\hat{x}_{i,j}$  denotes scaled experimental observations (from training objective j) while  $x(\mathbf{p}_k)_{i,j}$  denotes the simulation output (from training objective j). The quantity  $i$  denotes the sampled time-index or condition, and  $N$  denotes the number of time points or conditions for experiment j. The standard deviation,  $\hat{\sigma}_{i,j}$ , was calculated from at least three experimental repeats.  $\beta_j$  is a scaling factor which is required when considering experimental data that is accurate only to a multiplicative constant. In this study, the experimental data used for training and validation was typically band intensity from immunoblots, where intensity was estimated using the ImageJ software package [2]. The scaling factor used was chosen to minimize the normalized squared error [25]:

$$\beta_j = \frac{\sum_i (\hat{x}_{i,j} x_{i,j} / \hat{\sigma}_{i,j}^2)}{\sum_i (x_{i,j} / \hat{\sigma}_{i,j})^2} \quad (3.16)$$

By using the scaling factor, the concentration units on simulation results were arbitrary, which was consistent with the arbitrary units on the experimental training data. All simulation data was scaled by the corresponding  $\beta_j$ .

The cost function for the optimization problem can be expressed as:

$$\text{minimize } K(\mathbf{p}_k) = \sum_i^L \eta_j(\mathbf{p}_k) \quad (3.17)$$

where L is the number of objective functions used for training.

To begin PSO we randomly initialized a swarm of  $\mathcal{K}$ -dimensional particles (represented as  $\mathbf{x}_i$ ), which correspond to a  $\mathcal{K}$ -dimensional parameter vector. After running the necessary simulations, for each initial particle we calculated the particle error for all  $L$  objective functions, the total particle error ( $K$ ), and the velocity vector (initially set to zero). Next we determined the global best error (i.e. the lowest  $K$  value for all particles) and global best particle position. For each operation after initialization, the velocity ( $\mathbf{v}_{i,j}$ ) and position ( $\mathbf{x}_{i,j}$ ) of each particle were updated by the following equations:

$$\mathbf{v}_{i,j} = \theta \mathbf{v}_{i,j-1} + \mathcal{A} \mathbf{r}_1 (\mathcal{L}_i - \mathbf{x}_{i,j-1}) + \mathcal{B} \mathbf{r}_2 (\mathcal{G}\mathcal{L} - \mathbf{x}_{i,j-1}) \quad (3.18)$$

$$\mathbf{x}_{i,j} = \mathbf{x}_{i,j-1} + \mathbf{v}_{i,j} \quad (3.19)$$

where  $(\theta, \mathcal{A}, \mathcal{B})$  are adjustable parameters,  $\mathcal{L}_i$  denotes best local solution found by particle  $i$  up until function evaluation  $j - 1$ , and  $\mathcal{G}\mathcal{L}$  denotes the best global solution up until function evaluation  $j - 1$ . The quantities  $\mathbf{r}_1$  and  $\mathbf{r}_2$  denotes uniform random vectors with the same dimension as the number of unknown model parameters ( $\mathcal{K}x1$ ).

Again for each new particle position we calculated the particle error for all L objective functions, the total particle error (K), and the velocity vector. Using a greedy search we updated  $\mathcal{L}_i$  and  $\mathcal{GL}$  by the following rules:

```

if  $K_{i,j} < K_{best,i}$  then
     $K_{best,i} = K_{i,j}$ 
     $\mathcal{L}_i = \mathbf{x}_{i,j}$ 
    if  $K_{i,j} < K_{globalbest}$  then
         $K_{globalbest} = K_{i,j}$ 
         $\mathcal{GL} = \mathbf{x}_{i,j}$ 
    end
end

```

After J total operations we saved  $\mathcal{GL}$  and  $K_{globalbest}$  for the given model network structure.

## CHAPTER 4

### CONCLUSION AND FUTURE WORK

#### 4.0.1 Closing Remarks

Cancer is the second leading cause of death in the United States, and the probability of being diagnosed with invasive cancer is 43% for men and 38% for women [222]. One of the major obstacles of overcoming cancer has been the complexity of the biological systems involved. A computational modeling approach in combination with experiments should be used to understand the complex biology behind cancer. We must develop a better understanding of mechanisms involved to determine the development of drug resistance in cancers, predict combination therapies, and determine individualized treatment for cancer patients. Many mutations have been discovered in cancer to change cellular network responses, but the overall effects of these changes may be unknown, with small changes having broad-reaching effects [22]. Modeling approaches have been used to study p53, ErbB receptors, RAS, TGF- $\beta$ , and intracellular receptors, such as AR and RAR [140, 241, 242]. One promising drug candidate, MM-121, a human monoclonal antibody against ErbB3, was developed after revealing through sensitivity analysis that ErbB3 was a key node in their computational model of the ErbB signaling network [215]. The combination of experimental and computational methods is essential to understanding and treating cancer.

This work paired the use of computational models and experiments to determine the development of cancer subtypes in prostate cancer (ADPC vs CRPC) and leukemia (RA and D3 resistant subtypes). First we developed and analyzed

a population of mathematical models describing growth factor and hormone signal integration in androgen dependent, intermediate and resistant prostate cancer cells. The model described the integration of two simultaneous extracellular signaling inputs, androgen and mitogenic growth factors. Model parameters were identified from 43 studies in androgen dependent and resistant LNCaP cell lines. The model was validated by comparing simulations with an additional 29 data sets from LNCaP cell lines that were not used during training. Additionally, data from four drug trials was also used to evaluate the models performance. Sensitivity and robustness analysis, conducted over the population of prostate signaling models, suggested that simultaneously targeting the PI3K and MAPK pathways in addition to anti-androgen therapies could be an effective treatment for CRPC. We tested this hypothesis in both ADPC LNCaP cell lines and LNCaP derived CRPC C4-2 cells using three inhibitors: the androgen receptor inhibitor MDV3100 (enzalutamide), the Raf kinase inhibitor sorafenib, and the PI3K inhibitor LY294002. Consistent with model predictions, cell viability decreased at 72 hrs in the dual and triple inhibition cases in both the LNCaP and C4-2 cell lines. Additionally we observed crosstalk between regulatory pathways, as addition of inhibitors for one pathway increased activation of other pathways. These results suggest combination treatments are necessary to overcome the crosstalk between cell signaling pathways in prostate cancer.

The reverse engineering of biological networks has been studied in numerous contexts. It has been used in cancer networks to predict cancer outcomes, provide hypotheses for tumor progression, and explore cancer biomarkers [257]. One of the problems in reverse engineering is discriminating between model variants which accurately describe the experimental data [141]. In this study we determined that a network structure for a three node protein tran-

scription network could be found using sufficient experimental data. A good fit structure was found using only one experiment and two additional experiments were necessary to determine the correct model structure. The six leukemia cell lines, K562, HL60, NB4, U937, HL60 R38+ and HL60 R38-, have different responses to RA and D3 stimuli. Typically RA treatment leads to monocytic differentiation and D3 leads to granulocytic differentiation. The experiment results from Jensen *et al.* suggest that lineage determining transcription factors do not behave as expected and the mechanisms are unknown [122]. To determine the mechanisms involved we developed a 18 node transcription factor network of leukemia including CD38 and CD11b (myelomonocytic markers) and CD14 (monocytic specific marker). The model was simplified to exclude additional signaling interactions such as RXR dimerization with RAR and VDR. We determined better network structures from perturbation of an original best guess model. Additional work should be done to find better fits for certain experiments and network changes should be studied to see if they are all necessary for improvement of the model performance.

## Potential Future Projects

***Continue to test dual and triple inhibition in prostate cancer.*** It would be interesting to look at additional cell lines, such as CWR22v1 cells which have higher basal pERK expression and lower basal pAKT expression then LNCaP and C4-2 cells. Mouse studies in androgen dependent and castration resistant mice should also be performed. Also, AR activity should be measured in additional ways other then AR expression levels, including the use of an ARE-Luciferase reporter and qRT-PCR of androgen-regulated genes, such as PSA, Pbsn, and

Nkx3.1. It would also be interesting to look at the response of the cells to the drugs with the addition of DHT to the cells.

*Experimentally determine the role of EGF in prostate cancer signaling.* Identifying the mechanisms responsible for EGF regulation of AR and AR targeted genes could be of significance. To do this multiple prostate cancer cell lines, including LNCaP C-33, LNCaP C-81, CWR-R1, and C4-2, should be used to test whether EGF leads to a decrease in AR activation and expression levels. Since EGF is known to activate the PI3K/Akt pathway as well as the MAPK pathway, we would inhibit both pathways. The mRNA levels of AR as well as protein levels should be measured to determine if the decrease in AR expression levels is due to decreased stability of the AR protein or an increase in AR mRNA degradation. Through these studies we hope to determine the downstream effects of EGF on AR and the signaling pathways involved in different prostate cancer cell lines.

*Computationally determine the role of EGF in prostate cancer signaling.* In addition to experimentally identifying the mechanisms responsible for EGF regulation of AR and AR targeted genes, we could look at altered network structures to see if we can fit the data. This would be similar to the network identification problem in chapter 3.

*Improve model identification method.* The model identification method could be improved by adding a machine learning element to the algorithm. Currently we are just accepting models that are better than the current best model structure. Instead it might be more useful to look at the change in error response due to the perturbation and add an additional probability of choosing those perturbations in the future based on change in error. Also, it would be useful to find

a method to determine new experimental data necessary to find a better model structure. Additional experiments, such as mRNA data, may be necessary to determine correct model structures.

***Improve leukemia transcription factor models by using a population approach.*** Currently, we did not look at a population approach for fitting parameter data. For flow cytometry data in particular, a population approach may be able to fit the shifts in cell population responses better. Also, a population approach instead of a best fit solution, may improve data fits for the western blot data.

***Add a lineage component to the leukemia transcription factor model.*** Typically RA treatment leads to monocytic differentiation and D3 leads to granulocytic differentiation. As we saw, this may be cell line dependent and lineage direction may be dependent on specific levels of RA and D3 in combinations of the two stimuli. The ratio of PU.1 to C/EBPA $\alpha$  determines granulocytic vs. monocytic lineage selection [51]. CD38 and CD11b are myelomonocytic markers and CD14 is a monocytic specific marker. Using this information we may be able to add a function to the model that will determine lineage direction after a stimulus is added based on protein levels.

APPENDIX A  
CHAPTER 1 OF APPENDIX

## **Estimation of a population of models using Pareto Optimal Ensemble Techniques (POETs).**

We used multiobjective optimization to estimate an ensemble of prostate models. Although computationally more complex than single-objective formulations, multiobjective optimization can be used to address qualitative conflicts in training data arising from experimental error or cell-line artifacts [97]. In this study we used the Pareto Optimal Ensemble Technique (POETs) to perform the optimization. POETs integrates standard search strategies, e.g., Simulated Annealing (SA) or Local Pattern Search (PS) with a Pareto-rank fitness assignment [227]. The mean squared error,  $\eta$ , of parameter set  $\mathbf{k}$  for training objective  $j$  was defined as:

$$\eta_j(\mathbf{p}_k) = \frac{1}{N} \sum_i^N \frac{(\hat{x}_{i,j} - \beta_j x(\mathbf{p}_k)_{i,j})^2}{\hat{\sigma}_{i,j}^2} \quad (\text{A.1})$$

The symbol  $\hat{x}_{i,j}$  denotes scaled experimental observations (from training objective  $j$ ) while  $x(\mathbf{p}_k)_{i,j}$  denotes the simulation output (from training objective  $j$ ). The quantity  $i$  denotes the sampled time-index or condition, and  $N$  denotes the number of time points or conditions for experiment  $j$ . The standard deviation,  $\hat{\sigma}_{i,j}$ , was assumed to be equal to 10% of the reported observation, if no experimental error was reported.  $\beta_j$  is a scaling factor which is required when considering experimental data that is accurate only to a multiplicative constant. In this study, the experimental data used for training and validation was typically

band intensity from immunoblots, where intensity was estimated using the ImageJ software package [2]. The scaling factor used was chosen to minimize the normalized squared error [25]:

$$\beta_j = \frac{\sum_i (\hat{x}_{i,j} x_{i,j} / \hat{\sigma}_{i,j}^2)}{\sum_i (x_{i,j} / \hat{\sigma}_{i,j})^2} \quad (\text{A.2})$$

By using the scaling factor, the concentration units on simulation results were arbitrary, which was consistent with the arbitrary units on the experimental training data. All simulation data was scaled by the corresponding  $\beta_j$ .

We computed the Pareto rank of parameter set  $\mathbf{k}_{i+1}$  by comparing the simulation error at iteration  $i + 1$  against the simulation archive, denoted as  $\mathbf{K}_i$ . We used the Fonseca and Fleming ranking scheme [74] to estimate the rank of the parameter set  $\mathbf{k}_{i+1}$ . Parameter sets with increasing rank are progressively further away from the optimal trade-off surface. The parameter set  $\mathbf{k}_{i+1}$  was accepted or rejected by the SA with probability  $\mathcal{P}(\mathbf{k}_{i+1})$ :

$$\mathcal{P}(\mathbf{k}_{i+1}) \equiv \exp \{-\text{rank}(\mathbf{k}_{i+1} | \mathbf{K}_i) / T\} \quad (\text{A.3})$$

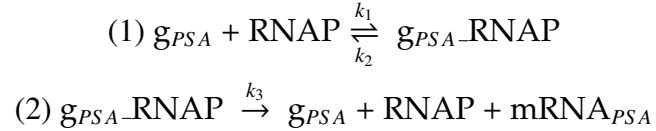
where  $T$  is the computational annealing temperature. The Pareto rank for  $\mathbf{k}_{i+1}$  is denoted by  $\text{rank}(\mathbf{k}_{i+1} | \mathbf{K}_i)$ . The annealing temperature was adjusted according to the schedule  $T_k = \beta^k T_0$  where  $\beta$  was defined as  $\beta = \left(\frac{T_f}{T_o}\right)^{1/10}$ . The initial temperature was given by  $T_0 = n/\log(2)$ , with  $n = 4$  and the final temperature  $T_f = 0.1$  used in this study. The epoch-counter  $k$  was incremented after the addition of 50 members to the ensemble. As the ensemble grew, the likelihood of accepting a high rank set decreased. Parameter sets were generated by applying a random perturbation in log space:

$$\log \mathbf{k}_{i+1} = \log \mathbf{k}_i + \mathcal{N}(0, \nu) \quad (\text{A.4})$$

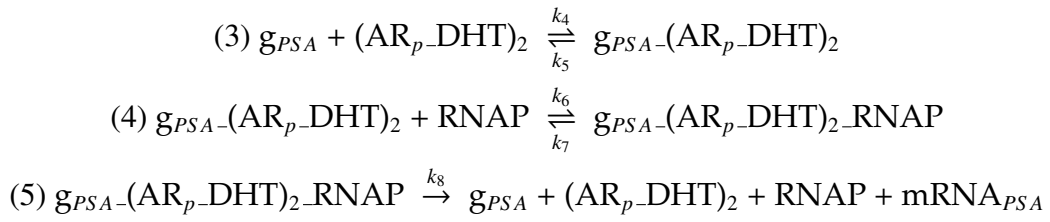
where  $\mathcal{N}(0, \nu)$  is a normally distributed random number with zero mean and variance  $\nu$ , set as 0.1 in this model. The perturbation was applied in log space to account for large variation in parameter scales and to ensure positive parameter values. We used a local pattern search every  $q$  steps, in our case 20, to minimize error for a single randomly selected objective. The local pattern-search algorithm used has been described previously [81].

## Translation and Transcription Template

We utilized the following template for the transcription of genes in the network without a transcription factor:



and with a transcription factor:



RNAP denotes RNA polymerase. Next translation was modeled by the following, where Ribo denotes ribosome:

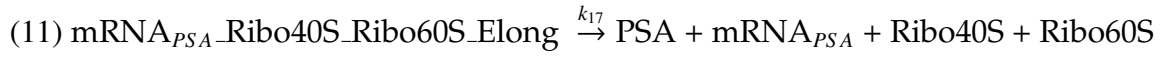
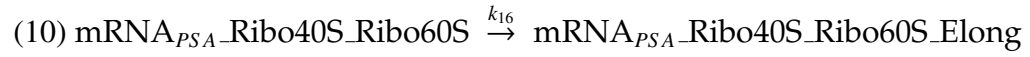
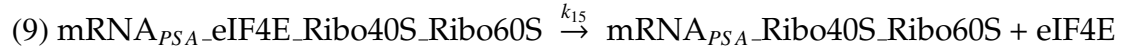
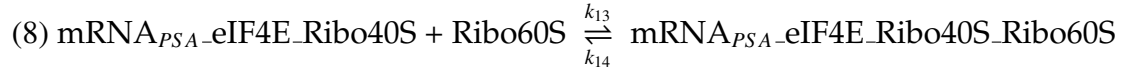
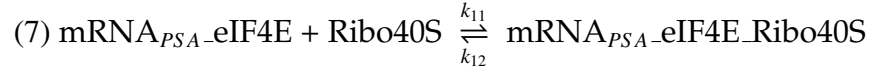
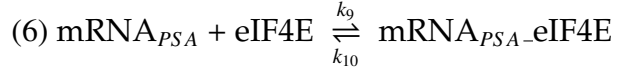


Table A.1: Objective function list along with species measured, stimulus, cell-type, steady state (SS) vs dynamic (D) and the corresponding literature reference.

O#	Species	Cell Type	Stimulus	SS or D	Source
O1	PSA	C33/C81	0	SS	[147]
O2	PSA	C33	DHT	D	[147]
O3	PSA	C81	DHT	D	[147]
O4	ERK-p	C33	DHT	D	[147]
O5	ERK-p	C81	DHT	D	[147]
O6	PSA	C33	HER2 Knockdown	SS	[147]
O7	PSA	C81	HER2 Knockdown	SS	[147]
O8	PSA	C33	MEK Up	SS	[147]
O9	PSA	C81	MEK Down	SS	[147]
O10	PSA	C33	HER2 Up	SS	[147]
O11	ERK-p	C33	HER2 Up	SS	[147]
O12	AR	C33/C51/C81	0	SS	[154]
O13	PAcP mRNA	C33	DHT	D	[154]
O14	PAcP mRNA	C51	DHT	D	[154]
O15	PAcP mRNA	C81	DHT	D	[154]
O16	HER2-p	C33/C51/C81	0	SS	[273]
O17	Cyclin D	C33/C81	0	SS	CITE
O18	Cyclin D	C33	EGF	D	[190]
O19	Cyclin D mRNA	C33	EGF	D	[190]
O20	AKT-p	C51/LNCaP-Rf	0	SS	[178]
O21	p27Kip1	C51/LNCaP-Rf	0	SS	[178]
O22	p21Cip1	C51/LNCaP-Rf	0	SS	[178]
O23	Rb-p	C33	DHT	D	[268]
O24	p70-p	C33	DHT	D	[268]
O25	p21Cip1	C33	DHT	D	[139]

O26	p27Kip1	C33	DHT	D	[139]
O27	PSA mRNA	C33	Cyclin E Up + DHT	D	[269]
O28	AR mRNA	C33	Cyclin E Up + DHT	D	[269]
O29	PSA mRNA	C33	HER2 Up	SS	[271]
O30	AKT-p	C33/C51	0	SS	[153]
O31	AR	C51	DHT	D	[153]
O32	AR	C33	DHT	D	[41]
O33	Cyclin D1b mRNA	C33	Sam68 Knockdown	SS	[187]
O34	AR mRNA	C33	E2F Up	SS	[56]
O35	AR	C33	E2F Up	SS	[56]
O36	AR Cyclin E	C33	E2F Up	SS	[56]
O37	PSA	C33	E2F Up	SS	[56]
O38	cPAcP	C33	DHT	D	[172]
O39	Cyclin D	C33	DHT	D	[268]
O40	4EBP1-p	C33	DHT	D	[268]
O41*	PAcP mRNA	C33/C51/C81	0	SS	[154]
O42*	p16INK4	C51/C81	0	SS	[178]
O43*	cPAcP	C33/C51/C81	0	SS	[155]

Table A.2: Blind Prediction list along with species measured, stimulus, cell-type, steady state (SS) vs dynamic (D) and the corresponding literature reference.

Prediction#	Species	Cell Type	Stimulus	SS or D	Source
P1	HER2-p	C33	DHT	D	[172]
P2	p27Kip1	C33	SHP Knockdown	D	[201]
P3	ERK-p	C33	PAcP Knockdown	SS	[44]
P4	AKT-p	C33	PAcP Knockdown	SS	[44]
P5	Cyclin D1	C33	PAcP Knockdown	SS	[44]
P6	EGFR-p	C33	EGF	D	[40]
P7	HER2-p	C33	EGF	D	[40]
P8	EGFR-p	LNCaP-AI	EGF	D	[40]
P9	HER2-p	LNCaP-AI	EGF	D	[40]
P10	CyclinE	C33	DHT	D	[139]
P11	CDK2	C33	DHT	D	[139]
P12	HER2-p	C33/C81	0	SS	[44]
P13	AR	C33	EGF	D	[32]
P14	AR	C33	EGF	D	[46]
P15	p27Kip1	C33	DHT	D	[69]
P16	Rb-p	C33	DHT	D	[139]
P17	AR	C33	DHT	D	[32]
P18	AKT-p	C33	DHT	D	[32]
P19	PSA	C33	EGF + DHT	D	[32]
P20	PSA	C33	EGF	D	[32]
P21	Cyclin D1	C33	Sam68 Knockdown	SS	[30]
P22	Shc	C33	DHT	D	[252]
P23	Shc	C33	EGF	D	[252]
P24	Shc	C33/C81	0	SS	[252]
P25	AR	C33	AKT-p Knockdown	SS	[92]
P26	AR	LNCaP AI	AKT-p Knockdown	SS	[92]

P27	4EBP1 bound eIF4E	C33/LNAI	0	SS	[88]
P28	Shc-p	C33/C51/C81	0	SS	[146]
P29	Shc-p	C33	EGF	D	[146]
P30	PSA Response	CRPC Patients	enzalutamide	D	[213]
P31	PSA Response	CRPC Patients	sorafenib	D	[52]
P32	PSA Response	CRPC Patients	lapatinib	D	[263]
P33	PSA Response	ADPC Patients	lapatinib	D	[157]

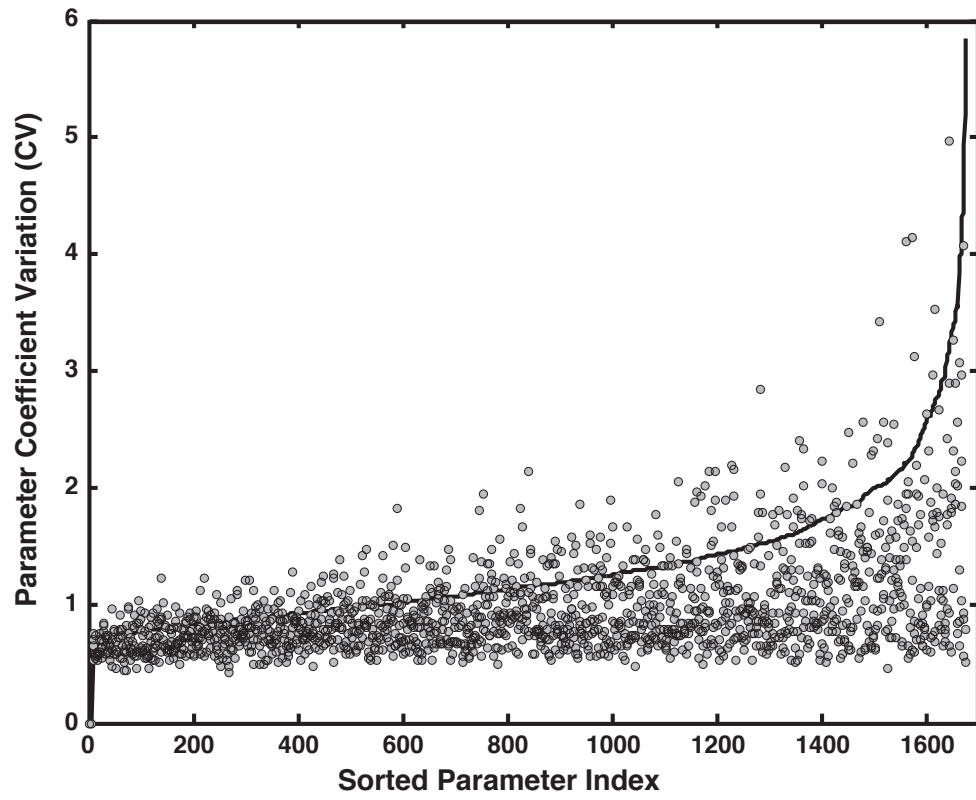


Figure A.1: Coefficient of variation (CV) of model parameters estimated using POETs. The solid line denotes the mean CV calculated over the entire ensemble ( $N = 5000$ ). The points denote the mean CV of the 500 ensemble members used for sensitivity and robustness calculations. Over the ensemble, the coefficient of variation (CV) of the kinetic parameters spanned 0.59 - 5.8, with 33% of the parameters having a CV of less than one.

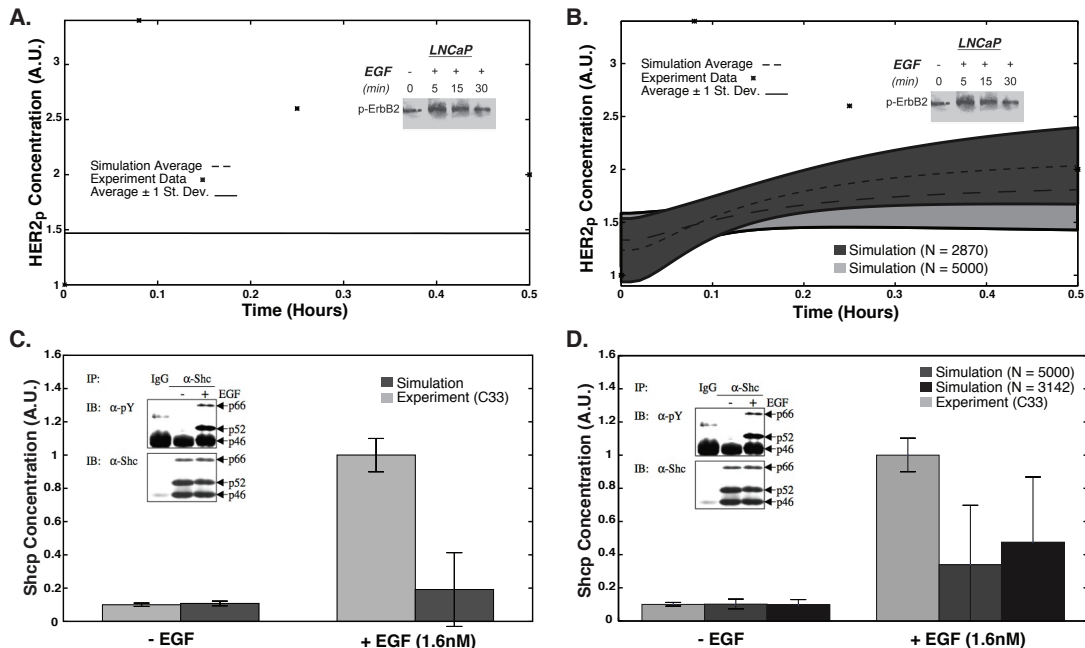
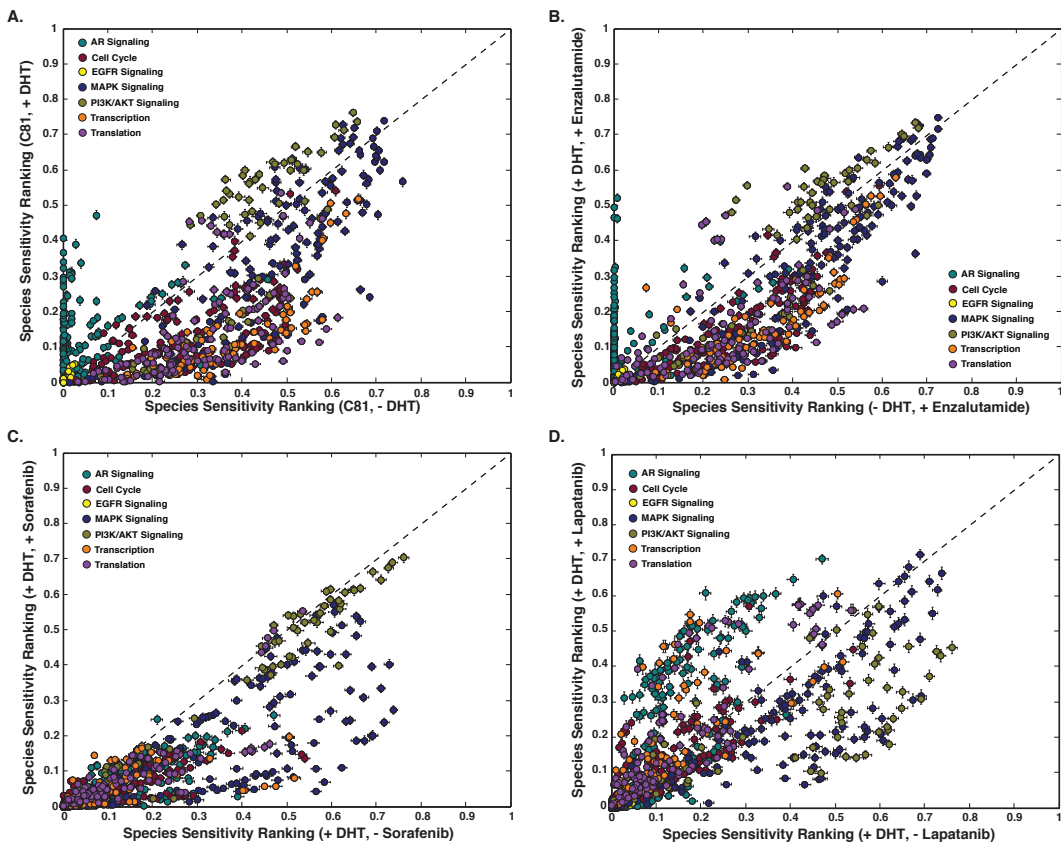


Figure A.2: Blind model predictions for the ensemble with the original and updated model (EGFR and HER2 heterodimer). **A, B.** Time course data for HER2 phosphorylation due to a stimulus of 1.6 nM EGF (LNCaP C-33, P7) for the old and new model, respectively. Dark grey shows only parameters improved by the updated model ( $N=2870$ ) while light grey show all parameter sets ( $N=5000$ ). **C, D.** Shc phosphorylation levels at 16 hrs in the presence and absence of 1.6 nM EGF (LNCaP C-33, P29) for the old and new model, respectively. Light grey denotes experimental data, mid grey denotes simulation results for all parameters ( $N=5000$ ), and black denotes only parameters improved by the updated model ( $N=3142$ ). Error bars denote plus and minus one standard deviation above the mean.



**Figure A.3:** Sensitivity analysis of a population of prostate models ( $N = 500$ ). Species with a low sensitivity are considered robust, while species with a high sensitivity ranking are considered fragile. **A.** Sensitivity ranking of network species in CR cells in the absence and presence of DHT. **B.** Sensitivity ranking of network species in CR cells in the presence of enzalutamide in the presence and absence of a DHT stimulus. **C., D.** Sensitivity ranking of network species in CR cells in the presence and absence of sorafenib and lapatinib, respectively, with a DHT stimulus. Error bars denote standard error with  $N = 500$ .

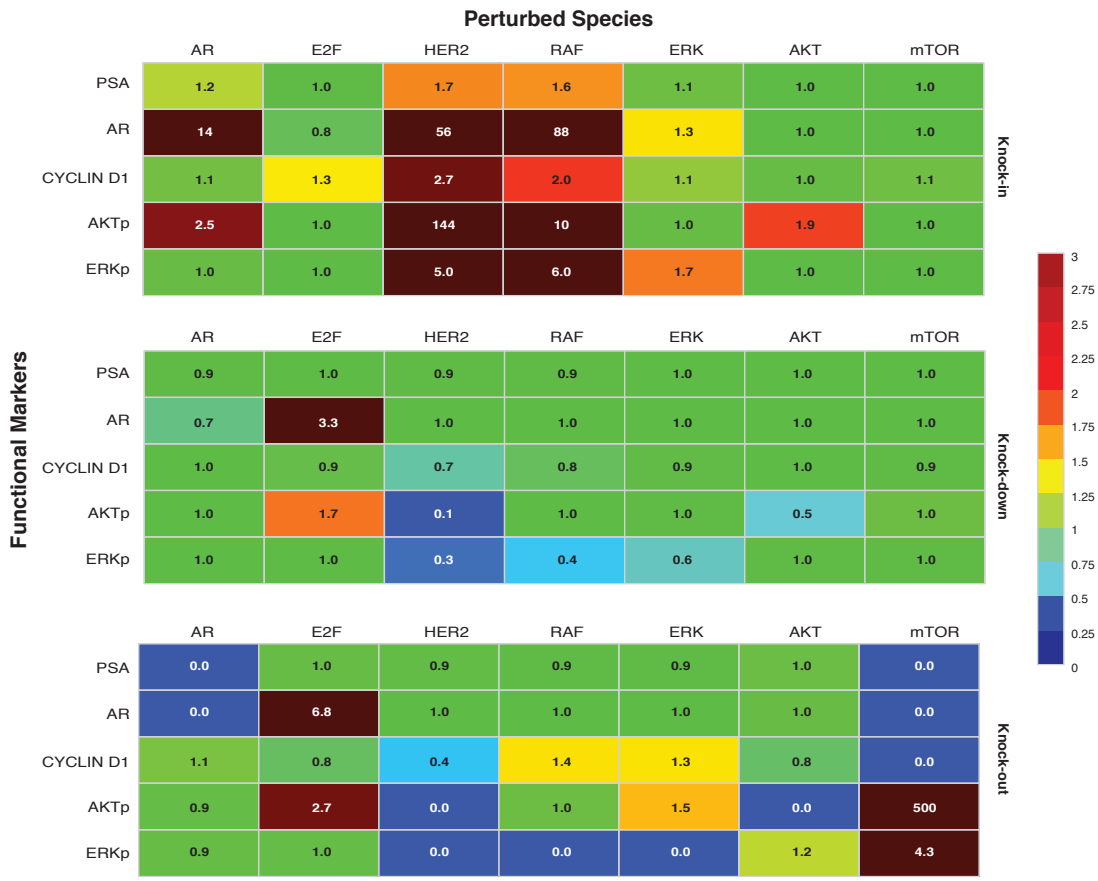


Figure A.4: Robustness analysis of protein markers. Expression level of key proteins was altered by a factor of 2, 0.1, or 0 (knock-in, knock-down, or knock-out) and robustness coefficients were calculated for five key protein markers. Simulations shown were from CR cells, with indicated perturbation. Mean of 500 ensemble members is shown.

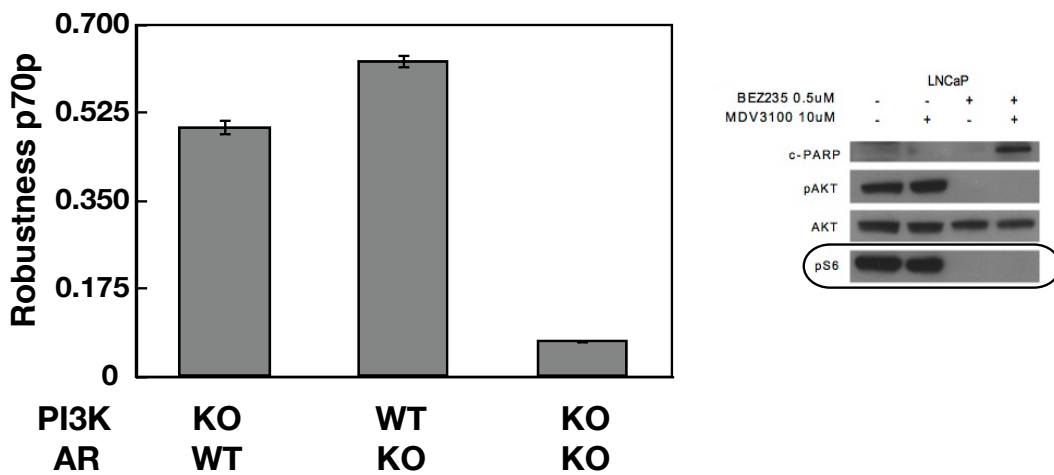


Figure A.5: Dual knock-out of AR and PI3K leads to decreased expression of activated p70. A., B, C. Robustness coefficient of activated p70 (S6) in the PI3K knock-out, AR knock-out, and dual knock-out cases, respectively. The control was the basal CR LNCaP wild type case. Error bars denote plus and minus one standard error above the mean with N = 500. Experimental data is from Carver, *et al.* [34].

**APPENDIX B**  
**CHAPTER 2 OF APPENDIX**

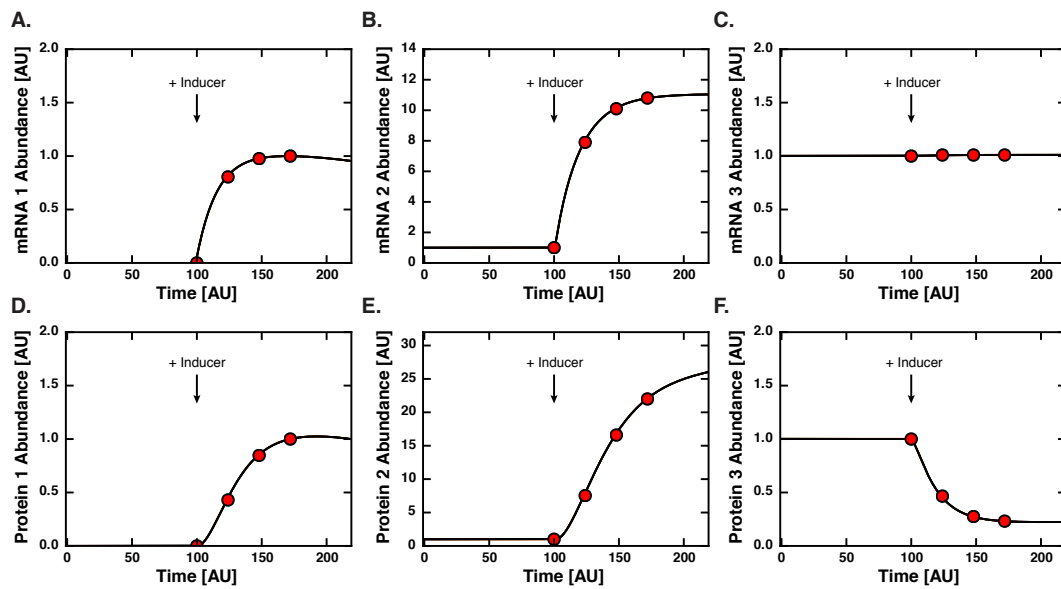


Figure B.1: Synthetic data running experiment 1 for true model of three node protein network. In experiment 1, inducer was added at Time = 100. **A, B, C.** Plots of mRNA concentration profiles for species 1, 2, and 3 after inducer added at Time = 100. **D, E, F.** Plots of protein concentration profiles for species 1, 2, and 3. Red dots denote data used for fitting (0, 24, 48, and 72 AU after stimulus).

Table B.1: Training objective function list with objective number, species measured, experiment and trials used in

Objective #	Species	Experiment #	Trial
O1	$mRNA_1$	Exp1	1, 2
O2	$mRNA_2$	Exp1	1, 2
O3	$mRNA_3$	Exp1	1, 2
O4	$P_2$	Exp1	1, 2
O5	$P_3$	Exp1	1, 2
O6	$mRNA_1$	Exp2	2
O7	$mRNA_2$	Exp2	2
O8	$P_1$	Exp2	2
O9	$P_2$	Exp2	2
O10	$P_3$	Exp2	2
O11	$mRNA_1$	Exp3	2
O12	$mRNA_2$	Exp3	2
O13	$mRNA_3$	Exp3	2
O14	$P_1$	Exp3	2
O15	$P_3$	Exp3	2

Table B.2: Prediction function list with prediction number, species measured, experiment and trials used in

Prediction #	Species	Experiment #	Trial
P1	$P_1$	Exp1	1, 2
P2	$mRNA_3$	Exp2	2
P3	$P_2$	Exp2	2

Table B.3: Experiment list with stimulus, species for training, and species for validation

Experiment #	Stimulus	Training Species	Validation Species
1	At t = 100, Inducer = +10	$mRNA_1, mRNA_2, mRNA_3,$ $P_2, P_3$	$P_1$
2	At t = 100, Inducer = +10 and inhibit binding of protein 2	$mRNA_1, mRNA_2, P_1, P_2,$ $P_3$	$mRNA_3$
3	At t = 100, 124, 148, 172, 196, Inducer = +1	$mRNA_1, mRNA_2, mRNA_3,$ $P_1, P_3$	$P_2$

Table B.4: Training objective function list with objective number, species measured, stimulus, and time points. The same 39 objective functions were used for all cell lines with data from [122].

Objective #	Species Measured	Stimulus	Time Point (hrs)
O1	C/EBP $\alpha$	1 $\mu$ M RA	48
O2	PU.1	1 $\mu$ M RA	48
O3	EGR1	1 $\mu$ M RA	48
O4	Gfi-1	1 $\mu$ M RA	48
O5	RAR $\alpha$	1 $\mu$ M RA	48
O6	VDR	1 $\mu$ M RA	48
O7	IRF-1	1 $\mu$ M RA	48
O8	Oct4	1 $\mu$ M RA	48
O9	AhR	1 $\mu$ M RA	48
O10	CD38	1 $\mu$ M RA	24, 48, 72
O11	CD11b	1 $\mu$ M RA	24, 48, 72
O12	CD14	1 $\mu$ M RA	24, 48, 72
O13	G1/G0	1 $\mu$ M RA	24, 48, 72
O14	C/EBP $\alpha$	0.5 $\mu$ M VD3	48
O15	PU.1	0.5 $\mu$ M VD3	48
O16	EGR1	0.5 $\mu$ M VD3	48
O17	Gfi-1	0.5 $\mu$ M VD3	48
O18	RAR $\alpha$	0.5 $\mu$ M VD3	48
O19	VDR	0.5 $\mu$ M VD3	48
O20	IRF-1	0.5 $\mu$ M VD3	48
O21	Oct4	0.5 $\mu$ M VD3	48
O22	AhR	0.5 $\mu$ M VD3	48
O23	CD38	0.5 $\mu$ M VD3	24, 48, 72
O24	CD11b	0.5 $\mu$ M VD3	24, 48, 72
O25	CD14	0.5 $\mu$ M VD3	24, 48, 72
O26	G1/G0	0.5 $\mu$ M VD3	24, 48, 72

O27	C/EBP $\alpha$	1 $\mu$ M RA, 0.5 $\mu$ M VD3	48
O28	PU.1	1 $\mu$ M RA, 0.5 $\mu$ M VD3	48
O29	EGR1	1 $\mu$ M RA, 0.5 $\mu$ M VD3	48
O30	Gfi-1	1 $\mu$ M RA, 0.5 $\mu$ M VD3	48
O31	RAR $\alpha$	1 $\mu$ M RA, 0.5 $\mu$ M VD3	48
O32	VDR	1 $\mu$ M RA, 0.5 $\mu$ M VD3	48
O33	IRF-1	1 $\mu$ M RA, 0.5 $\mu$ M VD3	48
O34	Oct4	1 $\mu$ M RA, 0.5 $\mu$ M VD3	48
O35	AhR	1 $\mu$ M RA, 0.5 $\mu$ M VD3	48
O36	CD38	1 $\mu$ M RA, 0.5 $\mu$ M VD3	24, 48, 72
O37	CD11b	1 $\mu$ M RA, 0.5 $\mu$ M VD3	24, 48, 72
O38	CD14	1 $\mu$ M RA, 0.5 $\mu$ M VD3	24, 48, 72
O39	G1/G0	1 $\mu$ M RA, 0.5 $\mu$ M VD3	24, 48, 72

## U937

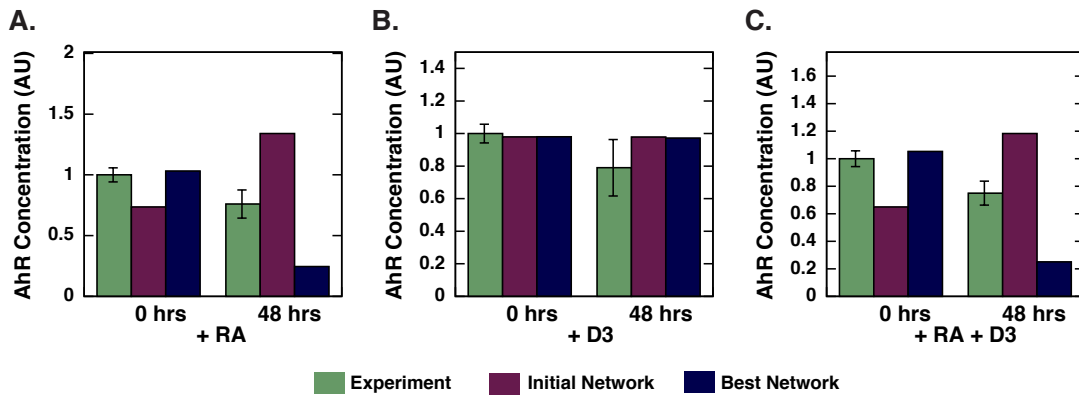


Figure B.2: Selected training results for the U937 cell line. A., B., C. Simulation and experimental results of change in AhR concentration due to RA, D3, and RA/D3 stimulus, respectively. Green denotes experimental data, pink denotes simulation data from the initial network, and blue denotes simulation data from the best network. The top parameter set is used, and error bars denote standard experimental error.

### HL60 R38+

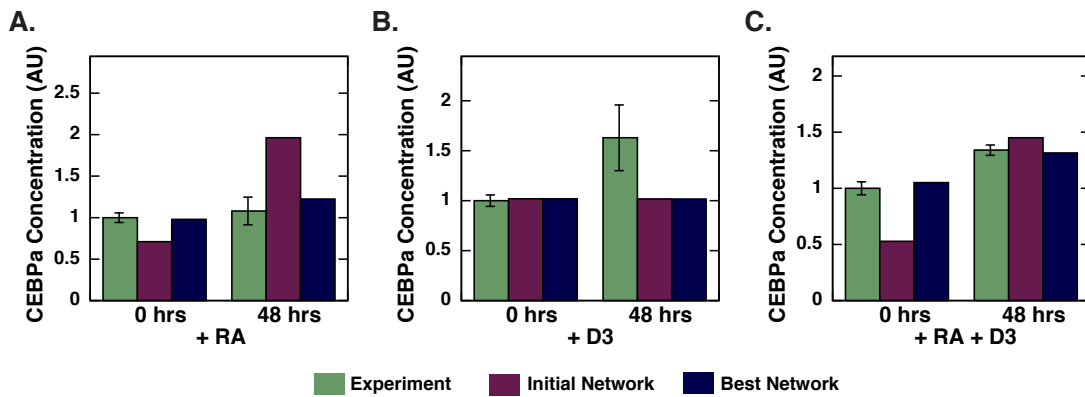


Figure B.3: Selected training results for the HL60 R38+ cell line. A., B., C. Simulation and experimental results of change in C/EBP $\alpha$  concentration due to RA, D3, and RA/D3 stimulus, respectively. Green denotes experimental data, pink denotes simulation data from the initial network, and blue denotes simulation data from the best network. The top parameter set is used, and error bars denote standard experimental error.

Table B.5: Model Updates for K562 cell line with edge number, action, transcription factor, general effect, target gene, and new references

Edge Number	Action	Transcription Factor	General Effect	Target Gene	Reference(s)
6	deleted	RAR $\alpha$	upregulates	AhR	
7	deleted	RAR $\alpha$	upregulates	C/EBP $\alpha$	
8	added	RAR $\alpha$	represses	Gfi-1	
9	deleted	RAR $\alpha$	upregulates	EGR1	
11	added	RAR $\alpha$	represses	AP-1	[18]
14	added	RAR $\alpha$	represses	CD14	
20	added	VDR	represses	VDR	
22	added	VDR	upregulates	IRF-1	
23	added	VDR	represses	Oct1	
25	added	VDR	represses	C/EBP $\alpha$	
27	added	VDR	represses	EGR1	
31	added	VDR	represses	CD11b	
32	added	VDR	upregulates	CD14	[204]
34	added	VDR	upregulates	E2F	
38	added	PPAR $\gamma$	upregulates	VDR	
49	added	PPAR $\gamma$	represses	CD11b	
50	deleted	PPAR $\gamma$	upregulates	CD14	
52	deleted	PPAR $\gamma$	represses	E2F	
56	added	IRF-1	represses	VDR	
59	added	IRF-1	upregulates	Oct1	
61	added	IRF-1	upregulates	C/EBP $\alpha$	
63	added	IRF-1	upregulates	EGR1	
64	added	IRF-1	represses	PU.1	
65	added	IRF-1	represses	AP-1	
67	added	IRF-1	upregulates	CD11b	
70	added	IRF-1	upregulates	E2F	
76	added	Oct1	represses	IRF-1	
77	added	Oct1	represses	Oct1	
78	added	Oct1	upregulates	AhR	
82	deleted	Oct1	upregulates	PU.1	
83	added	Oct1	upregulates	AP-1	[247]
86	added	Oct1	upregulates	CD14	
87	added	Oct1	represses	p21	
88	added	Oct1	upregulates	E2F	

89	added	Oct1	represses	p47phox	
90	added	Oct1	represses	Oct4	
92	added	AhR	upregulates	VDR	
97	added	AhR	represses	C/EBP $\alpha$	
99	added	AhR	upregulates	EGR1	[169]
102	added	AhR	represses	CD38	
107	added	AhR	upregulates	p47phox	
110	added	C/EBP $\alpha$	represses	VDR	
117	added	C/EBP $\alpha$	represses	EGR1	[100]
118	deleted	C/EBP $\alpha$	upregulates	PU.1	
121	added	C/EBP $\alpha$	upregulates	CD11b	
122	switched	C/EBP $\alpha$	represses	CD14	
128	added	Gfi-1	represses	VDR	
129	added	Gfi-1	represses	PPAR $\gamma$	
130	added	Gfi-1	represses	IRF-1	
134	added	Gfi-1	represses	Gfi-1	[63]
141	deleted	Gfi-1	represses	p21	
144	added	Gfi-1	represses	Oct4	
146	added	EGR1	represses	VDR	
147	switched	EGR1	represses	PPAR $\gamma$	
150	added	EGR1	upregulates	AhR	
155	added	EGR1	upregulates	AP-1	
157	added	EGR1	upregulates	CD11b	
162	added	EGR1	represses	Oct4	
164	deleted	PU.1	upregulates	VDR	
168	added	PU.1	represses	AhR	
169	added	PU.1	represses	C/EBP $\alpha$	
170	added	PU.1	upregulates	Gfi-1	[143]
173	deleted	PU.1	upregulates	AP-1	
174	added	PU.1	represses	CD38	
177	deleted	PU.1	upregulates	p21	
178	added	PU.1	upregulates	E2F	
179	switched	PU.1	represses	p47phox	
180	added	PU.1	upregulates	Oct4	
182	switched	AP-1	represses	VDR	
184	added	AP-1	upregulates	IRF-1	
187	deleted	AP-1	represses	C/EBP $\alpha$	
188	added	AP-1	upregulates	Gfi-1	

189	added	AP-1	upregulates	EGR1	
195	switched	AP-1	represses	p21	
198	added	AP-1	represses	Oct4	
255	added	p21	represses	PPAR $\gamma$	
257	added	p21	upregulates	Oct1	
258	added	p21	represses	AhR	
259	added	p21	represses	C/EBP $\alpha$	
260	added	p21	represses	Gfi-1	
263	added	p21	upregulates	AP-1	
265	added	p21	represses	CD11b	
274	added	E2F	upregulates	IRF-1	
275	added	E2F	represses	Oct1	
276	added	E2F	represses	AhR	
277	added	E2F	represses	C/EBP $\alpha$	[275]
279	added	E2F	upregulates	EGR1	
280	added	E2F	represses	PU.1	
281	added	E2F	represses	AP-1	
282	added	E2F	upregulates	CD38	
283	added	E2F	represses	CD11b	
284	added	E2F	represses	CD14	
286	switched	E2F	represses	E2F	
287	added	E2F	upregulates	p47phox	
313	added	Oct4	upregulates	C/EBP $\alpha$	
318	added	Oct4	represses	CD38	
319	added	Oct4	upregulates	CD11b	
320	added	Oct4	upregulates	CD14	
322	added	Oct4	represses	E2F	
324	added	Oct4	represses	Oct4	

Table B.6: Model Updates for NB4 cell line with edge number, action, transcription factor, general effect, target gene, and new references

Edge Number	Action	Transcription Factor	General Effect	Target Gene	Reference(s)
3	added	RAR $\alpha$	represses	PPAR $\gamma$	
6	deleted	RAR $\alpha$	upregulates	AhR	
9	switched	RAR $\alpha$	represses	EGR1	
10	switched	RAR $\alpha$	represses	PU.1	
11	added	RAR $\alpha$	upregulates	AP-1	
13	added	RAR $\alpha$	upregulates	CD11b	
16	added	RAR $\alpha$	represses	E2F	
17	added	RAR $\alpha$	upregulates	p47phox	[14]
18	switched	RAR $\alpha$	upregulates	Oct4	[17]
22	added	VDR	represses	IRF-1	
24	added	VDR	upregulates	AhR	
26	added	VDR	upregulates	Gfi-1	
36	added	VDR	upregulates	Oct4	
38	added	PPAR $\gamma$	upregulates	VDR	
39	added	PPAR $\gamma$	represses	PPAR $\gamma$	
45	deleted	PPAR $\gamma$	represses	EGR1	
46	added	PPAR $\gamma$	represses	PU.1	
58	added	IRF-1	represses	IRF-1	
60	added	IRF-1	represses	AhR	
62	added	IRF-1	upregulates	Gfi-1	
63	added	IRF-1	upregulates	EGR1	
66	switched	IRF-1	represses	CD38	
70	added	IRF-1	represses	E2F	
72	added	IRF-1	upregulates	Oct4	
76	added	Oct1	upregulates	IRF-1	
77	added	Oct1	upregulates	Oct1	[185]
81	added	Oct1	represses	EGR1	
83	added	Oct1	upregulates	AP-1	[247]
86	added	Oct1	represses	CD14	
89	added	Oct1	upregulates	p47phox	
90	added	Oct1	represses	Oct4	
92	added	AhR	upregulates	VDR	
96	added	AhR	upregulates	AhR	
98	added	AhR	upregulates	Gfi-1	

100	switched	AhR	upregulates	PU.1	
103	added	AhR	upregulates	CD11b	
104	added	AhR	represses	CD14	
106	added	AhR	represses	E2F	[168]
110	added	C/EBP $\alpha$	upregulates	VDR	
111	switched	C/EBP $\alpha$	represses	PPAR $\gamma$	
113	added	C/EBP $\alpha$	upregulates	Oct1	
114	added	C/EBP $\alpha$	upregulates	AhR	
116	deleted	C/EBP $\alpha$	upregulates	Gfi-1	
117	added	C/EBP $\alpha$	represses	EGR1	[100]
118	deleted	C/EBP $\alpha$	upregulates	PU.1	
122	switched	C/EBP $\alpha$	represses	CD14	
124	switched	C/EBP $\alpha$	upregulates	E2F	
129	added	Gfi-1	represses	PPAR $\gamma$	
133	deleted	Gfi-1	represses	C/EBP $\alpha$	
138	added	Gfi-1	represses	CD38	
143	added	Gfi-1	represses	p47phox	
152	switched	EGR1	upregulates	Gfi-1	
156	added	EGR1	represses	CD38	
157	added	EGR1	upregulates	CD11b	
167	added	PU.1	represses	Oct1	
172	switched	PU.1	represses	PU.1	
175	deleted	PU.1	upregulates	CD11b	
178	added	PU.1	upregulates	E2F	
180	added	PU.1	represses	Oct4	
182	deleted	AP-1	upregulates	VDR	
186	added	AP-1	upregulates	AhR	
188	added	AP-1	represses	Gfi-1	
189	added	AP-1	upregulates	EGR1	
190	deleted	AP-1	upregulates	PU.1	
191	added	AP-1	represses	AP-1	
193	added	AP-1	upregulates	CD11b	
196	added	AP-1	upregulates	E2F	[219]
197	added	AP-1	represses	p47phox	
254	added	p21	upregulates	VDR	
255	added	p21	upregulates	PPAR $\gamma$	
256	added	p21	represses	IRF-1	
260	added	p21	upregulates	Gfi-1	

262	added	p21	upregulates	PU.1	
265	added	p21	upregulates	CD11b	
268	added	p21	upregulates	E2F	
272	added	E2F	upregulates	VDR	
273	added	E2F	represses	PPAR $\gamma$	
274	added	E2F	upregulates	IRF-1	
276	added	E2F	upregulates	AhR	
281	added	E2F	upregulates	AP-1	
283	added	E2F	upregulates	CD11b	
284	added	E2F	upregulates	CD14	
286	switched	E2F	represses	E2F	
288	added	E2F	represses	Oct4	
309	added	Oct4	upregulates	PPAR $\gamma$	
310	added	Oct4	represses	IRF-1	
312	added	Oct4	upregulates	AhR	
314	added	Oct4	upregulates	Gfi-1	
317	added	Oct4	represses	AP-1	
320	added	Oct4	upregulates	CD14	

Table B.7: Model Updates for WT-HL60 cell line with edge number, action, transcription factor, general effect, target gene, and new references

Edge Number	Action	Transcription Factor	General Effect	Target Gene	Reference(s)
2	added	RAR $\alpha$	represses	VDR	
3	added	RAR $\alpha$	upregulates	PPAR $\gamma$	
5	added	RAR $\alpha$	represses	Oct1	
6	switched	RAR $\alpha$	represses	AhR	
7	switched	RAR $\alpha$	represses	C/EBP $\alpha$	
8	added	RAR $\alpha$	represses	Gfi-1	
13	added	RAR $\alpha$	upregulates	CD11b	
14	added	RAR $\alpha$	represses	CD14	
17	added	RAR $\alpha$	upregulates	p47phox	[14]
21	deleted	VDR	upregulates	PPAR $\gamma$	
27	added	VDR	represses	EGR1	
34	added	VDR	represses	E2F	
38	added	PPAR $\gamma$	upregulates	VDR	
39	added	PPAR $\gamma$	represses	PPAR $\gamma$	
40	switched	PPAR $\gamma$	represses	IRF-1	
42	added	PPAR $\gamma$	upregulates	AhR	
45	switched	PPAR $\gamma$	upregulates	EGR1	
48	deleted	PPAR $\gamma$	upregulates	CD38	
49	added	PPAR $\gamma$	upregulates	CD11b	
50	switched	PPAR $\gamma$	represses	CD14	
53	deleted	PPAR $\gamma$	represses	p47phox	
56	added	IRF-1	upregulates	VDR	
66	switched	IRF-1	represses	CD38	
68	added	IRF-1	represses	CD14	
70	added	IRF-1	represses	E2F	
74	switched	Oct1	represses	VDR	
78	added	Oct1	upregulates	AhR	
79	added	Oct1	upregulates	C/EBP $\alpha$	
83	added	Oct1	upregulates	AP1	[247]
85	added	Oct1	upregulates	CD11b	
87	added	Oct1	upregulates	p21	
88	added	Oct1	represses	E2F	
89	added	Oct1	represses	p47phox	
95	added	AhR	upregulates	Oct1	

96	added	AhR	represses	AhR	
100	switched	AhR	upregulates	PU.1	
101	deleted	AhR	upregulates	AP1	
103	added	AhR	represses	CD11b	
104	added	AhR	upregulates	CD14	
106	added	AhR	upregulates	E2F	[168]
110	added	C/EBP $\alpha$	upregulates	VDR	
113	added	C/EBP $\alpha$	represses	Oct1	
118	switched	C/EBP $\alpha$	represses	PU.1	
119	added	C/EBP $\alpha$	upregulates	AP1	
122	deleted	C/EBP $\alpha$	upregulates	CD14	
123	deleted	C/EBP $\alpha$	upregulates	p21	
125	added	C/EBP $\alpha$	upregulates	p47phox	
126	added	C/EBP $\alpha$	represses	Oct4	
136	deleted	Gfi-1	represses	PU.1	
141	deleted	Gfi-1	represses	p21	
142	deleted	Gfi-1	represses	E2F	
143	added	Gfi-1	represses	p47phox	
148	added	EGR1	upregulates	IRF-1	
149	added	EGR1	represses	Oct1	
151	added	EGR1	represses	C/EBP $\alpha$	
155	added	EGR1	represses	AP1	
158	deleted	EGR1	upregulates	CD14	
159	added	EGR1	upregulates	p21	
164	deleted	PU.1	upregulates	VDR	
165	deleted	PU.1	represses	PPAR $\gamma$	
167	added	PU.1	represses	Oct1	
174	added	PU.1	upregulates	CD38	
176	added	PU.1	represses	CD14	
179	deleted	PU.1	upregulates	p47phox	
181	added	AP1	upregulates	RAR $\alpha$	
182	deleted	AP1	upregulates	VDR	
183	added	AP1	represses	PPAR $\gamma$	[258]
185	added	AP1	represses	Oct1	
191	added	AP1	represses	AP1	
193	added	AP1	upregulates	CD11b	
254	added	p21	upregulates	VDR	
257	added	p21	upregulates	Oct1	

258	added	p21	upregulates	AhR
261	added	p21	represses	EGR1
262	added	p21	upregulates	PU.1
264	added	p21	upregulates	CD38
270	added	p21	upregulates	Oct4
272	added	E2F	represses	VDR
273	added	E2F	represses	PPAR $\gamma$
274	added	E2F	upregulates	IRF-1
275	added	E2F	represses	Oct1
276	added	E2F	upregulates	AhR
281	added	E2F	represses	AP1
283	added	E2F	represses	CD11b
312	added	Oct4	represses	AhR
314	added	Oct4	upregulates	Gfi-1
316	added	Oct4	upregulates	PU.1
317	added	Oct4	represses	AP1
319	added	Oct4	represses	CD11b
320	added	Oct4	represses	CD14
323	added	Oct4	upregulates	p47phox

Table B.8: Model Updates for HL60 R38+ cell line with edge number, action, transcription factor, general effect, target gene, and new references

Edge Number	Action	Transcription Factor	General Effect	Target Gene	Reference(s)
10	deleted	RAR $\alpha$	upregulates	PU.1	
13	added	RAR $\alpha$	upregulates	CD11b	
16	added	RAR $\alpha$	upregulates	E2F	
18	deleted	RAR $\alpha$	upregulates	Oct4	
21	switched	VDR	upregulates	PPAR $\gamma$	
22	added	VDR	upregulates	IRF-1	
23	added	VDR	upregulates	Oct1	
29	added	VDR	upregulates	AP1	[267]
31	added	VDR	upregulates	CD11b	
32	added	VDR	upregulates	CD14	[204]
36	added	VDR	upregulates	Oct4	
40	deleted	PPAR $\gamma$	upregulates	IRF-1	
44	added	PPAR $\gamma$	upregulates	Gfi-1	
52	deleted	PPAR $\gamma$	upregulates	E2F	
54	added	PPAR $\gamma$	upregulates	Oct4	
59	added	IRF-1	upregulates	Oct1	
62	added	IRF-1	upregulates	Gfi-1	
63	added	IRF-1	upregulates	EGR1	
64	added	IRF-1	upregulates	PU.1	
69	deleted	IRF-1	upregulates	p21	
71	added	IRF-1	upregulates	p47phox	
76	added	Oct1	upregulates	IRF-1	
81	added	Oct1	upregulates	EGR1	
82	switched	Oct1	upregulates	PU.1	
88	added	Oct1	upregulates	E2F	
90	added	Oct1	upregulates	Oct4	
94	deleted	AhR	upregulates	IRF-1	
99	added	AhR	upregulates	EGR1	[169]
100	deleted	AhR	upregulates	PU.1	
102	added	AhR	upregulates	CD38	
105	added	AhR	upregulates	p21	
107	added	AhR	upregulates	p47phox	
111	deleted	C/EBP $\alpha$	upregulates	PPAR $\gamma$	
112	added	C/EBP $\alpha$	upregulates	IRF-1	

114	added	C/EBP $\alpha$	upregulates	AhR	
116	switched	C/EBP $\alpha$	upregulates	Gfi-1	
117	added	C/EBP $\alpha$	upregulates	EGR1	
118	switched	C/EBP $\alpha$	upregulates	PU.1	
119	added	C/EBP $\alpha$	upregulates	AP1	
120	added	C/EBP $\alpha$	upregulates	CD38	
125	added	C/EBP $\alpha$	upregulates	p47phox	
131	added	Gfi-1	upregulates	Oct1	
132	added	Gfi-1	upregulates	AhR	
133	deleted	Gfi-1	upregulates	C/EBP $\alpha$	
135	deleted	Gfi-1	upregulates	EGR1	
139	added	Gfi-1	upregulates	CD11b	
142	deleted	Gfi-1	upregulates	E2F	
150	added	EGR1	upregulates	AhR	
152	deleted	EGR1	upregulates	Gfi-1	
154	added	EGR1	upregulates	PU.1	[78]
156	added	EGR1	upregulates	CD38	
161	added	EGR1	upregulates	p47phox	
165	switched	PU.1	upregulates	PPAR $\gamma$	
167	added	PU.1	upregulates	Oct1	
170	added	PU.1	upregulates	Gfi-1	
173	switched	PU.1	upregulates	AP1	
175	deleted	PU.1	upregulates	CD11b	
179	deleted	PU.1	upregulates	p47phox	
183	added	AP1	upregulates	PPAR $\gamma$	[258]
188	added	AP1	upregulates	Gfi-1	
192	added	AP1	upregulates	CD38	
195	deleted	AP1	upregulates	p21	
256	added	p21	upregulates	IRF-1	
261	added	p21	upregulates	EGR1	
266	added	p21	upregulates	CD14	
269	added	p21	upregulates	p47phox	
270	added	p21	upregulates	Oct4	
274	added	E2F	upregulates	IRF-1	
279	added	E2F	upregulates	EGR1	
310	added	Oct4	upregulates	IRF-1	
312	added	Oct4	upregulates	AhR	
315	added	Oct4	upregulates	EGR1	

318	added	Oct4	upregulates	CD38	
320	added	Oct4	upregulates	CD14	

Table B.9: Model Updates for HL60 R38- cell line with edge number, action, transcription factor, general effect, target gene, and new references

Edge Number	Action	Transcription Factor	General Effect	Target Gene	Reference(s)
7	deleted	RAR $\alpha$	upregulates	C/EBP $\alpha$	
9	switched	RAR $\alpha$	represses	EGR1	
14	added	RAR $\alpha$	represses	CD14	
16	added	RAR $\alpha$	upregulates	E2F	
21	deleted	VDR	upregulates	PPAR $\gamma$	
25	added	VDR	represses	C/EBP $\alpha$	
26	added	VDR	represses	Gfi-1	
29	added	VDR	represses	AP-1	[267]
40	deleted	PPAR $\gamma$	upregulates	IRF-1	
41	switched	PPAR $\gamma$	represses	Oct1	
43	switched	PPAR $\gamma$	represses	C/EBP $\alpha$	
46	added	PPAR $\gamma$	upregulates	PU.1	
47	switched	PPAR $\gamma$	upregulates	AP-1	
49	added	PPAR $\gamma$	upregulates	CD11b	
57	added	IRF-1	upregulates	PPAR $\gamma$	
58	added	IRF-1	upregulates	IRF-1	
62	added	IRF-1	represses	Gfi-1	
63	added	IRF-1	represses	EGR1	
64	added	IRF-1	upregulates	PU.1	
65	added	IRF-1	represses	AP-1	
66	deleted	IRF-1	upregulates	CD38	
67	added	IRF-1	upregulates	CD11b	
70	added	IRF-1	upregulates	E2F	
71	added	IRF-1	represses	p47phox	
73	added	Oct1	represses	RAR $\alpha$	[126]
75	added	Oct1	upregulates	PPAR $\gamma$	
78	added	Oct1	represses	AhR	
83	added	Oct1	represses	AP-1	[247]
87	added	Oct1	upregulates	p21	
89	added	Oct1	represses	p47phox	
91	added	AhR	upregulates	RAR $\alpha$	[264]
93	added	AhR	upregulates	PPAR $\gamma$	
94	deleted	AhR	upregulates	IRF-1	
100	deleted	AhR	represses	PU.1	

101	switched	AhR	represses	AP-1
104	added	AhR	represses	CD14
105	added	AhR	represses	p21
109	added	C/EBP $\alpha$	upregulates	RAR $\alpha$
110	added	C/EBP $\alpha$	upregulates	VDR
111	deleted	C/EBP $\alpha$	upregulates	PPAR $\gamma$
114	added	C/EBP $\alpha$	upregulates	AhR
116	deleted	C/EBP $\alpha$	upregulates	Gfi-1
118	deleted	C/EBP $\alpha$	upregulates	PU.1
119	added	C/EBP $\alpha$	upregulates	AP-1
124	deleted	C/EBP $\alpha$	represses	E2F
125	added	C/EBP $\alpha$	upregulates	p47phox
132	added	Gfi-1	represses	AhR
133	deleted	Gfi-1	represses	C/EBP $\alpha$
139	added	Gfi-1	represses	CD11b
140	added	Gfi-1	represses	CD14
141	deleted	Gfi-1	represses	p21
146	added	EGR1	represses	VDR
150	added	EGR1	upregulates	AhR
156	added	EGR1	upregulates	CD38
158	deleted	EGR1	upregulates	CD14
160	added	EGR1	represses	E2F
162	added	EGR1	upregulates	Oct4
176	added	PU.1	upregulates	CD14
178	added	PU.1	represses	E2F
180	added	PU.1	upregulates	Oct4
194	added	AP-1	represses	CD14
195	switched	AP-1	represses	p21
256	added	p21	upregulates	IRF-1
263	added	p21	upregulates	AP-1
266	added	p21	represses	CD14
269	added	p21	represses	p47phox
272	added	E2F	represses	VDR
275	added	E2F	represses	Oct1
279	added	E2F	represses	EGR1
283	added	E2F	upregulates	CD11b
309	added	Oct4	upregulates	PPAR $\gamma$
317	added	Oct4	represses	AP-1

318	added	Oct4	upregulates	CD38	
319	added	Oct4	upregulates	CD11b	
321	added	Oct4	upregulates	p21	
323	added	Oct4	upregulates	p47phox	

Table B.10: Model Updates for U937 cell line with edge number, action, transcription factor, general effect, target gene, and new references

Edge Number	Action	Transcription Factor	General Effect	Target Gene	Reference(s)
2	added	RAR $\alpha$	upregulates	VDR	
13	added	RAR $\alpha$	upregulates	CD11b	
14	added	RAR $\alpha$	represses	CD14	
17	added	RAR $\alpha$	upregulates	p47phox	
27	added	VDR	upregulates	EGR1	
36	added	VDR	upregulates	Oct4	
44	added	PPAR $\gamma$	upregulates	Gfi-1	
48	deleted	PPAR $\gamma$	upregulates	CD38	
62	added	IRF-1	upregulates	Gfi-1	
71	added	IRF-1	represses	p47phox	
72	added	IRF-1	represses	Oct4	
73	added	Oct1	upregulates	RAR $\alpha$	[126]
75	added	Oct1	represses	PPAR $\gamma$	
77	added	Oct1	upregulates	Oct1	[185]
80	added	Oct1	represses	Gfi-1	
92	added	AhR	upregulates	VDR	
96	added	AhR	upregulates	AhR	
97	added	AhR	upregulates	C/EBP $\alpha$	
100	switched	AhR	upregulates	PU.1	
103	added	AhR	upregulates	CD11b	
106	added	AhR	represses	E2F	[168]
110	added	C/EBP $\alpha$	upregulates	VDR	
114	added	C/EBP $\alpha$	upregulates	AhR	
117	added	C/EBP $\alpha$	represses	EGR1	[100]
119	added	C/EBP $\alpha$	represses	AP-1	
129	added	Gfi-1	represses	PPAR $\gamma$	
137	added	Gfi-1	represses	AP-1	
139	added	Gfi-1	represses	CD11b	
153	added	EGR1	upregulates	EGR1	
170	added	PU.1	represses	Gfi-1	[143]
178	added	PU.1	represses	E2F	
180	added	PU.1	upregulates	Oct4	
188	added	AP-1	upregulates	Gfi-1	
194	added	AP-1	upregulates	CD14	

196	added	AP-1	upregulates	E2F	
198	added	AP-1	upregulates	Oct4	
254	added	p21	represses	VDR	
268	added	p21	represses	E2F	
312	added	Oct4	represses	AhR	
317	added	Oct4	represses	AP-1	
320	added	Oct4	represses	CD14	

## BIBLIOGRAPHY

- [1] Robert G Abbott, Stephanie Forrest, and Kenneth J Pienta. Simulating the hallmarks of cancer. *Artif Life*, 12(4):617–34, 2006.
- [2] Ram S Abramoff M, Magelhaes P. Image processing with imagej. *Biophotonics Int*, 11:36–42, 2004.
- [3] John G Albeck, John M Burke, Bree B Aldridge, Mingsheng Zhang, Douglas A Lauffenburger, and Peter K Sorger. Quantitative analysis of pathways controlling extrinsic apoptosis in single cells. *Mol Cell*, 30(1):11–25, Apr 2008.
- [4] John G Albeck, John M Burke, Sabrina L Spencer, Douglas A Lauffenburger, and Peter K Sorger. Modeling a snap-action, variable-delay switch controlling extrinsic cell death. *PLoS Biol*, 6(12):2831–52, Dec 2008.
- [5] Bree B Aldridge, John M Burke, Douglas A Lauffenburger, and Peter K Sorger. Physicochemical modelling of cell signalling pathways. *Nat Cell Biol*, 8(11):1195–203, Nov 2006.
- [6] Bree B Aldridge, Julio Saez-Rodriguez, Jeremy L Muhlich, Peter K Sorger, and Douglas A Lauffenburger. Fuzzy logic analysis of kinase pathway crosstalk in tnf/egf/insulin-induced signaling. *PLoS Comput Biol*, 5(4):e1000340, Apr 2009.
- [7] Uri Alon. *An introduction to systems biology: design principles of biological circuits*, volume 10 of *Chapman & Hall/CRC mathematical and computational biology series*. Chapman & Hall/CRC, Boca Raton, FL, 2007.
- [8] S Altior, M Xu, and B M Spiegelman. Ppargamma induces cell cycle withdrawal: inhibition of e2f/dp dna-binding activity via down-regulation of pp2a. *Genes Dev*, 11(15):1987–98, Aug 1997.
- [9] Vivi Andasari, Ryan T Roper, Maciej H Swat, and Mark A J Chaplain. Integrating intracellular dynamics using compucell3d and bionetsolver: applications to multiscale modelling of cancer cell growth and invasion. *PLoS One*, 7(3):e33726, 2012.
- [10] Joshua F Apgar, David K Witmer, Forest M White, and Bruce Tidor. Sloppy models, parameter uncertainty, and the role of experimental design. *Mol Biosyst*, 6(10):1890–900, Oct 2010.

- [11] Ana Aranda and Angel Pascual. Nuclear and hormone receptors and gene expression. *Physiological Reviews*, 81(3):1269–1304, 2001.
- [12] Gerhardt Attard and Johann S de Bono. Prostate cancer: Psa as an intermediate end point in clinical trials. *Nat Rev Urol*, 6(9):473–5, Sep 2009.
- [13] J E Bailey. Complex biology with no parameters. *Nat Biotechnol*, 19(6):503–4, Jun 2001.
- [14] James E Balmer and Rune Blomhoff. Gene expression regulation by retinoic acid. *J Lipid Res*, 43(11):1773–808, Nov 2002.
- [15] B Bauvois, L Durant, J Laboureau, E Barthélémy, D Rouillard, G Boulla, and P Deterre. Upregulation of cd38 gene expression in leukemic b cells by interferon types i and ii. *J Interferon Cytokine Res*, 19(9):1059–66, Sep 1999.
- [16] G Behre, A J Whitmarsh, M P Coghlan, T Hoang, C L Carpenter, D E Zhang, R J Davis, and D G Tenen. c-jun is a jnk-independent coactivator of the pu.1 transcription factor. *J Biol Chem*, 274(8):4939–46, Feb 1999.
- [17] E Ben-Shushan, H Sharir, E Pikarsky, and Y Bergman. A dynamic balance between arp-1/coup-tfii, ear-3/coup-tfi, and retinoic acid receptor:retinoid x receptor heterodimers regulates oct-3/4 expression in embryonal carcinoma cells. *Mol Cell Biol*, 15(2):1034–48, Feb 1995.
- [18] Madjid Benkoussa, Céline Brand, Marie-Hélène Delmotte, Pierre Formstecher, and Philippe Lefebvre. Retinoic acid receptors inhibit ap1 activation by regulating extracellular signal-regulated kinase and cbp recruitment to an ap1-responsive promoter. *Mol Cell Biol*, 22(13):4522–34, Jul 2002.
- [19] Jeff Bezanson, Alan Edelman, Stefan Karpinski, and Viral B. Shah. Julia: A fresh approach to numerical computing. November 2014.
- [20] Upinder S Bhalla, Prahlad T Ram, and Ravi Iyengar. Map kinase phosphatase as a locus of flexibility in a mitogen-activated protein kinase signaling network. *Science*, 297(5583):1018–23, Aug 2002.
- [21] M Bhatia, J B Kirkland, and K A Meckling-Gill. M-csf and 1,25 dihydroxy vitamin d3 synergize with 12-o-tetradecanoylphorbol-13-acetate to

- induce macrophage differentiation in acute promyelocytic leukemia nb4 cells. *Leukemia*, 8(10):1744–9, Oct 1994.
- [22] M Bizzarri, A Cucina, F Conti, and F D'Anselmi. Beyond the oncogene paradigm: understanding complexity in cancerogenesis. *Acta Biotheor*, 56(3):173–96, Sep 2008.
- [23] Nikolay Borisov, Edita Aksamitiene, Anatoly Kiyatkin, Stefan Legewie, Jan Berkhout, Thomas Maiwald, Nikolai P Kaimachnikov, Jens Timmer, Jan B Hoek, and Boris N Kholodenko. Systems-level interactions between insulin-egf networks amplify mitogenic signaling. *Mol Syst Biol*, 5:256, 2009.
- [24] A O Brinkmann, L J Blok, P E de Ruiter, P Doesburg, K Steketee, C A Berrevoets, and J Trapman. Mechanisms of androgen receptor activation and function. *J Steroid Biochem Mol Biol*, 69(1-6):307–13, 1999.
- [25] Kevin S Brown and James P Sethna. Statistical mechanical approaches to models with many poorly known parameters. *Phys Rev E Stat Nonlin Soft Matter Phys*, 68(2 Pt 1):021904, Aug 2003.
- [26] Dennis Bruemmer, Fen Yin, Joey Liu, Joel P Berger, Toshiyuki Sakai, Florian Blaschke, Eckart Fleck, Andre J Van Herle, Barry M Forman, and Ronald E Law. Regulation of the growth arrest and dna damage-inducible gene 45 (gadd45) by peroxisome proliferator-activated receptor gamma in vascular smooth muscle cells. *Circ Res*, 93(4):e38–47, Aug 2003.
- [27] A Brunet, A Bonni, M J Zigmond, M Z Lin, P Juo, L S Hu, M J Anderson, K C Arden, J Blenis, and M E Greenberg. Akt promotes cell survival by phosphorylating and inhibiting a forkhead transcription factor. *Cell*, 96(6):857–68, Mar 1999.
- [28] Rodica P Bunaciu and Andrew Yen. Activation of the aryl hydrocarbon receptor ahr promotes retinoic acid-induced differentiation of myeloblastic leukemia cells by restricting expression of the stem cell transcription factor oct4. *Cancer Res*, 71(6):2371–80, Mar 2011.
- [29] Rodica P Bunaciu and Andrew Yen. 6-formylindolo (3,2-b)carbazole (ficz) enhances retinoic acid (ra)-induced differentiation of hl-60 myeloblastic leukemia cells. *Mol Cancer*, 12:39, 2013.
- [30] R Busà, M P Paronetto, D Farini, E Pierantozzi, F Botti, D F Angelini, F Attisani, G Vespasiani, and C Sette. The rna-binding protein sam68

- contributes to proliferation and survival of human prostate cancer cells. *Oncogene*, 26(30):4372–82, Jun 2007.
- [31] Nathan Bushue and Yu-Jui Yvonne Wan. Retinoid pathway and cancer therapeutics. *Adv Drug Deliv Rev*, 62(13):1285–98, Oct 2010.
- [32] Changmeng Cai, David C Portnoy, Hongyun Wang, Xinnong Jiang, Shaoyong Chen, and Steven P Balk. Androgen receptor expression in prostate cancer cells is suppressed by activation of epidermal growth factor receptor and erbB2. *Cancer Res*, 69(12):5202–9, Jun 2009.
- [33] Maria Rosaria Cardillo, Salvatore Monti, Franco Di Silverio, Vincenzo Gentile, Francesco Sciarra, and Vincenzo Toscano. Insulin-like growth factor (igf)-i, igf-ii and igf type i receptor (igfr-i) expression in prostatic cancer. *Anticancer Res*, 23(5A):3825–35, 2003.
- [34] Brett S Carver, Caren Chapinski, John Wongvipat, Haley Hieronymus, Yu Chen, Sarat Chandarlapaty, Vivek K Arora, Carl Le, Jason Koutcher, Howard Scher, Peter T Scardino, Neal Rosen, and Charles L Sawyers. Reciprocal feedback regulation of pi3k and androgen receptor signaling in pten-deficient prostate cancer. *Cancer Cell*, 19(5):575–86, May 2011.
- [35] Anirikh Chakrabarti, Scott Verbridge, Abraham D Stroock, Claudia Fischbach, and Jeffrey D Varner. Multiscale models of breast cancer progression. *Ann Biomed Eng*, 40(11):2488–500, Nov 2012.
- [36] Arvind K Chavali, Erwin P Gianchandani, Kenneth S Tung, Michael B Lawrence, Shayn M Peirce, and Jason A Papin. Characterizing emergent properties of immunological systems with multi-cellular rule-based computational modeling. *Trends Immunol*, 29(12):589–99, Dec 2008.
- [37] Fei Chen, Qing Wang, Xuening Wang, and George P Studzinski. Up-regulation of egr1 by 1,25-dihydroxyvitamin d3 contributes to increased expression of p35 activator of cyclin-dependent kinase 5 and consequent onset of the terminal phase of hl60 cell differentiation. *Cancer Res*, 64(15):5425–33, Aug 2004.
- [38] H Chen, D Ray-Gallet, P Zhang, C J Hetherington, D A Gonzalez, D E Zhang, F Moreau-Gachelin, and D G Tenen. Pu.1 (spi-1) autoregulates its expression in myeloid cells. *Oncogene*, 11(8):1549–60, Oct 1995.
- [39] H Chen, P Zhang, H S Radomska, C J Hetherington, D E Zhang, and

- D G Tenen. Octamer binding factors and their coactivator can activate the murine pu.1 (spi-1) promoter. *J Biol Chem*, 271(26):15743–52, Jun 1996.
- [40] Liqun Chen, Benjamin A Mooso, Maitreyee K Jathal, Anisha Madhav, Sherra D Johnson, Elyse van Spyk, Margarita Mikhailova, Alexandra Zierenberg-Ripoll, Lingru Xue, Ruth L Vinall, Ralph W deVere White, and Paramita M Ghosh. Dual egfr/her2 inhibition sensitizes prostate cancer cells to androgen withdrawal by suppressing erbB3. *Clin Cancer Res*, 17(19):6218–28, Oct 2011.
- [41] Shaoyong Chen, Cristina T Kesler, Bryce M Paschal, and Steven P Balk. Androgen receptor phosphorylation and activity are regulated by an association with protein phosphatase 1. *J Biol Chem*, 284(38):25576–84, Sep 2009.
- [42] Florence S G Cheung, Frank J Lovicu, and Juergen K V Reichardt. Current progress in using vitamin d and its analogs for cancer prevention and treatment. *Expert Rev Anticancer Ther*, 12(6):811–37, Jun 2012.
- [43] Yung-Tuen Chiu, Hui-Ying Han, Steve Chin-Lung Leung, Hiu-Fung Yuen, Chee-Wai Chau, Zhiyong Guo, Yun Qiu, Kwok-Wah Chan, Xianghong Wang, Yong-Chuan Wong, and Ming-Tat Ling. Cdc25a functions as a novel ar corepressor in prostate cancer cells. *J Mol Biol*, 385(2):446–56, Jan 2009.
- [44] Tsai-Der Chuang, Siu-Ju Chen, Fen-Fen Lin, Suresh Veeramani, Satyendra Kumar, Surinder K Batra, Yaping Tu, and Ming-Fong Lin. Human prostatic acid phosphatase, an authentic tyrosine phosphatase, dephosphorylates erbB-2 and regulates prostate cancer cell growth. *J Biol Chem*, 285(31):23598–606, Jul 2010.
- [45] Andrea Ciliberto, Béla Novak, and John J Tyson. Steady states and oscillations in the p53-mdm2 network. *Cell Cycle*, 4(3):488–93, Mar 2005.
- [46] Bekir Cinar, Arrigo De Benedetti, and Michael R Freeman. Post-transcriptional regulation of the androgen receptor by mammalian target of rapamycin. *Cancer Res*, 65(7):2547–53, Apr 2005.
- [47] A A Cohen, N Geva-Zatorsky, E Eden, M Frenkel-Morgenstern, I Issaeva, A Sigal, R Milo, C Cohen-Saidon, Y Liron, Z Kam, L Cohen, T Danon, N Perzov, and U Alon. Dynamic proteomics of individual cancer cells in response to a drug. *Science*, 322(5907):1511–6, Dec 2008.

- [48] C C Coombs, M Tavakkoli, and M S Tallman. Acute promyelocytic leukemia: where did we start, where are we now, and the future. *Blood Cancer J*, 5:e304, 2015.
- [49] N Craft, Y Shostak, M Carey, and C L Sawyers. A mechanism for hormone-independent prostate cancer through modulation of androgen receptor signaling by the her-2/neu tyrosine kinase. *Nat Med*, 5(3):280–5, Mar 1999.
- [50] Richard Dahl, Sangeeta R Iyer, Kristin S Owens, Dorothy D Cuylear, and M Celeste Simon. The transcriptional repressor gfi-1 antagonizes pu.1 activity through protein-protein interaction. *J Biol Chem*, 282(9):6473–83, Mar 2007.
- [51] Richard Dahl, Jonathan C Walsh, David Lancki, Peter Laslo, Sangeeta R Iyer, Harinder Singh, and M Celeste Simon. Regulation of macrophage and neutrophil cell fates by the pu.1:c/ebpalpha ratio and granulocyte colony-stimulating factor. *Nat Immunol*, 4(10):1029–36, Oct 2003.
- [52] William L Dahut, Charity Scripture, Edwin Posadas, Lokesh Jain, James L Gulley, Philip M Arlen, John J Wright, Yunkai Yu, Liang Cao, Seth M Steinberg, Jeanny B Aragon-Ching, Jürgen Venitz, Elizabeth Jones, Clara C Chen, and William D Figg. A phase ii clinical trial of sorafenib in androgen-independent prostate cancer. *Clin Cancer Res*, 14(1):209–14, Jan 2008.
- [53] Francesco D'Alo', Lisa M Johansen, Erik A Nelson, Hanna S Radom-ska, Erica K Evans, Pu Zhang, Claus Nerlov, and Daniel G Tenen. The amino terminal and e2f interaction domains are critical for c/ebp alpha-mediated induction of granulopoietic development of hematopoietic cells. *Blood*, 102(9):3163–71, Nov 2003.
- [54] W T Dalton, Jr, M J Ahearn, K B McCredie, E J Freireich, S A Stass, and J M Trujillo. HL-60 cell line was derived from a patient with fab-m2 and not fab-m3. *Blood*, 71(1):242–7, Jan 1988.
- [55] Bryan C Daniels, Yan-Jiun Chen, James P Sethna, Ryan N Gutenkunst, and Christopher R Myers. Sloppiness, robustness, and evolvability in systems biology. *Curr Opin Biotechnol*, 19(4):389–95, Aug 2008.
- [56] Joanne N Davis, Kirk J Wojno, Stephanie Daignault, Matthias D Hofer, Rainer Kuefer, Mark A Rubin, and Mark L Day. Elevated e2f1 inhibits

- transcription of the androgen receptor in metastatic hormone-resistant prostate cancer. *Cancer Res*, 66(24):11897–906, Dec 2006.
- [57] Johann Sebastian de Bono, Stephane Oudard, Mustafa Ozguroglu, Steinbjørn Hansen, Jean-Pascal Machiels, Ivo Kocak, Gwenaëlle Gravis, Istvan Bodrogi, Mary J Mackenzie, Liji Shen, Martin Roessner, Sunil Gupta, A Oliver Sartor, and TROPIC Investigators. Prednisone plus cabazitaxel or mitoxantrone for metastatic castration-resistant prostate cancer progressing after docetaxel treatment: a randomised open-label trial. *Lancet*, 376(9747):1147–54, Oct 2010.
- [58] H Defacque, T Commes, V Contet, C Sevilla, and J Marti. Differentiation of u937 myelomonocytic cell line by all-trans retinoic acid and 1,25-dihydroxyvitamin d<sub>3</sub>: synergistic effects on tissue transglutaminase. *Leukemia*, 9(10):1762–7, Oct 1995.
- [59] Thomas S Deisboeck, Zhihui Wang, Paul Macklin, and Vittorio Cristini. Multiscale cancer modeling. *Annu Rev Biomed Eng*, 13:127–55, Aug 2011.
- [60] P Delerive, K De Bosscher, S Besnard, W Vanden Berghe, J M Peters, F J Gonzalez, J C Fruchart, A Tedgui, G Haegeman, and B Staels. Peroxisome proliferator-activated receptor alpha negatively regulates the vascular inflammatory gene response by negative cross-talk with transcription factors nf-kappab and ap-1. *J Biol Chem*, 274(45):32048–54, Nov 1999.
- [61] R Dickinson and R Gelinas. Sensitivity analysis of ordinary differential equation systems—a direct method. *Journal of Computational Physics*, 21:123–143, 1976.
- [62] Joanna R Dispirito, Bin Fang, Fenfen Wang, and Mitchell A Lazar. Pruning of the adipocyte peroxisome proliferator-activated receptor cistrome by hematopoietic master regulator pu.1. *Mol Cell Biol*, 33(16):3354–64, Aug 2013.
- [63] Loretta L Doan, Susan D Porter, Zhijun Duan, Marcella M Flubacher, Diego Montoya, Philip N Tsichlis, Marshall Horwitz, C Blake Gilks, and H Leighton Grimes. Targeted transcriptional repression of gfi1 by gfi1 and gfi1b in lymphoid cells. *Nucleic Acids Res*, 32(8):2508–19, 2004.
- [64] Hartmut Döhner, Daniel J Weisdorf, and Clara D Bloomfield. Acute myeloid leukemia. *N Engl J Med*, 373(12):1136–52, Sep 2015.

- [65] J Drach, T McQueen, H Engel, M Andreeff, K A Robertson, S J Collins, F Malavasi, and K Mehta. Retinoic acid-induced expression of cd38 antigen in myeloid cells is mediated through retinoic acid receptor-alpha. *Cancer Res*, 54(7):1746–52, Apr 1994.
- [66] Zhijun Duan and Marshall Horwitz. Targets of the transcriptional repressor oncoprotein gfi-1. *Proc Natl Acad Sci U S A*, 100(10):5932–7, May 2003.
- [67] Thomas W Dunlop, Sami Väisänen, Christian Frank, Ferdinand Molnár, Lasse Sinkkonen, and Carsten Carlberg. The human peroxisome proliferator-activated receptor delta gene is a primary target of 1alpha,25-dihydroxyvitamin d<sub>3</sub> and its nuclear receptor. *J Mol Biol*, 349(2):248–60, Jun 2005.
- [68] R C Eberhart and J Kennedy. A new optimizer using particle swarm theory. *Proceedings of the Sixth International Symposium on Micro Machine and Human Science*, pages 39–43, 1995.
- [69] Zi Fang, Tao Zhang, Nishtman Dizeyi, Sen Chen, Hongyun Wang, Kenneth D Swanson, Changmeng Cai, Steven P Balk, and Xin Yuan. Androgen receptor enhances p27 degradation in prostate cancer cells through rapid and selective torc2 activation. *J Biol Chem*, 287(3):2090–8, Jan 2012.
- [70] Dana Faratian, Alexey Goltsov, Galina Lebedeva, Anatoly Sorokin, Stuart Moodie, Peter Mullen, Charlene Kay, In Hwa Um, Simon Langdon, Igor Goryanin, and David J Harrison. Systems biology reveals new strategies for personalizing cancer medicine and confirms the role of pten in resistance to trastuzumab. *Cancer Res*, 69(16):6713–20, Aug 2009.
- [71] Jia Fei, Carla Cook, Miriah Gillespie, Bangning Yu, Khyra Fullen, and Nalini Santanam. Atherogenic -6 lipids modulate ppar- egr-1 crosstalk in vascular cells. *PPAR Res*, 2011:753917, 2011.
- [72] B J Feldman and D Feldman. The development of androgen-independent prostate cancer. *Nat Rev Cancer*, 1(1):34–45, Oct 2001.
- [73] S C Ferreira, Jr, M L Martins, and M J Vilela. Reaction-diffusion model for the growth of avascular tumor. *Phys Rev E Stat Nonlin Soft Matter Phys*, 65(2 Pt 1):021907, Feb 2002.
- [74] Felming P Fonseca C. Genetic algorithms for multiobjective optimization: Formulation, discussion and generalization. In: *Proceedings of the fifth international conference on genetic algorithms Citeseer*, 423:416–423, 1993.

- [75] J A Fontana, D A Colbert, and A B Deisseroth. Identification of a population of bipotent stem cells in the hl60 human promyelocytic leukemia cell line. *Proc Natl Acad Sci U S A*, 78(6):3863–6, Jun 1981.
- [76] K E Forsten and D A Lauffenburger. The role of low-affinity interleukin-2 receptors in autocrine ligand binding: alternative mechanisms for enhanced binding effect. *Mol Immunol*, 31(10):739–51, Jul 1994.
- [77] A D Friedman. Transcriptional control of granulocyte and monocyte development. *Oncogene*, 26(47):6816–28, Oct 2007.
- [78] Alan D Friedman. Transcriptional regulation of myelopoiesis. *Int J Hematol*, 75(5):466–72, Jun 2002.
- [79] Mingui Fu, Jifeng Zhang, Yiming Lin, Xiaojun Zhu, Markus U Ehrengruber, and Yuqing E Chen. Early growth response factor-1 is a critical transcriptional mediator of peroxisome proliferator-activated receptor-gamma 1 gene expression in human aortic smooth muscle cells. *J Biol Chem*, 277(30):26808–14, Jul 2002.
- [80] K G Gadkar, J Varner, and F J Doyle, 3rd. Model identification of signal transduction networks from data using a state regulator problem. *Syst Biol (Stevenage)*, 2(1):17–30, Mar 2005.
- [81] Kapil G Gadkar, Francis J Doyle, 3rd, Timothy J Crowley, and Jeffrey D Varner. Cybernetic model predictive control of a continuous bioreactor with cell recycle. *Biotechnol Prog*, 19(5):1487–97, 2003.
- [82] Levi A Garraway and Pasi A Jänne. Circumventing cancer drug resistance in the era of personalized medicine. *Cancer Discov*, 2(3):214–26, Mar 2012.
- [83] Daniel Gioeli and Bryce M Paschal. Post-translational modification of the androgen receptor. *Mol Cell Endocrinol*, 352(1-2):70–8, Apr 2012.
- [84] Florian Göbel, Sabine Taschner, Jennifer Jurkin, Sabine Konradi, Christine Vaculik, Susanne Richter, Doris Kneidinger, Christina Mühlbacher, Christian Bieglmayer, Adelheid Elbe-Bürger, and Herbert Strobl. Reciprocal role of gata-1 and vitamin d receptor in human myeloid dendritic cell differentiation. *Blood*, 114(18):3813–21, Oct 2009.
- [85] Elżbieta Gocek, Aleksandra Marchwicka, Hanna Baurska, Agnieszka Chrobak, and Ewa Marcinkowska. Opposite regulation of vitamin d re-

- ceptor by atra in aml cells susceptible and resistant to vitamin d-induced differentiation. *J Steroid Biochem Mol Biol*, 132(3-5):220–6, Nov 2012.
- [86] J M Grad, J L Dai, S Wu, and K L Burnstein. Multiple androgen response elements and a myc consensus site in the androgen receptor (ar) coding region are involved in androgen-mediated up-regulation of ar messenger rna. *Mol Endocrinol*, 13(11):1896–911, Nov 1999.
- [87] J R Graff, B W Konicek, A M McNulty, Z Wang, K Houck, S Allen, J D Paul, A Hbaiu, R G Goode, G E Sandusky, R L Vessella, and B L Neubauer. Increased akt activity contributes to prostate cancer progression by dramatically accelerating prostate tumor growth and diminishing p27kip1 expression. *J Biol Chem*, 275(32):24500–5, Aug 2000.
- [88] Jeremy R Graff, Bruce W Konicek, Rebecca L Lynch, Chad A Dumstorf, Michele S Dowless, Ann M McNulty, Stephen H Parsons, Leslie H Brail, Bruce M Colligan, Jonathan W Koop, Bernadette M Hurst, James A Deddens, Blake L Neubauer, Louis F Stancato, Harry W Carter, Larry E Douglass, and Julia H Carter. eif4e activation is commonly elevated in advanced human prostate cancers and significantly related to reduced patient survival. *Cancer Res*, 69(9):3866–73, May 2009.
- [89] C W Gregory, B He, R T Johnson, O H Ford, J L Mohler, F S French, and E M Wilson. A mechanism for androgen receptor-mediated prostate cancer recurrence after androgen deprivation therapy. *Cancer Res*, 61(11):4315–9, Jun 2001.
- [90] Christopher W Gregory, Xiaoyin Fei, Liliana A Ponguta, Bin He, Heather M Bill, Frank S French, and Elizabeth M Wilson. Epidermal growth factor increases coactivation of the androgen receptor in recurrent prostate cancer. *J Biol Chem*, 279(8):7119–30, Feb 2004.
- [91] Zhiyong Guo, Bojie Dai, Tianyun Jiang, Kexin Xu, Yingqiu Xie, Oekyung Kim, Issa Nesheiwat, Xiangtian Kong, Jonathan Melamed, Venkatesh D Handratta, Vincent C O Njar, Angela M H Brodie, Li-Rong Yu, Timothy D Veenstra, Hegang Chen, and Yun Qiu. Regulation of androgen receptor activity by tyrosine phosphorylation. *Cancer Cell*, 10(4):309–19, Oct 2006.
- [92] Susan Ha, Rachel Ruoff, Nicole Kahoud, Thomas F Franke, and Susan K Logan. Androgen receptor levels are upregulated by akt in prostate cancer. *Endocr Relat Cancer*, 18(2):245–55, Apr 2011.
- [93] Tomoaki Hakariya, Yohei Shida, Hideki Sakai, Hiroshi Kanetake, and

- Tsukasa Igawa. Egfr signaling pathway negatively regulates psa expression and secretion via the pi3k-akt pathway in lncap prostate cancer cells. *Biochem Biophys Res Commun*, 342(1):92–100, Mar 2006.
- [94] Shouwei Han, Neil Sidell, Paul B Fisher, and Jesse Roman. Up-regulation of p21 gene expression by peroxisome proliferator-activated receptor gamma in human lung carcinoma cells. *Clin Cancer Res*, 10(6):1911–9, Mar 2004.
- [95] D Hanahan and R A Weinberg. The hallmarks of cancer. *Cell*, 100(1):57–70, Jan 2000.
- [96] Douglas Hanahan and Robert A Weinberg. Hallmarks of cancer: the next generation. *Cell*, 144(5):646–74, Mar 2011.
- [97] Julia Handl, Douglas B Kell, and Joshua Knowles. Multiobjective optimization in bioinformatics and computational biology. *IEEE/ACM Trans Comput Biol Bioinform*, 4(2):279–92, 2007.
- [98] T E Harris, J H Albrecht, M Nakanishi, and G J Darlington. Ccaat/enhancer-binding protein-alpha cooperates with p21 to inhibit cyclin-dependent kinase-2 activity and induces growth arrest independent of dna binding. *J Biol Chem*, 276(31):29200–9, Aug 2001.
- [99] William P Harris, Elahe A Mostaghel, Peter S Nelson, and Bruce Montgomery. Androgen deprivation therapy: progress in understanding mechanisms of resistance and optimizing androgen depletion. *Nat Clin Pract Urol*, 6(2):76–85, Feb 2009.
- [100] Marie S Hasemann, Felicia K B Lauridsen, Johannes Waage, Janus S Jakobsen, Anne-Katrine Frank, Mikkel B Schuster, Nicolas Rapin, Frederik O Bagger, Philipp S Hoppe, Timm Schroeder, and Bo T Porse. C/ebp is required for long-term self-renewal and lineage priming of hematopoietic stem cells and for the maintenance of epigenetic configurations in multipotent progenitors. *PLoS Genet*, 10(1):e1004079, Jan 2014.
- [101] Jan Hasenauer, Steffen Waldherr, Małgorzata Doszczak, Nicole Radde, Peter Scheurich, and Frank Allgöwer. Identification of models of heterogeneous cell populations from population snapshot data. *BMC Bioinformatics*, 12:125, 2011.
- [102] Johan Hattne, David Fange, and Johan Elf. Stochastic reaction-diffusion simulation with mesord. *Bioinformatics*, 21(12):2923–4, Jun 2005.

- [103] Hannelore V Heemers and Donald J Tindall. Androgen receptor (ar) coregulators: a diversity of functions converging on and regulating the ar transcriptional complex. *Endocr Rev*, 28(7):778–808, Dec 2007.
- [104] Cynthia A Heinlein and Chawnshang Chang. Androgen receptor (ar) coregulators: an overview. *Endocr Rev*, 23(2):175–200, Apr 2002.
- [105] Cynthia A Heinlein and Chawnshang Chang. Androgen receptor in prostate cancer. *Endocr Rev*, 25(2):276–308, Apr 2004.
- [106] Laura M Heiser, Nicholas J Wang, Carolyn L Talcott, Keith R Laderoute, Merrill Knapp, Yinghui Guan, Zhi Hu, Safiyyah Ziyad, Barbara L Weber, Sylvie Laquerre, Jeffrey R Jackson, Richard F Wooster, Wen Lin Kuo, Joe W Gray, and Paul T Spellman. Integrated analysis of breast cancer cell lines reveals unique signaling pathways. *Genome Biol*, 10(3):R31, 2009.
- [107] Bart S Hendriks, Lee K Opresko, H Steven Wiley, and Douglas Lauffenburger. Quantitative analysis of her2-mediated effects on her2 and epidermal growth factor receptor endocytosis: distribution of homo- and heterodimers depends on relative her2 levels. *J Biol Chem*, 278(26):23343–51, Jun 2003.
- [108] Alan Hindmarsh, Peter Brown, Keith Grant, Steven Lee, Radu Serban, Dan Shumaker, and Carol Woodward. Sundials: Suite of nonlinear and differential/algebraic equation solvers. *ACM Transactions on Mathematical Software*, 31:363–396, 2005.
- [109] Richard M Hoffman. Clinical practice. screening for prostate cancer. *N Engl J Med*, 365(21):2013–9, Nov 2011.
- [110] Alexander Hoffmann, Andre Levchenko, Martin L Scott, and David Baltimore. The ikappab-nf-kappab signaling module: temporal control and selective gene activation. *Science*, 298(5596):1241–5, Nov 2002.
- [111] J S Horoszewicz, S S Leong, E Kawinski, J P Karr, H Rosenthal, T M Chu, E A Mirand, and G P Murphy. LnCap model of human prostatic carcinoma. *Cancer Res*, 43(4):1809–18, Apr 1983.
- [112] S Huang and D E Ingber. Shape-dependent control of cell growth, differentiation, and apoptosis: switching between attractors in cell regulatory networks. *Exp Cell Res*, 261(1):91–103, Nov 2000.

- [113] C Huggins. Endocrine-induced regression of cancers. *Cancer Res*, 27(11):1925–30, Nov 1967.
- [114] Stephen P Hunger and Charles G Mullighan. Acute lymphoblastic leukemia in children. *N Engl J Med*, 373(16):1541–52, Oct 2015.
- [115] Lisa Hutchinson and Rebecca Kirk. High drug attrition rates—where are we going wrong? *Nat Rev Clin Oncol*, 8(4):189–90, Apr 2011.
- [116] Nancy E Hynes and Heidi A Lane. Erbb receptors and cancer: the complexity of targeted inhibitors. *Nat Rev Cancer*, 5(5):341–54, May 2005.
- [117] Sergio Iadevaia, Yiling Lu, Fabiana C Morales, Gordon B Mills, and Prahlad T Ram. Identification of optimal drug combinations targeting cellular networks: integrating phospho-proteomics and computational network analysis. *Cancer Res*, 70(17):6704–14, Sep 2010.
- [118] Tsukasa Igawa, Fen-Fen Lin, Ming-Shyue Lee, Dev Karan, Surinder K Batra, and Ming-Fong Lin. Establishment and characterization of androgen-independent human prostate cancer lncap cell model. *Prostate*, 50(4):222–35, Mar 2002.
- [119] Elias Jabbour and Hagop Kantarjian. Chronic myeloid leukemia: 2014 update on diagnosis, monitoring, and management. *Am J Hematol*, 89(5):547–56, May 2014.
- [120] Holly A Jensen, Rodica P Bunaciu, Christopher N Ibabao, Rebecca Myers, Jeffrey D Varner, and Andrew Yen. Retinoic acid therapy resistance progresses from unilineage to bilineage in hl-60 leukemic blasts. *PLoS One*, 9(6):e98929, 2014.
- [121] Holly A Jensen, Lauren E Styskal, Ryan Tassey, Rodica P Bunaciu, Johanna Congleton, Jeffrey D Varner, and Andrew Yen. The src-family kinase inhibitor pp2 rescues inducible differentiation events in emergent retinoic acid-resistant myeloblastic leukemia cells. *PLoS One*, 8(3):e58621, 2013.
- [122] Holly A Jensen, Harmony B Yourish, Rodica P Bunaciu, Jeffrey D Varner, and Andrew Yen. Induced myelomonocytic differentiation in leukemia cells is accompanied by noncanonical transcription factor expression. *FEBS Open Bio*, 5:789–800, 2015.

- [123] Yi Jiang, Jelena Pjesivac-Grbovic, Charles Cantrell, and James P Freyer. A multiscale model for avascular tumor growth. *Biophys J*, 89(6):3884–94, Dec 2005.
- [124] D G Johnson, K Ohtani, and J R Nevins. Autoregulatory control of e2f1 expression in response to positive and negative regulators of cell cycle progression. *Genes Dev*, 8(13):1514–25, Jul 1994.
- [125] E Jones, T Oliphant, and P Peterson. Scipy: Open source scientific tools for python, 2001.
- [126] T Kakizawa, T Miyamoto, K Ichikawa, A Kaneko, S Suzuki, M Hara, T Nagasawa, T Takeda, J i Mori, M Kumagai, and K Hashizume. Functional interaction between oct-1 and retinoid x receptor. *J Biol Chem*, 274(27):19103–8, Jul 1999.
- [127] Mridul K Kalita, Khachik Sargsyan, Bing Tian, Adriana Paulucci-Holthauzen, Habib N Najm, Bert J Debusschere, and Allan R Brasier. Sources of cell-to-cell variability in canonical nuclear factor-kappab (nf-kappab) signaling pathway inferred from single cell dynamic images. *J Biol Chem*, 286(43):37741–57, Oct 2011.
- [128] Philip W Kantoff, Celestia S Higano, Neal D Shore, E Roy Berger, Eric J Small, David F Penson, Charles H Redfern, Anna C Ferrari, Robert Dreicer, Robert B Sims, Yi Xu, Mark W Frohlich, Paul F Schellhammer, and IMPACT Study Investigators. Sipuleucel-t immunotherapy for castration-resistant prostate cancer. *N Engl J Med*, 363(5):411–22, Jul 2010.
- [129] T Karantanos, P G Corn, and T C Thompson. Prostate cancer progression after androgen deprivation therapy: mechanisms of castrate resistance and novel therapeutic approaches. *Oncogene*, Jun 2013.
- [130] D Kardassis, P Papakosta, K Pardali, and A Moustakas. c-jun transactivates the promoter of the human p21(waf1/cip1) gene by acting as a superactivator of the ubiquitous transcription factor sp1. *J Biol Chem*, 274(41):29572–81, Oct 1999.
- [131] S A Kauffman. Metabolic stability and epigenesis in randomly constructed genetic nets. *J Theor Biol*, 22(3):437–67, Mar 1969.
- [132] Himanshu Kaul and Yiannis Ventikos. Investigating biocomplexity through the agent-based paradigm. *Brief Bioinform*, Nov 2013.

- [133] Curtis T Keith, Alexis A Borisy, and Brent R Stockwell. Multicomponent therapeutics for networked systems. *Nat Rev Drug Discov*, 4(1):71–8, Jan 2005.
- [134] B N Kholodenko, O V Demin, G Moehren, and J B Hoek. Quantification of short term signaling by the epidermal growth factor receptor. *J Biol Chem*, 274(42):30169–81, Oct 1999.
- [135] Boris Kholodenko, Michael B Yaffe, and Walter Kolch. Computational approaches for analyzing information flow in biological networks. *Sci Signal*, 5(220):re1, Apr 2012.
- [136] D Kim, O Rath, W Kolch, and K-H Cho. A hidden oncogenic positive feedback loop caused by crosstalk between wnt and erk pathways. *Oncogene*, 26(31):4571–9, Jul 2007.
- [137] Daniel C Kirouac, Jin Y Du, Johanna Lahdenranta, Ryan Overland, Defne Yarar, Violette Paragas, Emily Pace, Charlotte F McDonagh, Ulrik B Nielsen, and Matthew D Onsum. Computational modeling of erbB2-amplified breast cancer identifies combined erbB2/3 blockade as superior to the combination of mek and akt inhibitors. *Sci Signal*, 6(288):ra68, Aug 2013.
- [138] Bertram Klinger, Anja Sieber, Raphaela Fritzsche-Guenther, Franziska Witzel, Leanne Berry, Dirk Schumacher, Yibing Yan, Pawel Durek, Mark Merchant, Reinhold Schäfer, Christine Sers, and Nils Blüthgen. Network quantification of egfr signaling unveils potential for targeted combination therapy. *Mol Syst Biol*, 9:673, 2013.
- [139] K E Knudsen, K C Arden, and W K Cavenee. Multiple g1 regulatory elements control the androgen-dependent proliferation of prostatic carcinoma cells. *J Biol Chem*, 273(32):20213–22, Aug 1998.
- [140] Pamela K Kreeger and Douglas A Lauffenburger. Cancer systems biology: a network modeling perspective. *Carcinogenesis*, 31(1):2–8, Jan 2010.
- [141] Andreas Kremling, Sophia Fischer, Kapil Gadkar, Francis J Doyle, Thomas Sauter, Eric Bullinger, Frank Allgöwer, and Ernst D Gilles. A benchmark for methods in reverse engineering and model discrimination: problem formulation and solutions. *Genome Res*, 14(9):1773–85, Sep 2004.
- [142] Silvia Lapenna and Antonio Giordano. Cell cycle kinases as therapeutic targets for cancer. *Nat Rev Drug Discov*, 8(7):547–66, Jul 2009.

- [143] Peter Laslo, Chauncey J Spooner, Aryeh Warmflash, David W Lancki, Hyun-Jun Lee, Roger Sciammas, Benjamin N Gantner, Aaron R Dinner, and Harinder Singh. Multilineage transcriptional priming and determination of alternate hematopoietic cell fates. *Cell*, 126(4):755–66, Aug 2006.
- [144] Yuri Lazebnik. What are the hallmarks of cancer? *Nat Rev Cancer*, 10(4):232–3, Apr 2010.
- [145] Michael J Lee, Albert S Ye, Alexandra K Gardino, Anne Margriet Heijink, Peter K Sorger, Gavin MacBeath, and Michael B Yaffe. Sequential application of anticancer drugs enhances cell death by rewiring apoptotic signaling networks. *Cell*, 149(4):780–94, May 2012.
- [146] Ming-Shyue Lee, Tsukasa Igawa, and Ming-Fong Lin. Tyrosine-317 of p52(shc) mediates androgen-stimulated proliferation signals in human prostate cancer cells. *Oncogene*, 23(17):3048–58, Apr 2004.
- [147] Ming-Shyue Lee, Tsukasa Igawa, Ta-Chun Yuan, Xiu-Qing Zhang, Fen-Fen Lin, and Ming-Fong Lin. Erbb-2 signaling is involved in regulating psa secretion in androgen-independent human prostate cancer lncap c-81 cells. *Oncogene*, 22(5):781–96, Feb 2003.
- [148] Joshua Lequieu, Anirikh Chakrabarti, Satyaprakash Nayak, and Jeffrey D Varner. Computational modeling and analysis of insulin induced eukaryotic translation initiation. *PLoS Comput Biol*, 7(11):e1002263, Nov 2011.
- [149] S L Li, W Schlegel, A J Valente, and R A Clark. Critical flanking sequences of pu.1 binding sites in myeloid-specific promoters. *J Biol Chem*, 274(45):32453–60, Nov 1999.
- [150] Maria Rosa Lidonnici, Alessandra Audia, Angela Rachele Soliera, Marco Prisco, Giovanna Ferrari-Amorotti, Todd Waldron, Nick Donato, Ying Zhang, Robert V Martinez, Tessa L Holyoake, and Bruno Calabretta. Expression of the transcriptional repressor gfi-1 is regulated by c/ebpalpha and is involved in its proliferation and colony formation-inhibitory effects in p210bcr/abl-expressing cells. *Cancer Res*, 70(20):7949–59, Oct 2010.
- [151] Jin T E Lim, Mahesh Mansukhani, and I Bernard Weinstein. Cyclin-dependent kinase 6 associates with the androgen receptor and enhances its transcriptional activity in prostate cancer cells. *Proc Natl Acad Sci U S A*, 102(14):5156–61, Apr 2005.

- [152] H K Lin, S Yeh, H Y Kang, and C Chang. Akt suppresses androgen-induced apoptosis by phosphorylating and inhibiting androgen receptor. *Proc Natl Acad Sci U S A*, 98(13):7200–5, Jun 2001.
- [153] Hui-Kuan Lin, Yueh-Chiang Hu, Lin Yang, Saleh Altuwaijri, Yen-Ta Chen, Hong-Yo Kang, and Chawnshang Chang. Suppression versus induction of androgen receptor functions by the phosphatidylinositol 3-kinase/akt pathway in prostate cancer lncap cells with different passage numbers. *J Biol Chem*, 278(51):50902–7, Dec 2003.
- [154] M F Lin, M S Lee, R Garcia-Arenas, and F F Lin. Differential responsiveness of prostatic acid phosphatase and prostate-specific antigen mRNA to androgen in prostate cancer cells. *Cell Biol Int*, 24(10):681–9, 2000.
- [155] M F Lin, M S Lee, X W Zhou, J C Andressen, T C Meng, S L Johansson, W W West, R J Taylor, J R Anderson, and F F Lin. Decreased expression of cellular prostatic acid phosphatase increases tumorigenicity of human prostate cancer cells. *J Urol*, 166(5):1943–50, Nov 2001.
- [156] Ralph K Lindemann, Melanie Braig, Pia Ballschmieter, Theresa A Guise, Alfred Nordheim, and Jürgen Dittmer. Protein kinase calpha regulates ets1 transcriptional activity in invasive breast cancer cells. *Int J Oncol*, 22(4):799–805, Apr 2003.
- [157] Glenn Liu, Yu-Hui Chen, Jill Kolesar, Wei Huang, Robert Dipaola, Michael Pins, Michael Carducci, Mark Stein, Glenn J Bubley, and George Wilding. Eastern cooperative oncology group phase ii trial of lapatinib in men with biochemically relapsed, androgen dependent prostate cancer. *Urol Oncol*, 31(2):211–8, Feb 2013.
- [158] M Liu and L P Freedman. Transcriptional synergism between the vitamin d3 receptor and other nonreceptor transcription factors. *Mol Endocrinol*, 8(12):1593–604, Dec 1994.
- [159] M Liu, A Iavarone, and L P Freedman. Transcriptional activation of the human p21(waf1/cip1) gene by retinoic acid receptor. correlation with retinoid induction of u937 cell differentiation. *J Biol Chem*, 271(49):31723–8, Dec 1996.
- [160] M Liu, M H Lee, M Cohen, M Bommakanti, and L P Freedman. Transcriptional activation of the cdk inhibitor p21 by vitamin d3 leads to the induced differentiation of the myelomonocytic cell line u937. *Genes Dev*, 10(2):142–53, Jan 1996.

- [161] Yuanbo Liu, Samarpan Majumder, Wesley McCall, Carolyn I Sartor, James L Mohler, Christopher W Gregory, H Shelton Earp, and Young E Whang. Inhibition of her-2/neu kinase impairs androgen receptor recruitment to the androgen responsive enhancer. *Cancer Res*, 65(8):3404–9, Apr 2005.
- [162] C B Lozzio and B B Lozzio. Human chronic myelogenous leukemia cell-line with positive philadelphia chromosome. *Blood*, 45(3):321–34, Mar 1975.
- [163] S Lu, S Y Tsai, and M J Tsai. Regulation of androgen-dependent prostatic cancer cell growth: androgen regulation of cdk2, cdk4, and cki p16 genes. *Cancer Res*, 57(20):4511–6, Oct 1997.
- [164] Deyan Luan, Fania Szlam, Kenichi A Tanaka, Philip S Barie, and Jeffrey D Varner. Ensembles of uncertain mathematical models can identify network response to therapeutic interventions. *Mol Biosyst*, 6(11):2272–86, Nov 2010.
- [165] Xin M Luo and A Catharine Ross. Retinoic acid exerts dual regulatory actions on the expression and nuclear localization of interferon regulatory factor-1. *Exp Biol Med (Maywood)*, 231(5):619–31, May 2006.
- [166] Ka Sin Mak, Alister P W Funnell, Richard C M Pearson, and Merlin Crossley. Pu.1 and haematopoietic cell fate: Dosage matters. *Int J Cell Biol*, 2011:808524, 2011.
- [167] D J Mangelsdorf, C Thummel, M Beato, P Herrlich, G Schütz, K Umesono, B Blumberg, P Kastner, M Mark, P Chambon, and R M Evans. The nuclear receptor superfamily: the second decade. *Cell*, 83(6):835–9, Dec 1995.
- [168] Jennifer L Marlowe, Erik S Knudsen, Sandy Schwemberger, and Alvaro Puga. The aryl hydrocarbon receptor displaces p300 from e2f-dependent promoters and represses s phase-specific gene expression. *J Biol Chem*, 279(28):29013–22, Jul 2004.
- [169] Jeanelle M Martinez, Seung Joon Baek, Donna M Mays, Patricia K Tithof, Thomas E Eling, and Nigel J Walker. Egr1 is a novel target for ahr agonists in human lung epithelial cells. *Toxicol Sci*, 82(2):429–35, Dec 2004.
- [170] Susan Christine Massey, Marcela C Assanah, Kim A Lopez, Peter Canoll, and Kristin R Swanson. Glial progenitor cell recruitment drives aggres-

- sive glioma growth: mathematical and experimental modelling. *J R Soc Interface*, 9(73):1757–66, Aug 2012.
- [171] R H Medema, G J Kops, J L Bos, and B M Burgering. Afx-like forkhead transcription factors mediate cell-cycle regulation by ras and pkb through p27kip1. *Nature*, 404(6779):782–7, Apr 2000.
- [172] T C Meng, M S Lee, and M F Lin. Interaction between protein tyrosine phosphatase and protein tyrosine kinase is involved in androgen-promoted growth of human prostate cancer cells. *Oncogene*, 19(22):2664–77, May 2000.
- [173] Carmen G Moles, Pedro Mendes, and Julio R Banga. Parameter estimation in biochemical pathways: a comparison of global optimization methods. *Genome Res*, 13(11):2467–74, Nov 2003.
- [174] Melody K Morris, Julio Saez-Rodriguez, Peter K Sorger, and Douglas A Lauffenburger. Logic-based models for the analysis of cell signaling networks. *Biochemistry*, 49(15):3216–24, Apr 2010.
- [175] Virginia A Moyer and U.S. Preventive Services Task Force. Screening for prostate cancer: U.s. preventive services task force recommendation statement. *Ann Intern Med*, 157(2):120–34, Jul 2012.
- [176] Beatrice U Mueller, Thomas Pabst, José Fos, Vibor Petkovic, Martin F Fey, Norio Asou, Ulrich Buergi, and Daniel G Tenen. Atra resolves the differentiation block in t(15;17) acute myeloid leukemia by restoring pu.1 expression. *Blood*, 107(8):3330–8, Apr 2006.
- [177] R Munker, A Norman, and H P Koeffler. Vitamin d compounds. effect on clonal proliferation and differentiation of human myeloid cells. *J Clin Invest*, 78(2):424–30, Aug 1986.
- [178] H Murillo, H Huang, L J Schmidt, D I Smith, and D J Tindall. Role of pi3k signaling in survival and progression of lncap prostate cancer cells to the androgen refractory state. *Endocrinology*, 142(11):4795–805, Nov 2001.
- [179] Chadi Nabhan and Steven T Rosen. Chronic lymphocytic leukemia: a clinical review. *JAMA*, 312(21):2265–76, Dec 2014.
- [180] H Nakajima, M Kizaki, H Ueno, A Muto, N Takayama, H Matsushita, A Sonoda, and Y Ikeda. All-trans and 9-cis retinoic acid enhance 1,25-

- dihydroxyvitamin d3-induced monocytic differentiation of u937 cells. *Leuk Res*, 20(8):665–76, Aug 1996.
- [181] Elly S W Ngan, Yoshihiro Hashimoto, Zhi-Qing Ma, Ming-Jer Tsai, and Sophia Y Tsai. Overexpression of cdc25b, an androgen receptor coactivator, in prostate cancer. *Oncogene*, 22(5):734–9, Feb 2003.
- [182] I L Olsson and T R Breitman. Induction of differentiation of the human histiocytic lymphoma cell line u-937 by retinoic acid and cyclic adenosine 3':5'-monophosphate-inducing agents. *Cancer Res*, 42(10):3924–7, Oct 1982.
- [183] H L Pahl, R J Scheibe, D E Zhang, H M Chen, D L Galson, R A Maki, and D G Tenen. The proto-oncogene pu.1 regulates expression of the myeloid-specific cd11b promoter. *J Biol Chem*, 268(7):5014–20, Mar 1993.
- [184] Z Pan, C J Hetherington, and D E Zhang. Ccaat/enhancer-binding protein activates the cd14 promoter and mediates transforming growth factor beta signaling in monocyte development. *J Biol Chem*, 274(33):23242–8, Aug 1999.
- [185] Elizaveta V Pankratova, Elena V Sytina, Nadejda N Luchina, and Ivan V Krivega. The regulation of the oct-1 gene transcription is mediated by two promoters. *Immunol Lett*, 88(1):15–20, Jul 2003.
- [186] C Parker, S Nilsson, D Heinrich, S I Helle, J M O'Sullivan, S D Foss, A Chodacki, P Wiechno, J Logue, M Seke, A Widmark, D C Johannessen, P Hoskin, D Bottomley, N D James, A Solberg, I Syndikus, J Kliment, S Wedel, S Boehmer, M Dall'Oglio, L Franzén, R Coleman, N J Vogelzang, C G O'Bryan-Tear, K Staudacher, J Garcia-Vargas, M Shan, Ø S Bruland, O Sartor, and ALSYMPCA Investigators. Alpha emitter radium-223 and survival in metastatic prostate cancer. *N Engl J Med*, 369(3):213–23, Jul 2013.
- [187] Maria Paola Paronetto, Manuela Cappellari, Roberta Busà, Simona Pedrotti, Roberta Vitali, Clay Comstock, Terry Hyslop, Karen E Knudsen, and Claudio Sette. Alternative splicing of the cyclin d1 proto-oncogene is regulated by the rna-binding protein sam68. *Cancer Res*, 70(1):229–39, Jan 2010.
- [188] Toby Passioura, Alla Dolnikov, Sylvie Shen, and Geoff Symonds. N-ras-induced growth suppression of myeloid cells is mediated by irf-1. *Cancer Res*, 65(3):797–804, Feb 2005.

- [189] Holger Perfahl, Helen M Byrne, Tingan Chen, Veronica Estrella, Tomás Alarcón, Alexei Lapin, Robert A Gatenby, Robert J Gillies, Mark C Lloyd, Philip K Maini, Matthias Reuss, and Markus R Owen. Multiscale modelling of vascular tumour growth in 3d: the roles of domain size and boundary conditions. *PLoS One*, 6(4):e14790, 2011.
- [190] J E Perry, M E Grossmann, and D J Tindall. Epidermal growth factor induces cyclin d1 in a human prostate cancer cell line. *Prostate*, 35(2):117–24, May 1998.
- [191] Christin E Petre-Draviam, Stephen L Cook, Craig J Burd, Thomas W Marshall, Yelena B Wetherill, and Karen E Knudsen. Specificity of cyclin d1 for androgen receptor regulation. *Cancer Res*, 63(16):4903–13, Aug 2003.
- [192] A Pollack. F.d.a. revokes approval of avastin for use as breast cancer drug. *The New York Times*, November 2011.
- [193] Liliana A Ponguta, Christopher W Gregory, Frank S French, and Elizabeth M Wilson. Site-specific androgen receptor serine phosphorylation linked to epidermal growth factor-dependent growth of castration-recurrent prostate cancer. *J Biol Chem*, 283(30):20989–1001, Jul 2008.
- [194] W B Pratt and D O Toft. Steroid receptor interactions with heat shock protein and immunophilin chaperones. *Endocr Rev*, 18(3):306–60, Jun 1997.
- [195] Jennifer Prescott and Gerhard A Coetzee. Molecular chaperones throughout the life cycle of the androgen receptor. *Cancer Lett*, 231(1):12–9, Jan 2006.
- [196] Amina A Qutub, Feilim Mac Gabhann, Emmanouil D Karagiannis, Prakash Vempati, and Aleksander S Popel. Multiscale models of angiogenesis. *IEEE Eng Med Biol Mag*, 28(2):14–31, 2009.
- [197] C C Reddy, S K Niyogi, A Wells, H S Wiley, and D A Lauffenburger. Engineering epidermal growth factor for enhanced mitogenic potency. *Nat Biotechnol*, 14(13):1696–9, Dec 1996.
- [198] Markus Rehm, Heinrich J Huber, Heiko Dussmann, and Jochen H M Prehn. Systems analysis of effector caspase activation and its control by x-linked inhibitor of apoptosis protein. *EMBO J*, 25(18):4338–49, Sep 2006.
- [199] A K Rishi, T M Gerald, Z M Shao, X S Li, R G Baumann, M I Dawson, and

- J A Fontana. Regulation of the human retinoic acid receptor alpha gene in the estrogen receptor negative human breast carcinoma cell lines skbr-3 and mda-mb-435. *Cancer Res*, 56(22):5246–52, Nov 1996.
- [200] K A Robertson, L Mueller, and S J Collins. Retinoic acid receptors in myeloid leukemia: characterization of receptors in retinoic acid-resistant k-562 cells. *Blood*, 77(2):340–7, Jan 1991.
- [201] F J Rodríguez-Ubreva, A E Cariaga-Martínez, M A Cortés, M Romero-De Pablos, S Ropero, P López-Ruiz, and B Colás. Knockdown of protein tyrosine phosphatase shp-1 inhibits g1/s progression in prostate cancer cells through the regulation of components of the cell-cycle machinery. *Oncogene*, 29(3):345–55, Jan 2010.
- [202] Evan D Rosen, Chung-Hsin Hsu, Xinzong Wang, Shuichi Sakai, Mason W Freeman, Frank J Gonzalez, and Bruce M Spiegelman. C/ebpalpha induces adipogenesis through ppargamma: a unified pathway. *Genes Dev*, 16(1):22–6, Jan 2002.
- [203] Karen A Ryall and Aik Choon Tan. Systems biology approaches for advancing the discovery of effective drug combinations. *J Cheminform*, 7:7, 2015.
- [204] Kambis Sadeghi, Barbara Wessner, Ute Laggner, Martin Ploder, Dietmar Tamandl, Josef Friedl, Ullrich Zügel, Andreas Steinmeyer, Arnold Pollak, Erich Roth, George Boltz-Nitulescu, and Andreas Spittler. Vitamin d3 down-regulates monocyte tlr expression and triggers hyporesponsiveness to pathogen-associated molecular patterns. *Eur J Immunol*, 36(2):361–70, Feb 2006.
- [205] Julio Saez-Rodriguez, Leonidas G Alexopoulos, Jonathan Epperlein, Regina Samaga, Douglas A Lauffenburger, Steffen Klamt, and Peter K Sorger. Discrete logic modelling as a means to link protein signalling networks with functional analysis of mammalian signal transduction. *Mol Syst Biol*, 5:331, 2009.
- [206] Julio Saez-Rodriguez, Leonidas G Alexopoulos, Mingsheng Zhang, Melody K Morris, Douglas A Lauffenburger, and Peter K Sorger. Comparing signaling networks between normal and transformed hepatocytes using discrete logical models. *Cancer Res*, 71(16):5400–11, Aug 2011.
- [207] Julio Saez-Rodriguez, Luca Simeoni, Jonathan A Lindquist, Rebecca Hemenway, Ursula Bommhardt, Boerge Arndt, Utz-Uwe Haus, Robert

- Weismantel, Ernst D Gilles, Steffen Klamt, and Burkhardt Schraven. A logical model provides insights into t cell receptor signaling. *PLoS Comput Biol*, 3(8):e163, Aug 2007.
- [208] Ozgür Sahin, Holger Fröhlich, Christian Löbke, Ulrike Korf, Sara Burmester, Meher Majety, Jens Mattern, Ingo Schupp, Claudine Chaouiya, Denis Thieffry, Annemarie Poustka, Stefan Wiemann, Tim Beissbarth, and Dorit Arlt. Modeling erbB receptor-regulated g1/s transition to find novel targets for de novo trastuzumab resistance. *BMC Syst Biol*, 3:1, 2009.
- [209] D S Salomon, R Brandt, F Ciardiello, and N Normanno. Epidermal growth factor-related peptides and their receptors in human malignancies. *Crit Rev Oncol Hematol*, 19(3):183–232, Jul 1995.
- [210] Regina Samaga, Julio Saez-Rodriguez, Leonidas G Alexopoulos, Peter K Sorger, and Steffen Klamt. The logic of egfr/erbB signaling: theoretical properties and analysis of high-throughput data. *PLoS Comput Biol*, 5(8):e1000438, Aug 2009.
- [211] Oliver Sartor and Sumanta K Pal. Abiraterone and its place in the treatment of metastatic crpc. *Nat Rev Clin Oncol*, 10(1):6–8, Jan 2013.
- [212] N Sato, M D Sadar, N Bruchovsky, F Saatcioglu, P S Rennie, S Sato, P H Lange, and M E Gleave. Androgenic induction of prostate-specific antigen gene is repressed by protein-protein interaction between the androgen receptor and ap-1/c-jun in the human prostate cancer cell line lncap. *J Biol Chem*, 272(28):17485–94, Jul 1997.
- [213] Howard I Scher, Karim Fizazi, Fred Saad, Mary-Ellen Taplin, Cora N Sternberg, Kurt Miller, Ronald de Wit, Peter Mulders, Kim N Chi, Neal D Shore, Andrew J Armstrong, Thomas W Flaig, Aude Fléchon, Paul Mainwaring, Mark Fleming, John D Hainsworth, Mohammad Hirmand, Bryan Selby, Lynn Seely, Johann S de Bono, and AFFIRM Investigators. Increased survival with enzalutamide in prostate cancer after chemotherapy. *N Engl J Med*, 367(13):1187–97, Sep 2012.
- [214] Birgit Schoeberl, Claudia Eichler-Jonsson, Ernst Dieter Gilles, and Gertraud Müller. Computational modeling of the dynamics of the map kinase cascade activated by surface and internalized egf receptors. *Nat Biotechnol*, 20(4):370–5, Apr 2002.
- [215] Birgit Schoeberl, Emily A Pace, Jonathan B Fitzgerald, Brian D Harms, Lihui Xu, Lin Nie, Bryan Linggi, Ashish Kalra, Violette Paragas, Raghida

- Bukhalid, Viara Grantcharova, Neeraj Kohli, Kip A West, Magdalena Leszczyniecka, Michael J Feldhaus, Arthur J Kudla, and Ulrik B Nielsen. Therapeutically targeting erbB3: a key node in ligand-induced activation of the erbB receptor-pi3k axis. *Sci Signal*, 2(77):ra31, 2009.
- [216] Angela Seaton, Paula Scullin, Pamela J Maxwell, Catherine Wilson, Johanna Pettigrew, Rebecca Gallagher, Joe M O'Sullivan, Patrick G Johnston, and David J J Waugh. Interleukin-8 signaling promotes androgen-independent proliferation of prostate cancer cells via induction of androgen receptor expression and activation. *Carcinogenesis*, 29(6):1148–56, Jun 2008.
- [217] Ankur Sharma, Wen-Shuz Yeow, Adam Ertel, Ilsa Coleman, Nigel Clegg, Chellappagounder Thangavel, Colm Morrissey, Xiaotun Zhang, Clay E S Comstock, Agnieszka K Witkiewicz, Leonard Gomella, Erik S Knudsen, Peter S Nelson, and Karen E Knudsen. The retinoblastoma tumor suppressor controls androgen signaling and human prostate cancer progression. *J Clin Invest*, 120(12):4478–92, Dec 2010.
- [218] Miaoqing Shen, Rodica P Bunaciu, Johanna Congleton, Holly A Jensen, Lavanya G Sayam, Jeffrey D Varner, and Andrew Yen. Interferon regulatory factor-1 binds c-cbl, enhances mitogen activated protein kinase signaling and promotes retinoic acid-induced differentiation of hl-60 human myelo-monoblastic leukemia cells. *Leuk Lymphoma*, 52(12):2372–9, Dec 2011.
- [219] Q Shen, I P Uray, Y Li, T I Krisko, T E Strecker, H-T Kim, and P H Brown. The ap-1 transcription factor regulates breast cancer cell growth via cyclins and e2f factors. *Oncogene*, 27(3):366–77, Jan 2008.
- [220] C J Sherr and J M Roberts. Cdk inhibitors: positive and negative regulators of g1-phase progression. *Genes Dev*, 13(12):1501–12, Jun 1999.
- [221] Rebecca Siegel, Deepa Naishadham, and Ahmedin Jemal. Cancer statistics, 2013. *CA Cancer J Clin*, 63(1):11–30, Jan 2013.
- [222] Rebecca L Siegel, Kimberly D Miller, and Ahmedin Jemal. Cancer statistics, 2015. *CA Cancer J Clin*, 65(1):5–29, 2015.
- [223] Elizabeth Sklar. Netlogo, a multi-agent simulation environment. *Artif Life*, 13(3):303–11, 2007.

- [224] D J Slamon, W Godolphin, L A Jones, J A Holt, S G Wong, D E Keith, W J Levin, S G Stuart, J Udove, and A Ullrich. Studies of the her-2/neu proto-oncogene in human breast and ovarian cancer. *Science*, 244(4905):707–12, May 1989.
- [225] R E Sobel and M D Sadar. Cell lines used in prostate cancer research: a compendium of old and new lines—part 1. *J Urol*, 173(2):342–59, Feb 2005.
- [226] Eun-Kyung Song, Young-Rae Lee, Yu-Ri Kim, Ji-Hyun Yeom, Chae-Hwa Yoo, Hyun-Kag Kim, Hye-Min Park, Hyung-Sub Kang, Jong-Suk Kim, Uh-Hyun Kim, and Myung-Kwan Han. Naadp mediates insulin-stimulated glucose uptake and insulin sensitization by ppar in adipocytes. *Cell Rep*, 2(6):1607–19, Dec 2012.
- [227] Sang Ok Song, Anirikh Chakrabarti, and Jeffrey D Varner. Ensembles of signal transduction models using pareto optimal ensemble techniques (poets). *Biotechnol J*, 5(7):768–80, Jul 2010.
- [228] Sang Ok Song and Jeffrey Varner. Modeling and analysis of the molecular basis of pain in sensory neurons. *PLoS One*, 4(9):e6758, 2009.
- [229] C Starbuck and D A Lauffenburger. Mathematical model for the effects of epidermal growth factor receptor trafficking dynamics on fibroblast proliferation responses. *Biotechnol Prog*, 8(2):132–43, 1992.
- [230] Ulrich Steidl, Frank Rosenbauer, Roel G W Verhaak, Xuesong Gu, Alexander Ebralidze, Hasan H Otu, Steffen Klippel, Christian Steidl, Ingmar Bruns, Daniel B Costa, Katharina Wagner, Manuel Aivado, Guido Kobbe, Peter J M Valk, Emmanuelle Passegué, Towia A Libermann, Ruud Delwel, and Daniel G Tenen. Essential role of jun family transcription factors in pu.1 knockdown-induced leukemic stem cells. *Nat Genet*, 38(11):1269–77, Nov 2006.
- [231] Jaehong Suh, Young Jin Jeon, Hwan Mook Kim, Jong Soon Kang, Norbert E Kaminski, and Kyu-Hwan Yang. Aryl hydrocarbon receptor-dependent inhibition of ap-1 activity by 2,3,7,8-tetrachlorodibenzo-p-dioxin in activated b cells. *Toxicol Appl Pharmacol*, 181(2):116–23, Jun 2002.
- [232] I Swameye, T G Muller, J Timmer, O Sandra, and U Klingmuller. Identification of nucleocytoplasmic cycling as a remote sensor in cellular signaling by databased modeling. *Proc Natl Acad Sci U S A*, 100(3):1028–33, Feb 2003.

- [233] Kristin R Swanson, Lawrence D True, and J D Murray. On the use of quantitative modeling to help understand prostate-specific antigen dynamics and other medical problems. *Am J Clin Pathol*, 119(1):14–7, Jan 2003.
- [234] I Sylvester and H R Schöler. Regulation of the oct-4 gene by nuclear receptors. *Nucleic Acids Res*, 22(6):901–11, Mar 1994.
- [235] Attila Szanto and Laszlo Nagy. Retinoids potentiate peroxisome proliferator-activated receptor gamma action in differentiation, gene expression, and lipid metabolic processes in developing myeloid cells. *Mol Pharmacol*, 67(6):1935–43, Jun 2005.
- [236] H Takaishi, H Konishi, H Matsuzaki, Y Ono, Y Shirai, N Saito, T Kitamura, W Ogawa, M Kasuga, U Kikkawa, and Y Nishizuka. Regulation of nuclear translocation of forkhead transcription factor *afx* by protein kinase b. *Proc Natl Acad Sci U S A*, 96(21):11836–41, Oct 1999.
- [237] L Tam, L M McGlynn, P Traynor, R Mukherjee, J M S Bartlett, and J Edwards. Expression levels of the jak/stat pathway in the transition from hormone-sensitive to hormone-refractory prostate cancer. *Br J Cancer*, 97(3):378–83, Aug 2007.
- [238] Samir S Taneja, Susan Ha, Nicole K Swenson, Hong Ying Huang, Peng Lee, Jonathan Melamed, Ellen Shapiro, Michael J Garabedian, and Susan K Logan. Cell-specific regulation of androgen receptor phosphorylation in vivo. *J Biol Chem*, 280(49):40916–24, Dec 2005.
- [239] Xiao-Han Tang and Lorraine J Gudas. Retinoids, retinoic acid receptors, and cancer. *Annu Rev Pathol*, 6:345–64, 2011.
- [240] Ian F Tannock, Ronald de Wit, William R Berry, Jozsef Horti, Anna Pluzanska, Kim N Chi, Stephane Oudard, Christine Théodore, Nicholas D James, Ingela Turesson, Mark A Rosenthal, Mario A Eisenberger, and TAX 327 Investigators. Docetaxel plus prednisone or mitoxantrone plus prednisone for advanced prostate cancer. *N Engl J Med*, 351(15):1502–12, Oct 2004.
- [241] Ryan Tasseff, Satyaprakash Nayak, Saniya Salim, Poorvi Kaushik, Noreen Rizvi, and Jeffrey D Varner. Analysis of the molecular networks in androgen dependent and independent prostate cancer revealed fragile and robust subsystems. *PLoS One*, 5(1):e8864, 2010.
- [242] Ryan Tasseff, Satyaprakash Nayak, Sang Ok Song, Andrew Yen, and Jeffrey D Varner. Modeling and analysis of retinoic acid induced differentia-

- tion of uncommitted precursor cells. *Integr Biol (Camb)*, 3(5):578–91, May 2011.
- [243] U Testa, F Grignani, T Barberi, M Fagioli, R Masciulli, P F Ferrucci, D Seripa, A Camagna, M Alcalay, and P G Pelicci. Pml/rar alpha+ u937 mutant and nb4 cell lines: retinoic acid restores the monocytic differentiation response to vitamin d3. *Cancer Res*, 54(16):4508–15, Aug 1994.
- [244] G N Thalmann, P E Anezinis, S M Chang, H E Zhau, E E Kim, V L Hopwood, S Pathak, A C von Eschenbach, and L W Chung. Androgen-independent cancer progression and bone metastasis in the lncap model of human prostate cancer. *Cancer Res*, 54(10):2577–81, May 1994.
- [245] N Timchenko, D R Wilson, L R Taylor, S Abdelsayed, M Wilde, M Sawadogo, and G J Darlington. Autoregulation of the human c/ebp alpha gene by stimulation of upstream stimulatory factor binding. *Mol Cell Biol*, 15(3):1192–202, Mar 1995.
- [246] National Cancer Institute U. S. National Institutes of Health. Seer training modules, classification, December 2013.
- [247] K S Ullman, J P Northrop, A Admon, and G R Crabtree. Jun family members are controlled by a calcium-regulated, cyclosporin a-sensitive signaling pathway in activated t lymphocytes. *Genes Dev*, 7(2):188–96, Feb 1993.
- [248] I M M van Leeuwen, G R Mirams, A Walter, A Fletcher, P Murray, J Osborne, S Varma, S J Young, J Cooper, B Doyle, J Pitt-Francis, L Momtahan, P Pathmanathan, J P Whiteley, S J Chapman, D J Gavaghan, O E Jensen, J R King, P K Maini, S L Waters, and H M Byrne. An integrative computational model for intestinal tissue renewal. *Cell Prolif*, 42(5):617–36, Oct 2009.
- [249] Ingeborg M M van Leeuwen, Helen M Byrne, Oliver E Jensen, and John R King. Elucidating the interactions between the adhesive and transcriptional functions of beta-catenin in normal and cancerous cells. *J Theor Biol*, 247(1):77–102, Jul 2007.
- [250] Matthew Vanneman and Glenn Dranoff. Combining immunotherapy and targeted therapies in cancer treatment. *Nat Rev Cancer*, 12(4):237–51, Apr 2012.
- [251] C L Varley, E J Bacon, J C Holder, and J Southgate. Foxa1 and irf-1 in-

- termediary transcriptional regulators of ppargamma-induced urothelial cytodifferentiation. *Cell Death Differ*, 16(1):103–14, Jan 2009.
- [252] Suresh Veeramani, Tsukasa Igawa, Ta-Chun Yuan, Fen-Fen Lin, Ming-Shyue Lee, Jamie S Lin, Sonny L Johansson, and Ming-Fong Lin. Expression of p66(shc) protein correlates with proliferation of human prostate cancer cells. *Oncogene*, 24(48):7203–12, Nov 2005.
- [253] Suresh Veeramani, Ta-Chun Yuan, Siu-Ju Chen, Fen-Fen Lin, Juliette E Petersen, Syed Shaheduzzaman, Shiv Srivastava, Richard G MacDonald, and Ming-Fong Lin. Cellular prostatic acid phosphatase: a protein tyrosine phosphatase involved in androgen-independent proliferation of prostate cancer. *Endocr Relat Cancer*, 12(4):805–22, Dec 2005.
- [254] Julio Vera, Julie Bachmann, Andrea C Pfeifer, Verena Becker, Jose A Hormiga, Nestor V Torres Darias, Jens Timmer, Ursula Klingmüller, and Olaf Wolkenhauer. A systems biology approach to analyse amplification in the jak2-stat5 signalling pathway. *BMC Syst Biol*, 2:38, 2008.
- [255] Alejandro F Villaverde and Julio R Banga. Reverse engineering and identification in systems biology: strategies, perspectives and challenges. *J R Soc Interface*, 11(91):20130505, Feb 2014.
- [256] Andreas Von Knethen and Bernhard Brüne. Activation of peroxisome proliferator-activated receptor gamma by nitric oxide in monocytes/macrophages down-regulates p47phox and attenuates the respiratory burst. *J Immunol*, 169(5):2619–26, Sep 2002.
- [257] Jinlian Wang, Yiming Zuo, Yan-Gao Man, Itzhak Avital, Alexander Stojadinovic, Meng Liu, Xiaowei Yang, Rency S Varghese, Mahlet G Tadesse, and Habtom W Ressom. Pathway and network approaches for identification of cancer signature markers from omics data. *J Cancer*, 6(1):54–65, 2015.
- [258] Nanping Wang, Lynne Verna, Neng-Guin Chen, Jasmine Chen, Hongling Li, Barry Marc Forman, and Michael B Stemerman. Constitutive activation of peroxisome proliferator-activated receptor-gamma suppresses pro-inflammatory adhesion molecules in human vascular endothelial cells. *J Biol Chem*, 277(37):34176–81, Sep 2002.
- [259] Zhihui Wang, Christina M Birch, Jonathan Sagotsky, and Thomas S Deisboeck. Cross-scale, cross-pathway evaluation using an agent-based non-small cell lung cancer model. *Bioinformatics*, 25(18):2389–96, Sep 2009.

- [260] J Wayman and J Varner. Biological systems modeling of metabolic and signaling networks. *Curr Opin Chem Eng*, 2:365 – 372, 2013.
- [261] Michael J Weber and Daniel Gioeli. Ras signaling in prostate cancer progression. *J Cell Biochem*, 91(1):13–25, Jan 2004.
- [262] Y Wen, M C Hu, K Makino, B Spohn, G Bartholomeusz, D H Yan, and M C Hung. Her-2/neu promotes androgen-independent survival and growth of prostate cancer cells through the akt pathway. *Cancer Res*, 60(24):6841–5, Dec 2000.
- [263] Young E Whang, Andrew J Armstrong, W Kimryn Rathmell, Paul A Godley, William Y Kim, Raj S Pruthi, Eric M Wallen, Jeffrey M Crane, Dominic T Moore, Gayle Grigson, Karla Morris, Catharine P Watkins, and Daniel J George. A phase ii study of lapatinib, a dual egfr and her-2 tyrosine kinase inhibitor, in patients with castration-resistant prostate cancer. *Urol Oncol*, 31(1):82–6, Jan 2013.
- [264] Magdalena Widerak, Christelle Ghoneim, Marie-France Dumontier, Monique Quesne, Marie Therese Corvol, and Jean-Francois Savouret. The aryl hydrocarbon receptor activates the retinoic acid receptoralpha through smrt antagonism. *Biochimie*, 88(3-4):387–97, 2006.
- [265] H Steven Wiley, Stanislav Y Shvartsman, and Douglas A Lauffenburger. Computational modeling of the egf-receptor system: a paradigm for systems biology. *Trends Cell Biol*, 13(1):43–50, Jan 2003.
- [266] M G Wilkinson and J B Millar. Control of the eukaryotic cell cycle by map kinase signaling pathways. *FASEB J*, 14(14):2147–57, Nov 2000.
- [267] Wei Wu, Xiaoyu Zhang, and Laura P Zanello. 1alpha,25-dihydroxyvitamin d(3) antiproliferative actions involve vitamin d receptor-mediated activation of mapk pathways and ap-1/p21(waf1) upregulation in human osteosarcoma. *Cancer Lett*, 254(1):75–86, Aug 2007.
- [268] Youyuan Xu, Shao-Yong Chen, Kenneth N Ross, and Steven P Balk. Androgens induce prostate cancer cell proliferation through mammalian target of rapamycin activation and post-transcriptional increases in cyclin d proteins. *Cancer Res*, 66(15):7783–92, Aug 2006.
- [269] A Yamamoto, Y Hashimoto, K Kohri, E Ogata, S Kato, K Ikeda, and

- M Nakanishi. Cyclin e as a coactivator of the androgen receptor. *J Cell Biol*, 150(4):873–80, Aug 2000.
- [270] Y Yarden and M X Sliwkowski. Untangling the erbB signalling network. *Nat Rev Mol Cell Biol*, 2(2):127–37, Feb 2001.
- [271] S Yeh, H K Lin, H Y Kang, T H Thin, M F Lin, and C Chang. From her2/neu signal cascade to androgen receptor and its coactivators: a novel pathway by induction of androgen target genes through map kinase in prostate cancer cells. *Proc Natl Acad Sci U S A*, 96(10):5458–63, May 1999.
- [272] S Yeh, H Miyamoto, K Nishimura, H Kang, J Ludlow, P Hsiao, C Wang, C Su, and C Chang. Retinoblastoma, a tumor suppressor, is a coactivator for the androgen receptor in human prostate cancer du145 cells. *Biochem Biophys Res Commun*, 248(2):361–7, Jul 1998.
- [273] T-C Yuan, F-F Lin, S Veeramani, S-J Chen, H S Earp, 3rd, and M-F Lin. Erbb-2 via pyk2 upregulates the adhesive ability of androgen receptor-positive human prostate cancer cells. *Oncogene*, 26(54):7552–9, Nov 2007.
- [274] Hiromichi Yuki, Shikiko Ueno, Hiro Tatetsu, Hiroaki Niilo, Tadafumi Iino, Shinya Endo, Yawara Kawano, Yoshihiro Komohara, Motohiro Takeya, Hiroyuki Hata, Seiji Okada, Toshiki Watanabe, Koichi Akashi, Hiroaki Mitsuya, and Yutaka Okuno. Pu.1 is a potent tumor suppressor in classical hodgkin lymphoma cells. *Blood*, 121(6):962–70, Feb 2013.
- [275] Katrin Zaragoza, Valérie Bégay, Anja Schuetz, Udo Heinemann, and Achim Leutz. Repression of transcriptional activity of c/ebpalpha by e2f-dimerization partner complexes. *Mol Cell Biol*, 30(9):2293–304, May 2010.
- [276] Ranran Zhang, Mithun Vinod Shah, Jun Yang, Susan B Nyland, Xin Liu, Jong K Yun, Réka Albert, and Thomas P Loughran, Jr. Network model of survival signaling in large granular lymphocyte leukemia. *Proc Natl Acad Sci U S A*, 105(42):16308–13, Oct 2008.